

THE UNIVERSITY OF MICHIGAN

College of Engineering  
Department of Mechanical Engineering

Final Report

THERMAL REACTOR DEVELOPMENT FOR  
SMALL ROTARY ENGINES

*(Handwritten)*  
F. Ament

D. E. Cole

D. J. Patterson

Period: September 15, 1972 to January 31, 1974

ORA Project 320229

supported by:

Walker Manufacturing Company  
Research & Engineering Center  
Grass Lake, Michigan

administered through

Office of Research Administration Ann Arbor

June 1974

TABLE OF CONTENTS

	<u>PAGE</u>
GENERAL INTRODUCTION	2
OVERALL CONCLUSIONS	4
PHASE I - STEADY-STATE PERFORMANCE OF THE MODEL A REACTOR	6
PHASE II - TRANSIENT PERFORMANCE OF THE MODEL A REACTOR	74
PHASE III - THE EFFECT OF VOLUME AND GEOMETRY VARIATIONS ON THE STEADY-STATE PERFORMANCE OF SIMILAR REACTORS	112
DISTRIBUTION LIST	167

## GENERAL INTRODUCTION

### Background

During the past few years, interest in air pollution on both the local and national level has increased rapidly and the internal combustion engine has been receiving much criticism for its contribution to the problem. In some special cases, notably Los Angeles with its photochemical smog, the automotive spark-ignited engine is responsible for the major portion of the total problem. California, in fact, became the first governmental body to legislate control of automotive exhaust emissions in 1961.

From this beginning, rapid legislative progress has resulted in the formulation of very restrictive Federal emission standards for CO, HC, and NO<sub>x</sub>. The 1970 Clean Air Act called for emission reduction of more than 90% from pre-control automotive emission levels. Only a temporary delay has prevented these standards from being applied in the 1975 model year. At the same time, rapid progress has been made in the control of emissions from stationary sources such as power generation and industrial processing plants.

As the more significant pollution sources, such as the automobile and industrial stack effluents, are controlled, emissions from small utility and recreational vehicles will most certainly increase in importance on a relative scale. We believe that federal regulations governing currently uncontrolled engines are imminent and will appear in the near future. The recently completed EPA sponsored study by the Southwest Research Institute entitled, "Exhaust Emissions from Uncontrolled Vehicles and Related Equipment Using Internal Combustion Engines", strengthens our view of increasing

government interest in these areas. It is desirable to have positive and valid technical information available at the time the small engine industry is requested or required to participate in the formulation of regulations or standards governing their products. It is imperative that fair and equitable laws be written that are cognizant of both the requirements of the general public for reasonably priced, efficient, non-polluting power systems, and the manufacturer's problems of designing and building their engines.

With few exceptions, little attention has been directed at the problem of emission control for small engines, and it is reasonable to expect rotary engines to assume a good share of the future small engine market. The development of a reasonably inexpensive exhaust clean-up device for the rotary class of small engines may offer a practical solution to a segment of the industry. Since the rotary engine has a characteristically higher exhaust temperature, a well designed exhaust thermal reactor could be effective in meeting future HC and CO emission standards as the low emission results of this research program suggest.

#### Program Outline

The purpose of this research was to develop and test effective, yet easily manufacturable, exhaust thermal reactor designs for small rotary engines. Furthermore, it was hoped that technology could be developed that would lead to a better understanding of rotary engine emissions and the important criteria for thermal reactor design.



Dynamometer and vehicle tests were run with an Outboard Marine Corporation 35 HP (32 CID) rotary (Wankel) engine and snowmobile. Five similar bottle-shaped exhaust reactors, with internal volumes ranging from 52.5 to 84 in<sup>3</sup>, were individually evaluated. The best reactor, Model A, was more extensively evaluated at several test points representative of snowmobile operation including warmup, idle, deceleration, and cruise. Some theoretical performance predictions were made using the UM-CRC model and a two-stirred tank model.

The program was divided into three phases:

- I. Steady-State Performance of the Model A Reactor
- II. Transient Performance of the Model A reactor
- III. Effect of Volume and Geometry Variations on the Steady-State Performance of Similar Reactors

#### OVERALL CONCLUSIONS

Small exhaust reactors of simple design can react 98% of exhaust CO and HC from the OMC rotary engine when air injection quantity is properly controlled. High engine exhaust temperatures, coupled with a large heat of combustion from the typically CO rich (6%) exhaust, minimize thermal reactor ignition problems and permit air injection directly into the reactor which in turn provides excellent mixing. Moderate volume and geometry variations of the basic reactor design provide virtually equivalent performance.

The best reactor, Model A, exhibits the ability to ignite itself at idle and remain lit during transient decelerations. Very high reactor shell temperatures of 1700<sup>o</sup>F or higher may pose severe metallurgical and packaging problems. Some form of reactor insulating and cooling will be required

for safety.

Based on the general design of the five reactors tested, a simple two-stirred tank math model was developed. While it predicted the directional effects of volume, shape, temperature, flow rate, and composition for the conditions tested, additional verification is needed before absolute predictions can be relied upon.

PHASE I

STEADY-STATE PERFORMANCE OF THE MODEL A REACTOR

	<u>Page</u>
I. Introduction	8
II. Conclusions	9
III. Test Equipment	10
A. Dynamometer Installation	10
B. Exhaust Gas Sampling	13
C. Exhaust Gas Analysis	15
1. Carbon Monoxide	15
2. NDIR Carbon Monoxide, Carbon Dioxide, and Nitric Oxide	15
3. FID Hydrocarbons	17
4. Exhaust Gas Oxygen Analysis	18
5. Exhaust Aldehyde Measurement	19
D. Temperature Measurement	20
E. Secondary Air Injection	23
F. Engine A/F Measurement	23
1. Engine Air Measurement	24
2. Engine Fuel Measurement	24
IV. Test Procedure	25
V. Discussion	27
A. Air Injection Fraction as a Mixing Indicator	27
B. Reactor Description	28
C. Reactor Evaluation	29
1. Carbon Monoxide and Hydrocarbon Oxidation	29
2. Nitric Oxide	32
3. Aldehyde Emissions	34
D. Reactor Skin Temperatures	34
VI. References for Phase I	37
Appendix	
A. Data Expression	65
B. FID HC Parameter Optimization	68

## Introduction

The initial phase of this program was devoted to developing a flexible testing installation, including a complete range of emission transducers. Supportive structures had to be built, and sampling and analyzing techniques had to be developed or modified to suit the rotary's unique characteristics. In addition, a number of safety features had to be incorporated to provide protection during long, high speed, high temperature runs. During this set-up period, detailed test and data reduction procedures were also developed.

At the same time, a mathematical model development program was initiated. This consisted of a major revision of the model formulated during the previous two years as part of the CRC-APRAC CAPE 8-68 program,<sup>7</sup> and the development of a new model specific to the reactor designs of this program. The theoretical work is described in Phase III under Discussion - Part D.

The model A reactor was tested over a wide range of engine operating conditions. HC, CO, and NO emissions and temperature were measured at the exhaust port, at various positions along the reactor centerline, and at the reactor exit. The HC, CO, and aldehyde conversion efficiency of the model A reactor as a function of air injection fraction was determined at several test conditions.

After the conversion efficiency of the A reactor was established, modifications designed to improve the performance and simplify manufacturability were tested.

## II. Conclusions

1. Thermal reactors with CO and HC conversion efficiencies in excess of 95% and of easily manufacturable design, can be adapted to the OMC rotary snowmobile engine.
2. High reactor skin temperatures of 1700<sup>o</sup>F or higher are expected to pose severe material and/or design problems for rich engine reactors. Some form of internal or external cooling may be required.
3. In designing thermal reactors for rotary engines, mixing of exhaust and injected air is of prime importance. Because of the high reactor temperatures, conversion efficiency under warmed-up conditions is most often mixing, rather than reaction rate, limited.
4. The air injection fraction, and possibly the NO concentration, measured at various points in the reactor may be used as an experimental indicator of relative mixing efficiency.
5. All current data suggest that NO is not increased in the reactor.
6. The well-mixed model A reactor appears attractive for lean rotary engines also. The OMC rotary engine's rich mixture requirements have prevented any attempt at using the highly efficient design as a lean reactor.
7. Because of the effectiveness of this reactor, it should be scaled to the size required by an automotive rotary engine and tested for both lean and rich reactor application.

### III. Test Equipment

#### A. Dynamometer Installation

The Outboard Marine Corporation (OMC) 35 HP, air-charge cooled, single rotor engine was installed in Room 254 of the University of Michigan Automotive Laboratory. Key engine features are listed in Table 1.

The engine was coupled to a 200 HP General Electric motoring-absorbing dynamometer, with speed control, by a 9/16" shaft mounted in a rubber damper at one end. To prevent possible injury from shaft failure, the entire length of the shaft was covered by a heavy steel guard which was bolted to the bedplate. Figure 1 shows an overview of the engine dynamometer installation, and Figure 2 shows the control console.

To facilitate reactor attachment, a special engine stand was designed and fabricated. Because of its low vibration, the engine was mounted rigidly to the support stand and shimmed for proper alignment with the dynamometer shaft. The ignition components were assembled in a tray and bolted to the front of the engine stand for easy access. To reduce heating of the fan cooling air, the 2 in. diameter exhaust pipe was routed close to the bedplate, into the laboratory exhaust system. The exhaust pipe was covered with an expanded steel shield, and the muffler was mounted in the trench below the bedplate to prevent possible injury from severe "back-popping". A thin steel radiation shield was mounted between the engine and reactor to minimize heat transfer to the engine housing, which could lead to over-heating. To provide cooling air for the engine fan and prevent stagnation

Table 1

OMC Rotary Engine (Type D471) - Key Features

No. of Rotors	1
Actual Displacement	32.3 in. <sup>3</sup> (528 cc)
Compression Ratio	8.75:1
Max. Rated HP at RPM	35 at 5500
Size l/w/h <sup>(1)</sup>	14 in/13 in/11.5 in.
Weight <sup>(2)</sup>	67 pounds
Intake port/area	Peripheral + side/.785 in <sup>2</sup> + .5 in. <sup>2</sup>
Exhaust port/area	Peripheral/.99 in <sup>2</sup>
Ignition	15° BTDC (fixed)
Carburetion <sup>(3)</sup>	SU type HS - 1-1/2 in. dia.
Cooling	Housing - forced air Rotor - intake charge cooling
Rotor Width (w)	3.060 in. (78 mm)
Radius (R)	3.63 in. (92 mm)
Eccentricity (e)	.55 in. (14 mm)
K factor (R/e)	6.6
Q factor (W/4e)	1.39

---

(1) not including standard carburetor

(2) including starter and carburetor

(3) engine comes with production OMC carburetor



of hot air, a large fan was mounted in front of the engine fan inlet.

For better air-fuel control, the OMC carburetor and diaphragm fuel pump were replaced by a 1-1/2 inch, constant vacuum, SU carburetor and Bendix 12-volt, electric fuel pump. The SU carburetor was chosen because of its simplicity and ability to deliver a constant and controllable air-fuel mixture. The air-fuel ratio can be precisely controlled by adjusting the position of the jet with respect to the fuel metering rod. Since the engine was operated at constant speed, the SAE 20 oil recommended for the carburetor damper was replaced with SAE 30 to minimize metering piston pulsation, which was originally found to be a minor problem. The electric fuel pump and 6 gallon fuel tank were mounted behind the dynamometer away from the engine and exhaust system.

To prevent the fuel in the carburetor bowl from boiling out the vent, the outside of the carburetor bowl was water-cooled and a radiation shield was placed between the carburetor and engine housing. Carburetor heating was a problem because the air that cools the end housing was exhausted directly at the carburetor. (This is not a problem in the snowmobile installation because the carburetor is completely isolated from the engine compartment).

## B. Exhaust Gas Sampling

The reactor and exhaust sampling circuit are shown in Figure 3. Four sample probes were used. The exhaust port probe and the two downstream probes, located 9 and 20 inches from the reactor exit, could be positioned to sample anywhere across the diameter of the exhaust pipe. The reactor sample probe could be adjusted to sample axially along the centerline of the reactor and into the first three inches of the exhaust pipe.

Two types of water-cooled, stainless steel sample probes were used to collect the hot exhaust gas. The concentrically-cooled reactor probe (shown in Figure 4) was cooled at the sample inlet. The water-jacket probe (shown in Figure 5) was not cooled at the sample inlet.

The 5/16" diameter reactor probe (Figure 4) was designed to quench the entire exhaust sample and minimize the possibility of further chemical reactions in the sample line. The "quenched" sample was then ducted, at room temperature, to the analytical instruments. To enable coolant flow near the sample inlet, it was necessary to use a single stagnation inlet hole at the probe tip. Because of its larger diameter, this concentrically cooled "quench" probe was not practical for sampling at the exhaust port or in the exhaust pipe. For sampling in the small diameter sections, the "delayed quench" probe shown in Figure 5 was used. This design combined the advantages of a small diameter tube, for minimum exhaust

system restriction, with the "quench" effect of water cooling. It is felt that the measurements were not significantly effected by the chemical reactions that occurred in the short uncooled section. This design also allowed the use of multiple inlets which are useful in obtaining a more representative sample from a pulsating exhaust flow. While these probes could be positioned to sample anywhere across the diameter of the pipe, early tests indicated no significant concentration gradient across the diameter of the exhaust pipe downstream of the reactor. As a result, the probes were adjusted to sample from the middle of the exhaust stream.

Teflon tubing (1/4") was used for all sample lines involved with HC measurement and nylon tubing (1/4") for the remainder of the sampling circuit. Previous work by Papa (1 ) on exhaust sampling bags indicated that many common tubing materials, including nylon, absorb hydrocarbons readily. Because the reactor HC concentrations were very low and the inside of tubing comprises such a large surface area, Teflon tubing was used for any lines involved in HC measurement.

To prevent water vapor and particulate contamination, an ice bath and particulate filter were installed in both the HC and in the CO sampling circuits ahead of the analyzers. The 115 mm glass fiber filter made by Gelman Instrument Company was quite effective in removing particulates from the sample. In addition, a 12" column of calcium sulfate dessicant was placed ahead of the NO analyzer cell to remove any water in the sample.

Because the NO sample cell is long, 10 inches, and the NO concentrations may be extremely low, water vapor can cause interference in NO measurement. The exhaust gas analytical system is shown in Figure 6.

### C. Exhaust Gas Analysis

The various exhaust gas analysis techniques are summarized in Table 2, and the analyzer cart with some of the bottled gases is shown in Figure 7.

#### 1. Carbon Monoxide

For rich reactors, carbon monoxide is the most important exhaust component for determining reactor efficiency. Recent reactor studies (2) indicate that HC and H<sub>2</sub> oxidize at lower temperatures and with higher rates than CO. H<sub>2</sub> and HC also tend to consume O<sub>2</sub> before CO does. These findings indicate that, because CO oxidation requires more time and higher temperatures, when the CO conversion is high, the HC conversion will be at least equal or better.

#### 2. NDIR Carbon Monoxide, Carbon Dioxide, and Nitric Oxide

Carbon monoxide, carbon dioxide, and nitric oxide concentrations were measured by Beckman 315A NDIR analyzers. This technique measures the differential absorption of infrared energy between a fixed reference gas and the exhaust sample gas. Because of the high concentrations of CO, (0-10%) and CO<sub>2</sub> (0-15%), short sample cells were used

Table 2

Gas Analysis Techniques

<u>Exhaust Specie</u>	<u>Technique</u>	<u>Manufacturer</u>	<u>Range</u>
Carbon monoxide	NDIR <sup>1,2</sup>	Beckman Inst Model 315A	0-10%
Carbon dioxide	NDIR <sup>1,2</sup>	Beckman Inst. Model 315A	0-15%
Nitric oxide	NDIR <sup>1</sup>	Beckman Inst. Model 315A	0-1000 ppm
Hydrocarbon	FID <sup>3</sup>	Beckman Inst. Model 109A	0-1450 ppm
Oxygen	Amperometric	Beckman Inst. Model 715	0-5% or 0-25%
Aldehydes	DNPH <sup>4</sup>	Wet chemical and Bausch & Lomb Spectronic 20 spectrophotometer	

- 
1. NDIR - nondispersive infrared
  2. Calibration gases check by Orsat analysis
  3. FID - flame ionization detector
  4. DNPH - dinitrophenylhydrazone wet chemical method.

for rapid response. Unlike the CO and CO<sub>2</sub>, the NO concentration ranged from 0-700 ppm, (0-.07%). To provide the necessary sensitivity for measuring these low concentrations, a 10" sample cell was used.

Before each test, the NDIR analyzers were calibrated with dry N<sub>2</sub> as a zero gas and several known span gases. Calibration gases of 8.2% CO and 4.9% CO were used and periodically the lower range of the CO analyzer was checked with .5% CO and .19% CO. The CO analyzer response was found to be very accurate, being able to distinguish between concentrations of .05 and .1% CO. Since the exhaust CO<sub>2</sub> concentration was consistently between 10-15%, a calibration gas of 13.45% CO<sub>2</sub> was chosen. The 8.2% and 4.9% CO and 13.45% CO<sub>2</sub> gases were checked by Orsat analysis and found to be within 5% of the specified composition. The .5% CO and .19% CO gases were obtained from the Ford Motor Company and were checked by them. A mixture of 675 ppm NO in pure N<sub>2</sub> was used as a span gas for the NO analyzer.

### 3. FID Hydrocarbons

A Beckman 109A flame ionization detector (FID) was used to measure total hydrocarbons in the exhaust. This instrument is typical of those used by EPA for hydrocarbon measurement. The FID uses positive pressure to force the sample through the detector which makes the instrument less susceptible to leakage at the various fittings. The sample, fuel, and air flow rates are controlled by capillary tubes. Figure 8 shows the hydrocarbon analytical branch.

A separate HC sampling circuit, complete with condensate trap, pump, and particulate filter was branched off the main sample line as indicated in Figure 6. Sample flow rate to the detector was maintained between 2.8-2.9 l/min by a Fischer and Porter rotameter. Since the accuracy of the FID is greatly affected by the sample bypass flow, a Fischer and Porter 7.0 SCFH, rotameter was installed in the bypass line to insure the sample flow and calibration gas flow through the burner were equal.

While the instrument was used in conventional form, the operating parameters were optimized, as explained in Appendix B, to minimize any error due to  $O_2$  interference and to provide equal response to the various HC in the exhaust. A mixture of 40%  $H_2$  and 60% He was used as the FID fuel.

#### 4. Exhaust Gas Oxygen Analysis

The oxygen concentration in the exhaust was measured with a Beckman Model 715 amperometric oxygen analyzer. Since the composition of the dry exhaust gas is not altered by passage through the NDIR analyzers, the oxygen transducer was placed at the outlet of the  $CO_2$  analyzer. The stopcock on the  $O_2$  meter outlet sealed the sensor from atmospheric oxygen when it was not in use. This is shown schematically in Figure 6.

Since this instrument has a linear response to oxygen concentration (actually partial pressure of  $O_2$ ), it was calibrated with pure  $N_2$  as the zero gas and atmospheric oxygen as the 21%  $O_2$  span gas.

Several gases can cause  $O_2$  interference, including  $SO_2$ ,  $Cl_2$ ,  $H_2S$ , and  $NO$ . Since most of these compounds are not present in measurable concentrations, only  $NO$  could cause significant interference. However, because the  $NO$  concentrations ranged from 100-700 ppm, its interference is also negligible.

The  $O_2$  meter provides temperature compensation for gas temperatures between  $32-110^{\circ}F$ . After passing through the ice bath, the sample temperature is within this range.

#### 5. Exhaust Aldehyde Measurement

Total exhaust aldehyde emissions were determined colorimetrically using the DNPH (dinitrophenylhydrazine) wet chemical method (references 3-5). In this procedure, a small portion of the exhaust is bubbled through 2,4-dinitrophenylhydrazine solution. This gas volume is measured with a wet test meter. The precipitate formed is recovered, dissolved and treated with various chemicals until a color producing ion is formed. The optical density of this mixture is measured by a Bausch and Lomb spectronic 20. Since the optical density is directly proportional to the amount of carbonyls in the sample and the principal carbonyl in the exhaust is formaldehyde, the DNPH wet chemical test is a good measurement of the aldehyde concentration in the exhaust.

The aldehyde sample was taken 20" downstream of the thermal reactor. Heater tape wrapped around the sampling line maintained the sample temperature between  $220-240^{\circ}F$  to prevent condensation of heavy aldehydes and water.



#### D. Temperature Measurement

To provide necessary information for analytical modeling and for material selection, it was important to know both the composition and temperature of the exhaust gas. Besides exhaust temperatures, close monitoring of engine and ambient temperatures was also necessary. All temperature measurements were made using thermocouples and various potentiometer read-out devices. The various types of thermocouples and their read-out devices are summarized in Table 3.

A Brown dual-range, continuous indicating potentiometer was used to read the copper-constantan (0-250<sup>o</sup>F) and chromel-alumel (0-1800<sup>o</sup>F) thermocouples. The temperatures at the exhaust port and at the two downstream "delayed quench" sample probes were measured using bayonet-type chromel-alumel thermocouples. These were positioned about 3/8 of the way across the pipe diameter and at 90<sup>o</sup> to the sample probes. These thermocouples were unshielded, and therefore the actual gas temperatures are higher than those measured because of the radiation losses from the thermocouple to the cooler exhaust pipe surfaces.

Because the temperatures within the thermal reactor exceeded the range of the chromel-alumel thermocouple, a platinum-platinum, 13% rhodium thermocouple was built. According to the manufacturer's specifications, temperatures between 1000-2900<sup>o</sup>F could be measured with  $\pm 1/2\%$  error. Since reactor core temperatures ranged from 1000-2000<sup>o</sup>F,

Table 3

Temperature Measurements

Temperature Measured	Type of * Thermocouple	Specified Error at Operating Temperature Range	Read out Device	Maximum Temperature Observed
Fan cooling air	T	$\pm 1^{\circ}\text{F}$	Brown, Range 1	120 $^{\circ}\text{F}$
Laminar flow meter	T	$\pm 1^{\circ}\text{F}$	" "	120 $^{\circ}\text{F}$
Carburetor inlet	T	$\pm 1^{\circ}\text{F}$	" "	120 $^{\circ}\text{F}$
Fuel in burette	T	$\pm 1^{\circ}\text{F}$	" "	130 $^{\circ}\text{F}$
Engine charge	K	$\pm 4^{\circ}\text{F}$	Brown, Range 2	300 $^{\circ}\text{F}$
Spark plug metal	K	$\pm 4^{\circ}\text{F}$	" "	510 $^{\circ}\text{F}$
Exhaust region metal	K	$\pm 4^{\circ}\text{F}$	" "	550 $^{\circ}\text{F}$
Exhaust port gas	K	$\pm 3/4\%$	" "	1800 $^{\circ}\text{F}$
Reactor skin	K	$\pm 3/4\%$	" "	1800 $^{\circ}\text{F}$
Downstream exhaust gas	K	$\pm 3/4\%$	" "	1800 $^{\circ}\text{F}$
Reactor Center line gas	R	$\pm 1/2\%$	Westronic M11D2	2000 $^{\circ}\text{F}$

\* T - copper-constantan  
 K - chromel-alumel  
 R - platinum-platinum, 13% rhodium

this thermocouple proved to be adequate. The output was recorded on a Westonics Model M11D2, 0-3000°F, strip recorder supplied and calibrated by Walker Research. The thermocouple wires were inserted through a 16 in. ceramic insulating core which was contained in a 1/4 in., 304 stainless steel sheath. The sheath was extended 1/4 in. beyond the thermocouple junction to act as a radiation shield.

To allow simultaneous measurement of the average concentration and temperature along the centerline of the reactor, the shielded, Pt-Rh immersion thermocouple was installed adjacent to the transversing, water-cooled sample probe. The sample inlet and thermocouple junction were positioned to sample the same longitudinal point of the reactor. A cylindrical guide was welded to the end of the reactor to support and seal the adjustable assembly as shown in Figs. 9a and b. A measuring rod was mounted adjacent to sampling assembly to determine the exact sampling position along the length of the reactor.

To estimate reactor metal temperatures, six unshielded chromel-alumel thermocouples were bonded to the exterior of the reactor at different distances from the reactor inlet. The position and attachment of the skin thermocouples is shown in Figure 9a. Ceramic insulators were used to prevent shorting of the uninsulated wires.

Figure 10 shows the reactor sampling assembly used in a typical test.

### E. Secondary Air Injection

Because of its insensitivity to downstream pressure, a critical flow meter was used to deliver secondary combustion air to the reactor. The use of critical flow prevented injection blow-out by the high pressure exhaust pulse. A schematic of the critical flow meter system is shown in Fig. 11. Shop air at 80 psig was supplied to the flow meter. Oil and water in the air was removed by a swirl-filter trap before the air pressure was regulated and passed through the orifices. The four critical orifices in parallel provided air flow rates between 11 to 305 lbm/hr. A large precision gage measured the upstream pressure, while a smaller gage was used to measure downstream pressure. The upstream/downstream pressure ratio was constantly checked to insure the flow remained critical. All orifices were calibrated using a large positive displacement tank.

Before each test, the water content of the shop air was determined from the wet and dry bulb readings of a sling psychrometer placed in the air stream. The dry air flow was determined from the psychometric chart. Although the secondary dry air flow rate was not used directly in the data expression, it served as a check for repeatability and provided data for air pump requirements.

### F. Engine A/F Measurement

To obtain meaningful reactor conversion data, it was important that the reactor input remained relatively constant. This required close control of the engine A/F mixture over a considerable period of time.

As previously mentioned, the SU carburetor and Bendix electric fuel pump greatly simplified the task.

### 1. Engine Air Measurement

Carburetor air flow was measured by a Meriam, model 50MC2-2F, 100 CFM laminar flow element in conjunction with a Meriam, Model 34FB2, micromanometer. The laminar flow element calibration was checked with the critical orifice air meter, which had been calibrated with a large displacement tank. The difference between the two instruments was less than 1%, well within experimental error. To minimize flow pulsations through the laminar element, the flow meter was mounted on the inlet of a large (1155 in<sup>3</sup>) surge tank. The surge tank was equipped with a "blow-out" membrane to prevent damage to the tank and flow meter in case of "back-fire". The entire system is shown schematically in Figure 12.

Using the calibration curve provided with the flow element, the differential pressure across the flow element was converted to a volumetric flow rate. This flow rate was corrected for temperature, viscosity, pressure, and humidity to obtain a dry air mass flow rate. Before and after each test, the humidity was determined from wet and dry bulb temperature readings taken with a sling psychrometer.

### 2. Engine Fuel Measurement

The fuel measurement system is shown in Figure 13. The fuel flow rate was determined using a burette and timer system. The timer was triggered by electric contacts when the fuel in the burette was displaced by

electrolyte. While several fuel volumes were available, the 148.4 ml volume was commonly used because it allowed at least three fuel measurements to be taken during a typical run. The air flow measurements were taken at the same time the fuel measurements were being made. In this way, any abnormalities in fuel or air consumption could be detected and noted when evaluating the data. If the fuel readings were relatively constant throughout the run, the average of the readings was taken as representative of the fuel consumption during the run.

Since the fuel volume was measured, it was necessary to know the fuel density at the time and location of measurement. Before each test, the API (American Petroleum Institute) number for the 50:1 fuel-oil mixture was determined at room temperature with an API Hygrometer. With this basic information, the specific gravity of the fuel could be determined at any time by knowing the fuel temperature and correcting the original API number accordingly. The fuel temperature was measured at the burette inlet.

#### IV. Test Procedure

All data was taken at steady speed and fixed throttle, with engine temperatures stabilized. During a test, the engine air-fuel ratio was adjusted when necessary to maintain a constant CO and CO<sub>2</sub> input to the reactor. The engine torque decreased slightly with increasing air injection fraction (back pressure effect) and no attempt was made to hold it constant. The percent engine load was determined from the ratio of the observed torque during the test, to the w.o.t. torque at the same speed.

Before sampling within the reactor, the emissions were measured at the exhaust port and then the sampling circuit was switched to sample the desired reactor position. After the reactor measurements were made, the system was switched back to sample the exhaust port to ensure constant reactor input during the run. This alternating sampling technique was used for each reactor position and air injection fraction tested.

While this alternating sampling technique allowed accurate calculation of the air injection fraction, it resulted in high HC readings due to "hang up" in the sample lines. As a result of alternating between HC concentrations of 600-1000 ppm at the exhaust port, and 10-50 ppm in the reactor, an extremely long time was required for the lower HC readings to stabilize. Finally, each reactor HC reading was given a fixed amount of time before the measurement was recorded. To check the magnitude of the "hang-up" error, a test was made at 4000 rpm, 29 ft. -lbs. in which the reactor exit was sampled continuously. This was compared to the alternating sampling method at the same conditions and the results are shown in Figure 20.

In subsequent tests, a separate parallel "low HC" sampling line and selector valve was installed just ahead of the analyzers. This eliminated the HC "hang-up" problem indicated above.

## V. Discussion

### A. Air Injection Fraction as a Mixing Indicator

One of the most difficult parameters to estimate is the extent of mixing of exhaust gas and injected air throughout a thermal reactor.

Yet, this parameter is extremely important in determining the shape-volume design for the reactor and in tailoring an analytical model.

While analyzing the data, it was noted that the calculated air injection fraction varied along the length of the reactor. The air injection fraction by volume or mole percent,  $F$ , is defined as the ratio of moles injected air to moles of dry exhaust determined from a carbon balance (see Appendix A). Actually, the air injection fraction is constant along the length of the reactor. Any observed variation indicates that the exhaust products and secondary air were not well mixed at every sampling position. Thus, when the air injection fraction determined at any point in the reactor is greater than that measured at a relatively well mixed position, such as the reactor outlet, the sample probe is seeing a non-homogeneous mixture of exhaust gas and air.

We believe that the observed result arises when packets of injected air not mixed with exhaust are sampled. When mixing is poor, the exhaust is rapidly passed through the reactor during blowdown without contacting much injected air. The bulk of this rejected air thus resides in the reactor for a relatively long period. As a result, a continuously



drawing sample probe sees more than the average amount of air. As mixing proceeds throughout the reactor, the observed air injection fraction gradually decreases to a constant level at sampling stations further downstream. Figures 14a and b show typical observations. Thus, when the undiluted exhaust at the port and the diluted exhaust in the reactor are measured in a test, the calculated air injection fraction provides an indication of the reactor mixing profile. We recommend further development of this experimental mixing assessment to provide good mixing coefficient estimates for the computer model.

#### B. Reactor Description

In this phase of the work two reactors, Models A and B, were designed and built for the OMC engine. Both reactors are shown in Figures 15 and 16. The outstanding feature of these reactors is the injection of air directly into the reactor, as opposed to the conventional injection into the exhaust port. This method of air injection with induced tangential swirl provides good mixing, while minimizing back pressure.

The model A reactor, in which the air is injected in the direction of the exhaust flow, but at  $180^{\circ}$  around the perimeter of the reactor, has proven to be an excellent design. The B reactor was built with the air injected at the exhaust inlet, but this design was found to be less efficient. A higher injection pressure is required to deliver the same air mass flow rate for the B reactor than for reactor A, as shown in Figure 17. The air inlet tubes and openings were the same diameter for both reactors, but the B reactor had a  $90^{\circ}$  bend in the inlet tube. The B reactor also created a slightly higher back pressure. While the HC and CO conversion

efficiencies of both reactors typically exceed 95%, major test efforts have focused on the model A reactor.

### C. Reactor Evaluation

#### 1. Carbon Monoxide and Hydrocarbon Oxidation

Figures 18 - 21 show the emission and temperature result for the model A and B reactors tested over a wide engine operating range. The first point, without air injection, is representative of the CO input to the reactor for all the air injection fractions. Without air injection, no significant CO oxidation occurred. Subsequent test points were run at various increasing air injection fractions to some arbitrary maximum air flow rate. At each test point, sufficient time was allowed for temperature and concentration stabilization.

Because of the high reactor temperatures normally observed, hysteresis was small in all tests and therefore not shown. Hysteresis is a well established reactor characteristic of obtaining better conversion at a given air injection fraction when changing from a hotter to a new cooler operating point, as opposed to attaining the same new point from an initially cooler condition. All data shown was taken for increasing air injection fractions.

As found in previous work ( 2 ), CO is more difficult to oxidize than HC and therefore is a good indicator of reactor efficiency. If the CO conversion is high, it is reasonable to assume the HC conversion is at least comparable.

With the exception of the 2100 rpm condition for the model B reactor, greater than 95% CO reduction was attained with both reactors at optimum air injection fractions between .2 and .55. Even the addition of small amounts of air resulted in significant CO reduction. For example, an injection fraction of .1 resulted in between 79-83% CO conversion for the A reactor and between 74-80% CO conversion for the B reactor showing that large air pumps may not be necessary. The CO emissions began to increase for air injection fractions greater than .55. Considering the slight variations in air-fuel ratio and throttle opening between tests, the temperatures for the two reactors are approximately equal at comparable conditions.

As predicted, good HC reduction was attained at a lower air injection fraction than for CO. Maximum HC oxidation occurred at air injection fractions between .10 and .55. HC oxidation remained relatively good beyond .55, and emissions did not increase as rapidly as for CO.

It is interesting to compare the actual reactor temperature increase due to the HC and CO oxidation with the theoretical value if heat losses are ignored. The theoretical adiabatic flame temperature increase from the oxidation of 5.5% CO and 2.7% H<sub>2</sub> and 30 mole percent secondary air at 70<sup>o</sup>F would be approximately 600<sup>o</sup>F. Our experimental data shows typically less than a 400<sup>o</sup>F increase. It is evident that considerable external cooling of the reactor occurs and cooling will be an extremely important future consideration for rich engine reactors for Wankel engines.

The HC emissions indicated by the open symbols in Figures 20 and 21 are thought to be higher than the true value because of the HC "hang-up" resulting from alternately measuring the high exhaust and low reactor concentrations. This problem has been discussed previously. To estimate the magnitude of the hang up problem, continuous sampling of HC was made in separate runs with no switching to check inlet composition. These data are plotted also in Figure 20 and they represent more accurately the actual HC level exiting the reactor. Note that all the HC curves of Figures 20 and 21 exhibit the same trend, but the actual magnitude of the HC reduction is diminished by sample line hang up. HC conversion was at least greater than 90% and probably between 98% and 99% as the continuous sampling data suggest.

CO conversion as a function of air injection fraction for reactors A and B is compared in Figure 22. Reactor A appears slightly more efficient at lower and higher air injection fractions. For F's between .2 and .4, both reactors yielded 97-99% CO conversion. This extremely high conversion efficiency can be achieved over a relatively large air injection range, which is an important consideration for possible vehicle use where the air cannot be precisely controlled. There appears to be no significant difference in conversion efficiency between the A and B reactors at the 3000 rpm condition. This particular operating point was chosen because the input variables for the two reactors were approximately the same and the temperature was sufficiently high (above 1600<sup>o</sup>F) that the reactions were not temperature limited. Thus, results emphasize mixing differences between the reactors.

Tests run at conditions where temperature was a limiting factor showed the A reactor more efficient. This is probably due to the manner in which the air is injected in the two reactors. In the B reactor, the entire air flow blows across the exhaust products at the reactor entry, cooling the reactants and suppressing light off. In the A reactor the air is injected into the other half of the reactor. Because of intensive back mixing some of the exhaust products react partially with preheated air and liberate heat prior to mixing with cool freshly injected air.

The B reactor's higher downstream air injection pressure for the same injection rate (Fig. 17) indicates that there was a pressure build-up in the air injection line due to flow from the high pressure exhaust pulse. Reactor A also created slightly less engine back pressure than reactor B.

## 2. Nitric Oxide

All present data indicate that the thermal reactor had no significant effect on nitric oxide (NO) emissions. Typical NO results are shown in Figure 23. This operating point was chosen because the sample temperature exceeded 1900<sup>o</sup>F and any major effect would be more apt to appear at the higher temperature.

At first glance, Figure 23 indicates that NO is produced in the reactor. This is unlikely since the equilibrium NO concentration in the reactor temperature range (1800-1900<sup>o</sup>F) is considerably less than the 230-330 ppm concentration observed in the reactor. If any NO reaction occurred, a slight NO reduction would be expected. The apparent NO increase in the cylindrical section of the reactor is attributed to mixing effects. Because the air was injected near the 3/4" sampling position, the probe

sampled a non-homogeneous mixture of exhaust products and air, but mostly air. The average NO increase between the 5 in. and 9-1/4 in. position was considerably less because the sample was better mixed and more representative of the actual composition as indicated by air injection fraction at each position.

The differences between the 5 in. and 9-1/4 in. position are due to slight mixing effects and small variations in engine A/F ratio. At this rich A/F mixture, the smallest variation in A/F ratio causes a measurable change in NO. As expected, the difference in NO between the 3/4 in. and 5 in. sampling positions increased with larger air injection fractions. The greater the air flow near the sample probe, the more air and less exhaust the probe will see.

The results shown in Figure 23 are typical of the data taken from both A and B reactors in that the engine richened slightly when air was injected and this in itself reduces NO. The NO was corrected using the air injection fraction calculated at the 9-1/4 in. sampling position. This value is most representative of the actual exhaust composition.

In conclusion, no significant change in NO emissions arose in our tests as a result of the thermal reactor. Compared to the engine exhaust (reactor input) NO concentration, the concentration at the reactor exit was slightly and consistently lower. In addition to engine richening, such a reduction could arise from increased back pressure and more exhaust residual in the cylinder, or an actual NO reduction in the reactor through oxidation to NO<sub>2</sub>. NO<sub>2</sub> was not detected by our instrument.

### 3. Aldehyde Emissions

Optimum aldehyde reduction coincided with total hydrocarbon reduction. Results for the B reactor at two different engine conditions are shown in Figure 24. At 2100 rpm, the aldehyde and hydrocarbon emissions were extremely high, 142 ppmc and 1370 ppmc<sub>6</sub> respectively. As secondary air was added, the HC and aldehyde concentrations were reduced sharply. Aldehydes were reduced by more than 95% with .2 air injection fraction and to under 4 ppmc with additional air. At 3500 rpm, A/F = 11.4, the exhaust aldehyde emissions were much lower (richer mixture) and reduced by 90% with an air injection fraction of .1 to about 2 ppmc. Data taken at air injection fractions up to .60 showed no significant increase in aldehydes. Tests with the model A reactor showed similar results.

#### D. Reactor Skin Temperatures

The high reactor operating temperatures made it obvious that material limitations would be a major factor in any future application. To obtain an estimate of the reactor metal temperatures for a wide range of engine conditions, six chromel-alumel thermocouples were bonded to the outer surface of the A reactor. Two thermocouples, each 180° apart, were mounted 2-1/2 in., 4-3/4 in., and 7-1/8 in. from the inlet end of the reactor. The unshielded thermocouple junctions were welded to the reactor surface by Walker Research. Thermocouple locations and temperature results for three engine conditions are shown in Figures 25-27.

Thermocouples 1 and 3 failed early in the testing, therefore no results are shown for these positions. However, since the calculated air injection fraction along the centerline of the reactor at positions 3 and 4

indicates good mixing, it is reasonable to assume that temperatures 3 and 4 would be approximately equal. Unfortunately, the same assumption cannot be made for temperatures 1 and 2 because the metal at position 1 is always a duller color than at 2, which indicates a lower metal temperature. In fact, the area around 1 is always the duller color of the entire reactor surface, and therefore should not be of primary concern. The temperature difference between 1 and 2 is primarily due to the direct impingement of the hot exhaust gas and the initial  $H_2$ , HC and CO oxidation near 2, and the swirling non-homogeneous mixture, of mostly air, cooling the area around 1.

The data from the three engine conditions show that the skin temperatures follow the same trend as the reactor exit sample temperatures, but are lower in magnitude. It should be kept in mind that the external skin temperatures are the net result of the heat transfer from the reactor, the flow and heat release pattern inside the reactor, and the cooling and flow effects of the injected air. The maximum skin and reactor exit temperatures occurred at a reactor A/F ratio of approximately 13.5. With a greater air injection quantity, the cooling effect of the injected air and heat loss from the reactor surpassed the heat released from the oxidation of  $H_2$ , HC, and CO, and a drop in reactor temperature resulted.

Temperature 2 is considerably higher than the other skin temperatures, being between  $180^{\circ}$ - $220^{\circ}$ F lower than the reactor exit sample temperature at 2500 and 3500 rpm and between  $270^{\circ}$ - $300^{\circ}$ F lower at 4000 rpm.



For reactor A/F ratios between 11.5 - 18.0 temperatures 4, 5, and 6 are approximately the same.

The practical conclusions to be drawn from this data are: 1) external reactor skin temperatures can exceed 1700°F, without some method of external cooling, 2) the highest metal temperatures will occur in the area around thermocouple 2, and 3) the highest metal temperatures occur at a reactor A/F ratio of approximately 13.5.

VI. References for Phase I.

1. Papa, Louis J., Gas Chromatography - "Measuring Exhaust Hydrocarbons Down to Parts Per Billion", E. I. DuPont De Nemours & Co., SAE 670494, 1967.
2. Lord, H. A., E. A. Sondreal, R. H. Kadlec, and D. J. Patterson, "Reactor Studies for Exhaust Oxidation Rates", University of Michigan, SAE 730203, 1973.
3. Oberdorfer, P. E., "Determination of Aldehydes in Automobile Exhaust Gas", SAE paper 670123, January 1967.
4. U.S. Bureau of Mines, "Procedures for Determining Exhaust Carbonyls as 2, 4-Dinitrophenylhydrazones", APRAC Project CAPE-11-68, Final Report, 1968.
5. Papa, L. J., "Colorimetric Determination of Carbonyl Compounds in Automotive Exhaust as 2, 4-Dinitrophenylhydrazones", Env. Sci. Tech. 3, No. 4, April 1969, p. 397.
6. Teague, D. M., E. J. Lesniak Jr., and E. H. Loeser, "A Recommended Flame Ionization Detector Procedure for Automotive Exhaust Hydrocarbons", Chrysler Corp., SAE 700468, 1970.
7. Patterson, D. J., et al., "Kinetics of Oxidation and Quenching of Combustibles in Exhaust Systems of Gasoline Engines", Three Annual Progress Reports to CRC, 1969-1972.

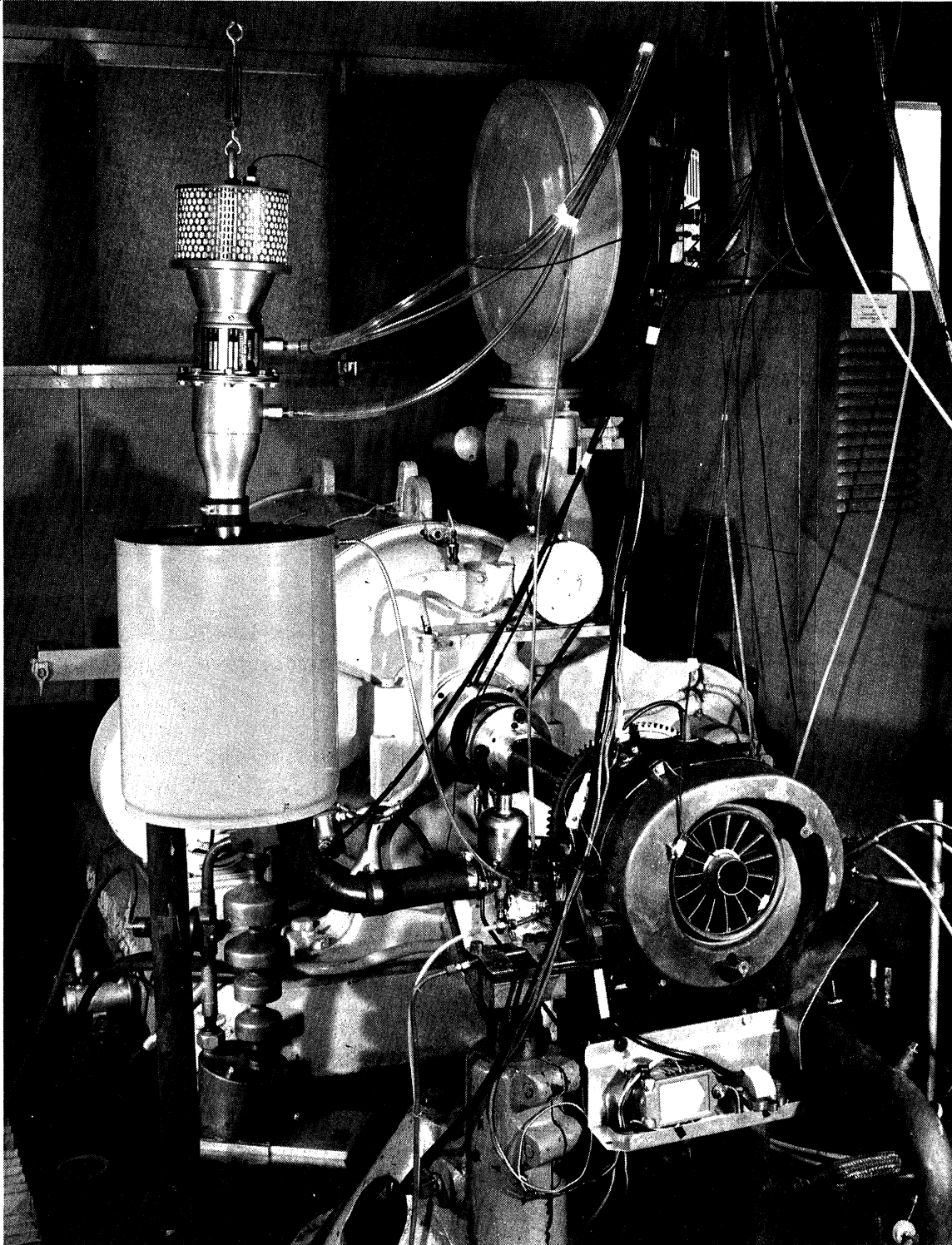


Figure 1 - Engine dynamometer installation

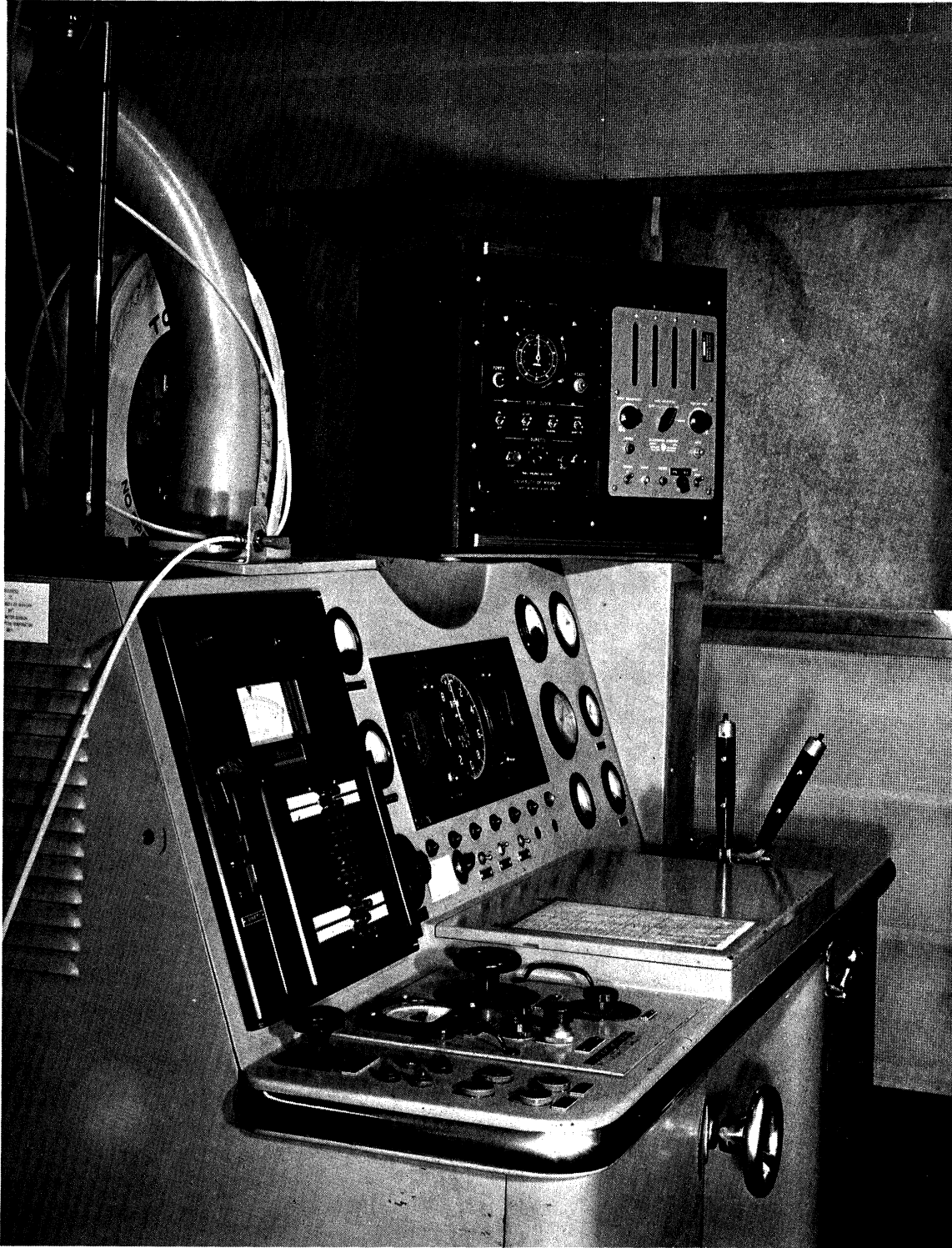


Figure 2 - Dynamometer control console and fuel timer

- A thermal reactor
- B reactor sample probe
- C first downstream sample probe
- D second downstream sample probe
- E two way valve
- F 1/4" teflon tubing
- G to analyzer cart
- I cooling water in
- O cooling water out
- P exhaust port sample probe
- Q three way valve

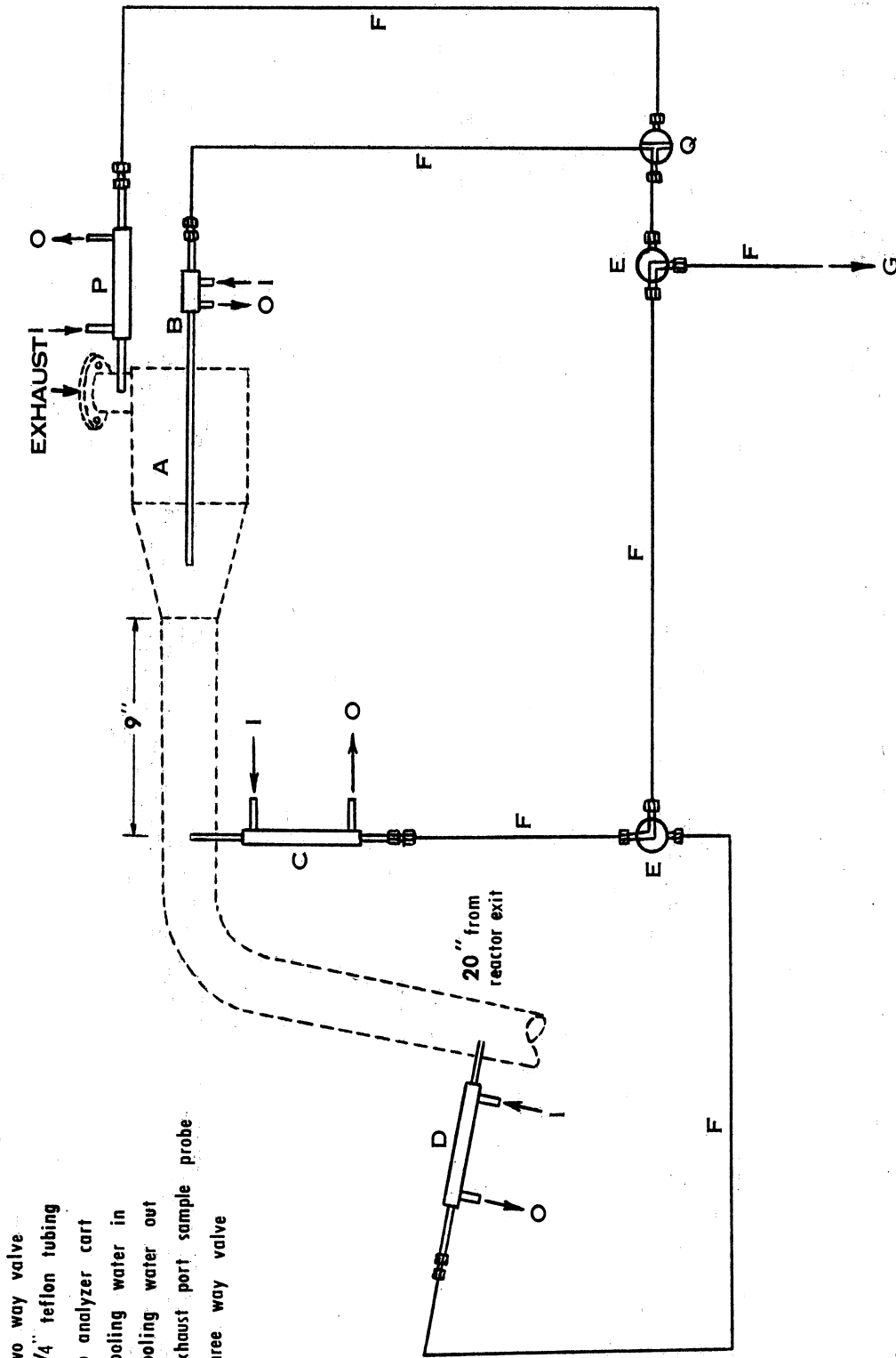


FIG 3 - SAMPLE PROBE PLUMBING for MODEL A & B REACTORS

- A sample inlet
- B cooling water in
- C cooling water out

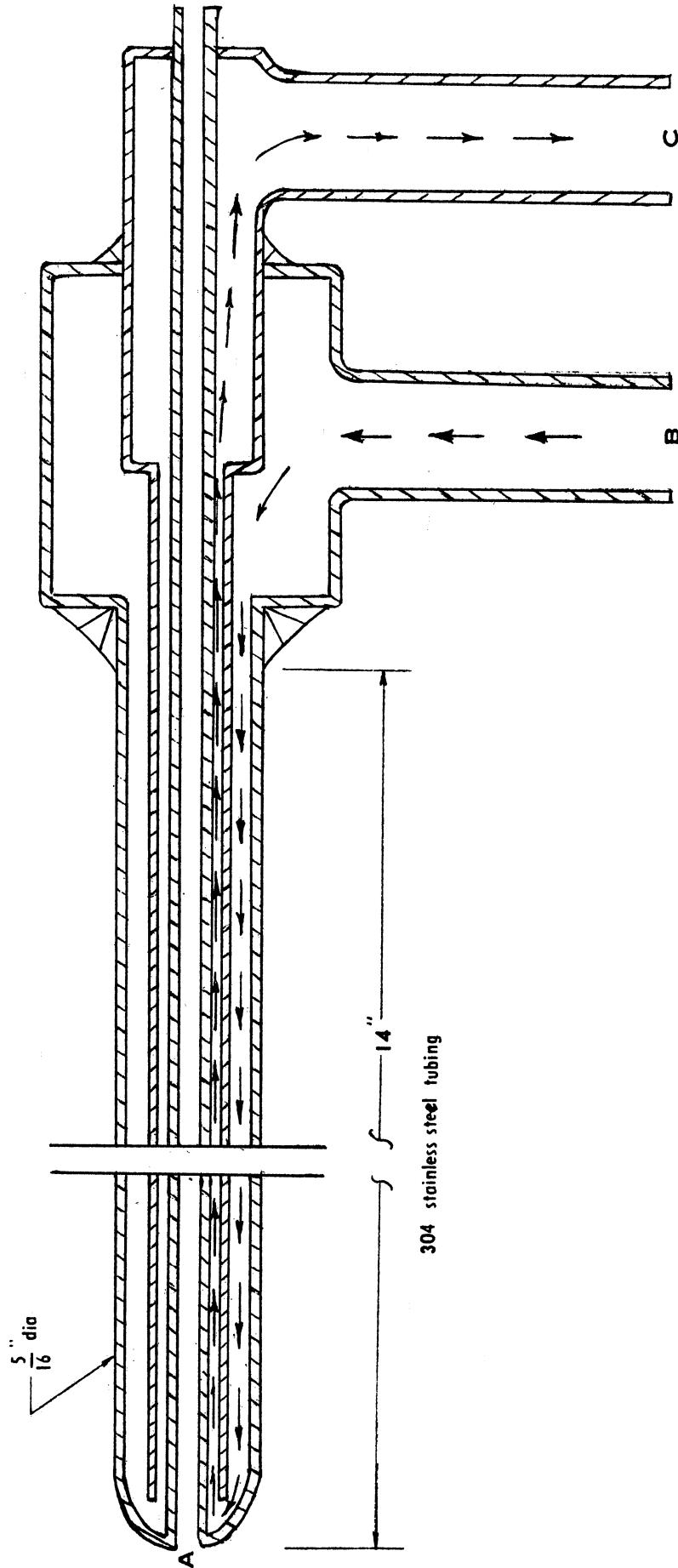


FIG 4 - WATER-COOLED REACTOR SAMPLE PROBE

- A sample inlet
- B cooling water in
- C cooling water out

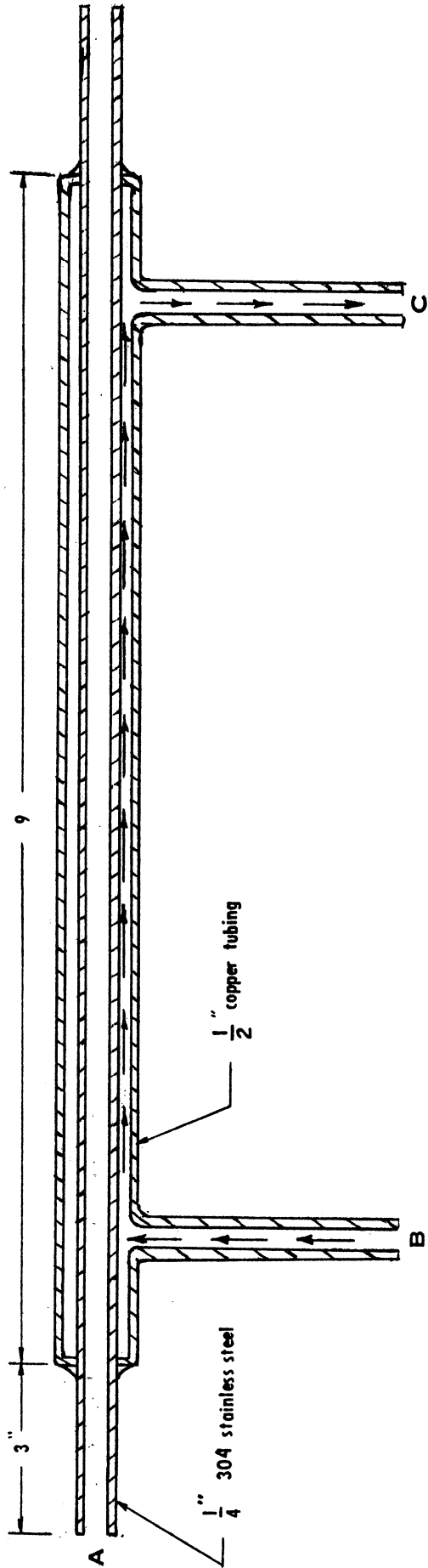


FIG 5 - WATER-COOLED  
DOWNSTREAM SAMPLE PROBE

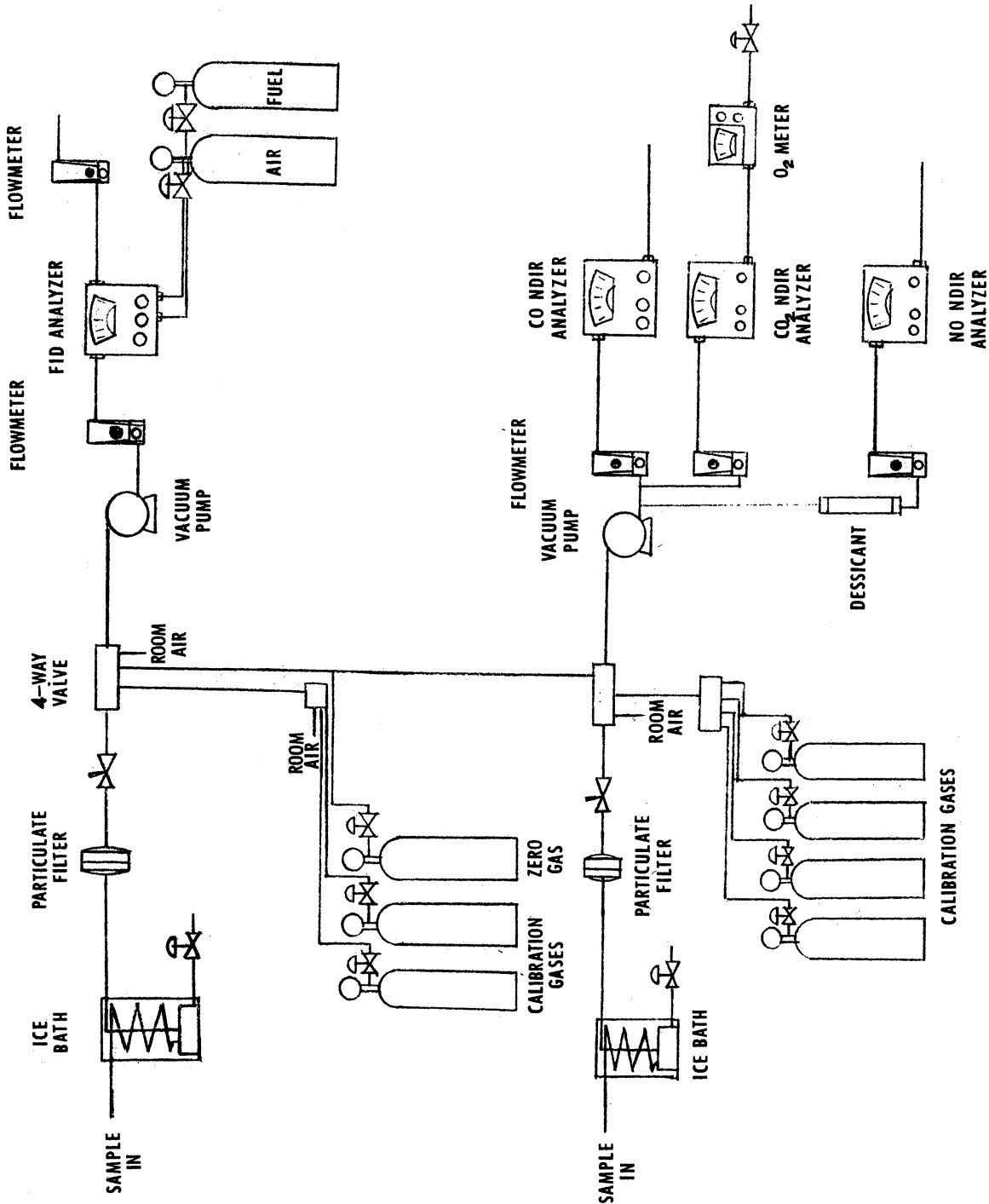


FIG 6 - SCHEMATIC OF ANALYTICAL SYSTEM



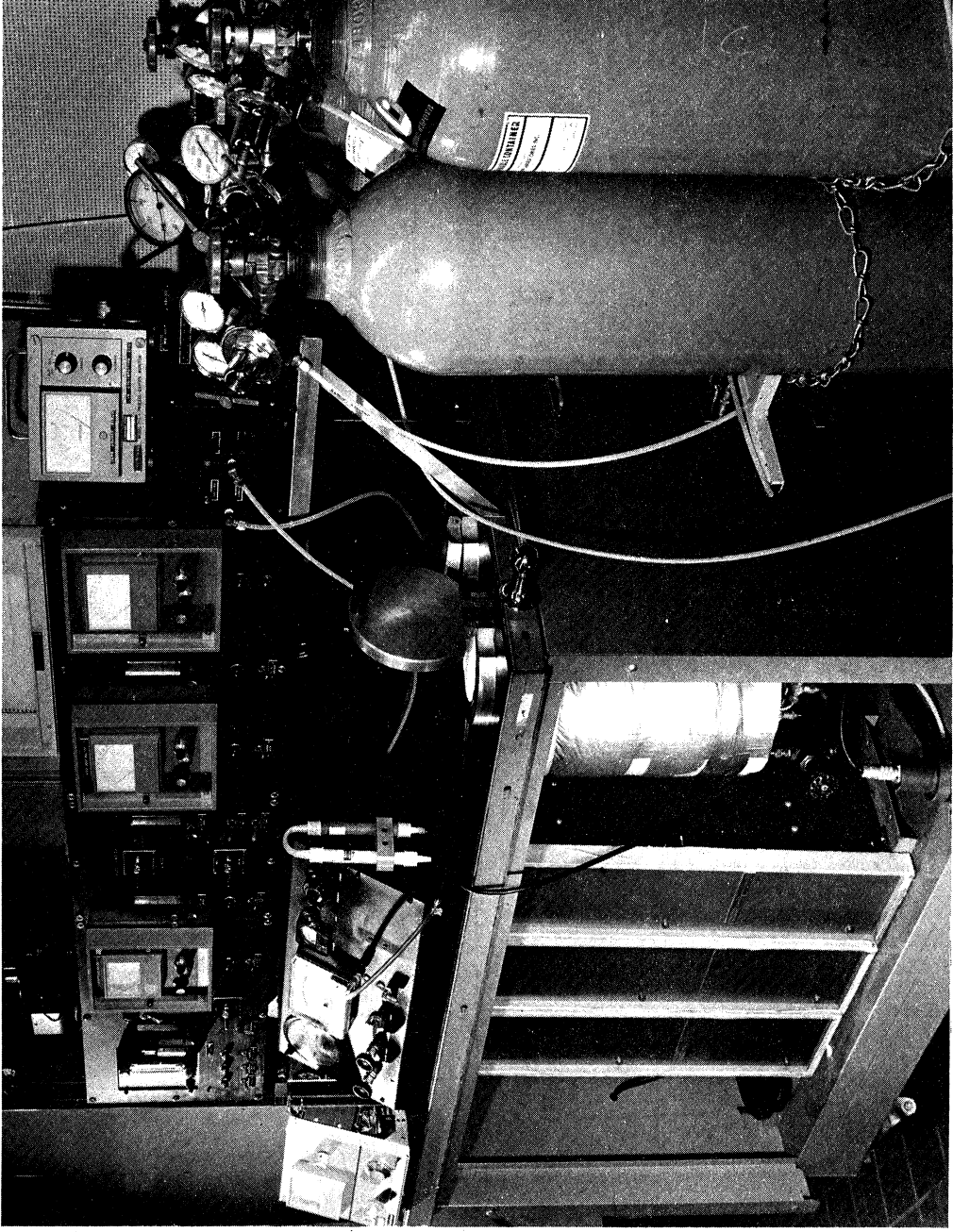


Figure 7 - Exhaust gas analyzer cart

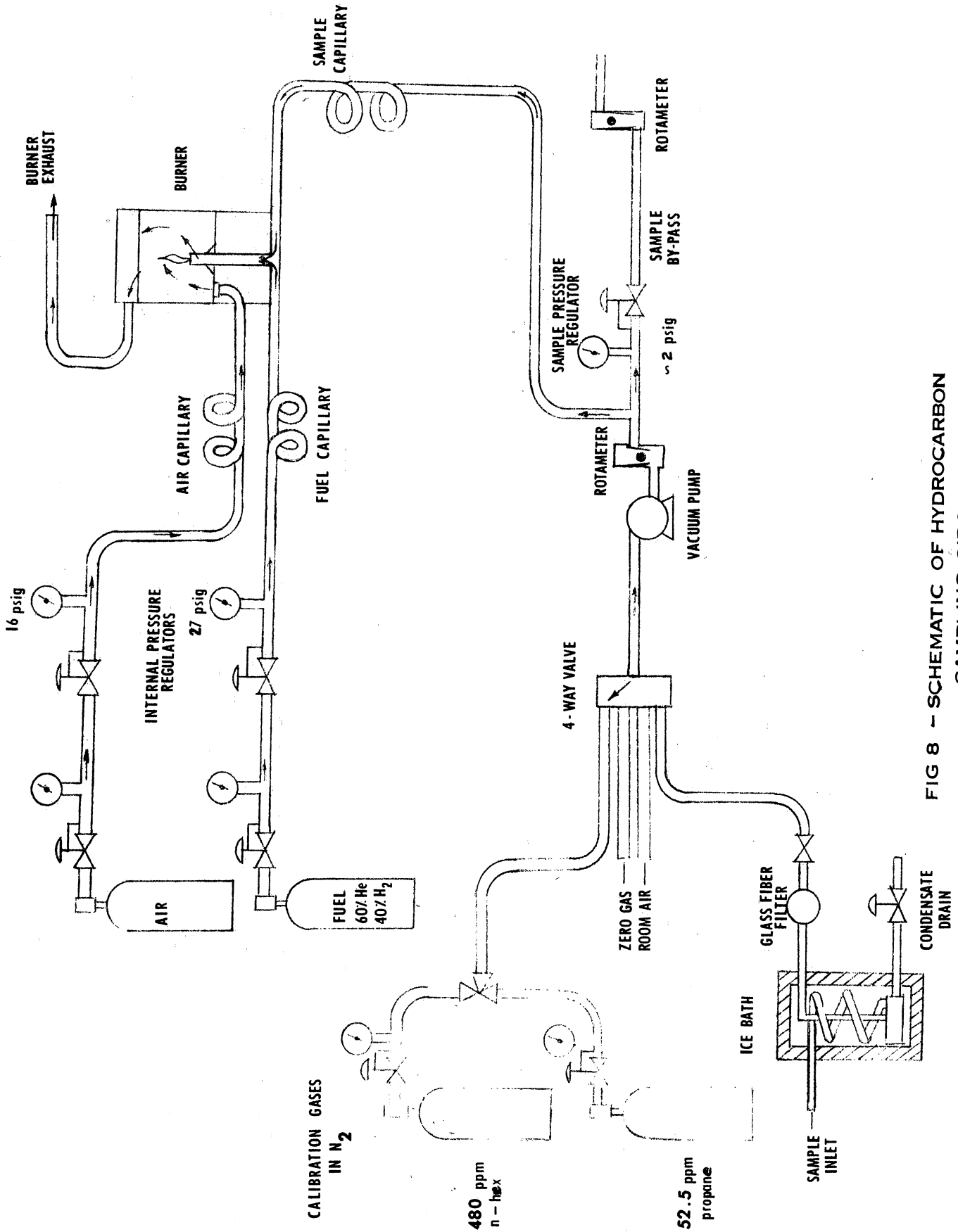


FIG 8 - SCHEMATIC OF HYDROCARBON SAMPLING CIRCUIT

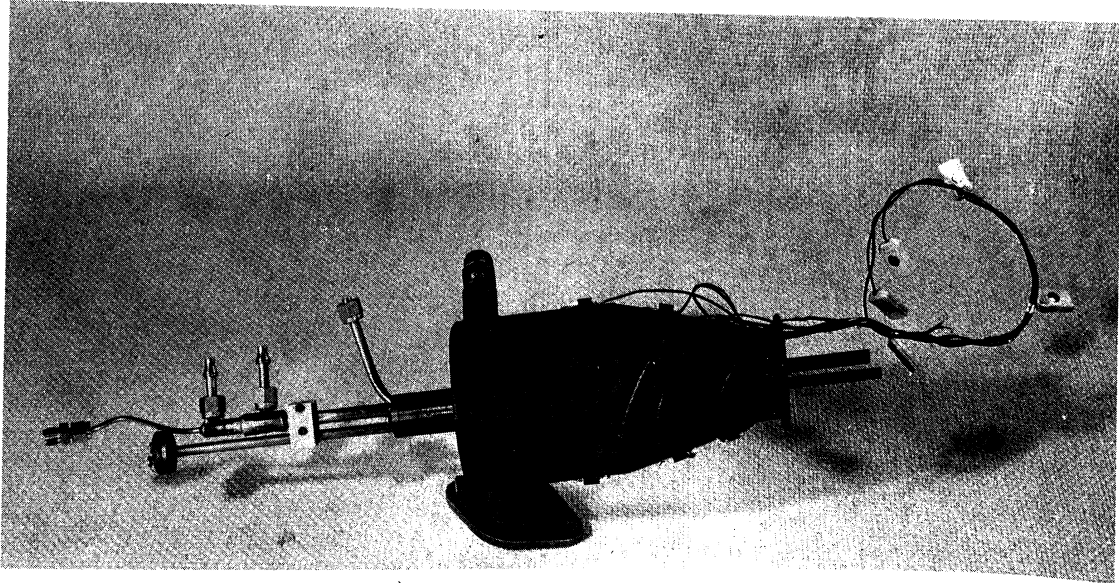


Figure 9a - Adjustable reactor sampling assembly installed in the A reactor. (A reactor is equipped with skin temperature thermocouples)

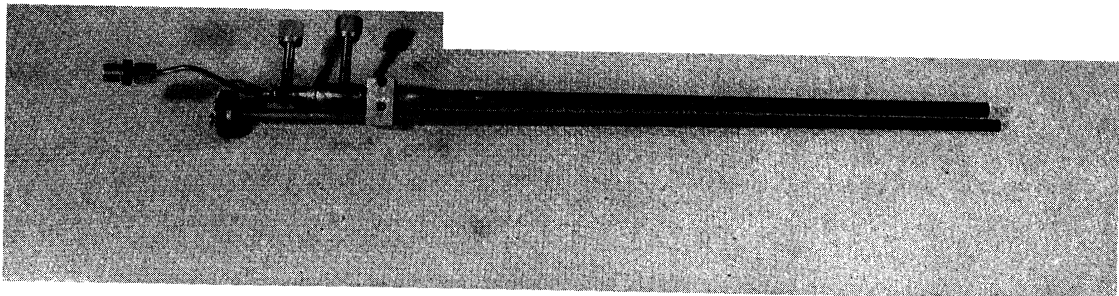


Figure 9b - Shielded immersion thermocouple and transversing water-cooled sample probe assembly to simultaneously measure the average concentration and temperature along the centerline of the reactor.

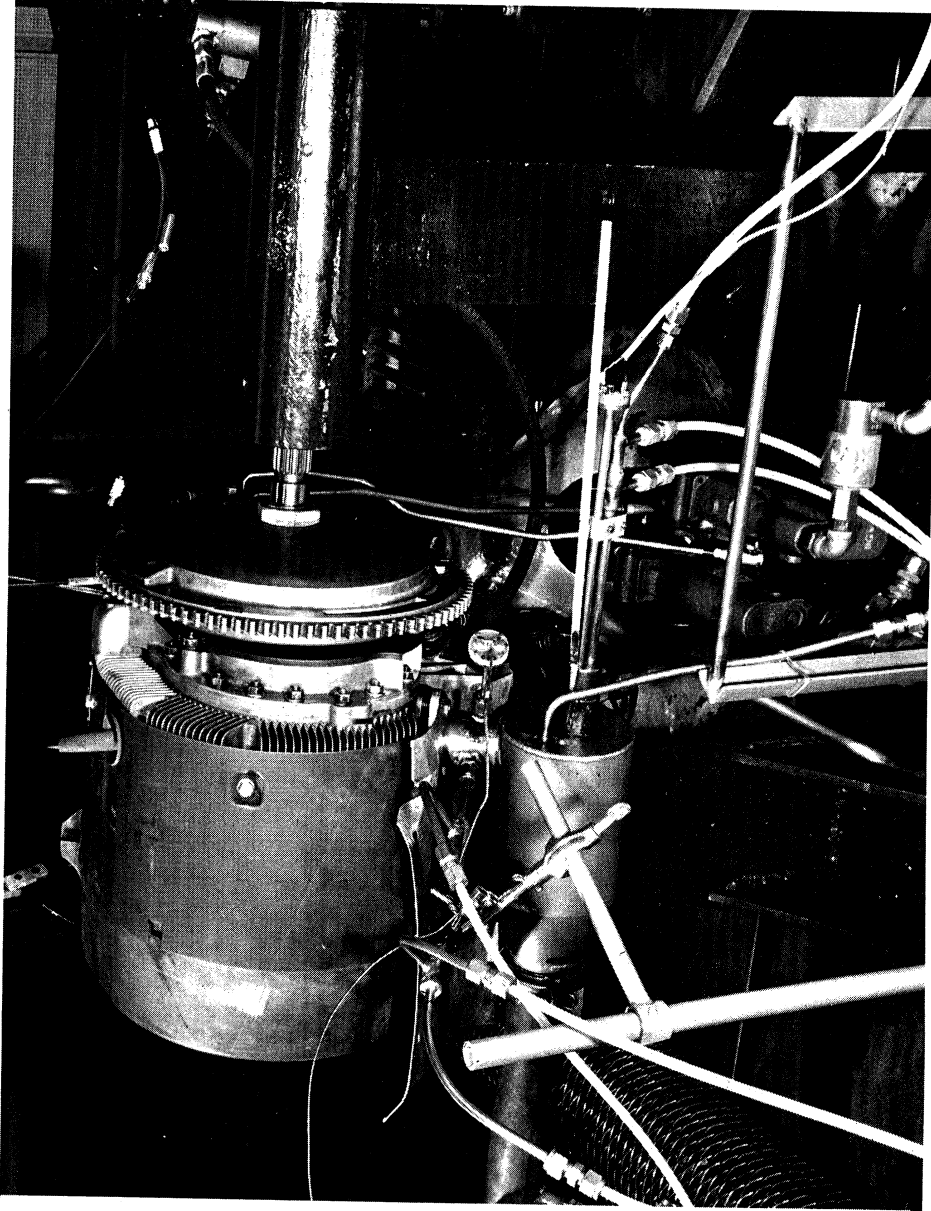


Figure 10 - Thermal reactor sampling assembly showing "delayed quench" sampling probe and thermocouple at reactor inlet, the adjustable reactor centerline sampling assembly, and measuring rod.

- A shop air in, 80 psig
- B swirl-filter trap
- C pressure regulator
- D up stream pressure gage, psia
- E valve
- F orifice plate
- G surge tank
- H downstream pressure gage, psig
- I to reactor

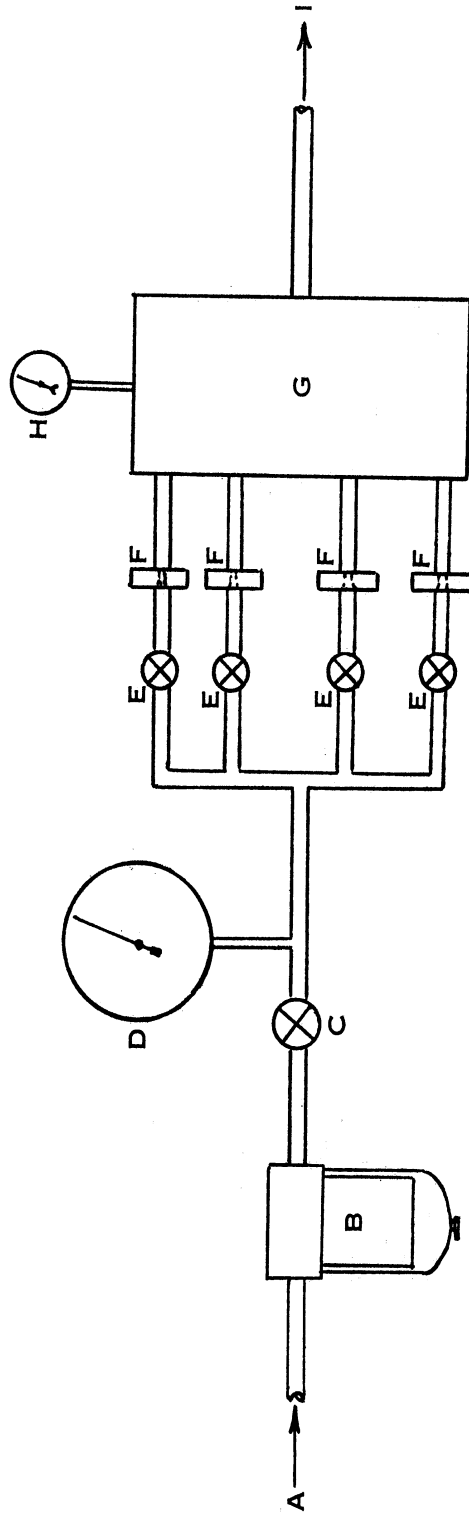


FIG 11 -FLOW SCHEMATIC for CRITICAL FLOW ORIFICE SYSTEM used for SECONDARY AIR INJECTION

- A Meriam laminar flow meter
- B 1155 cu. in. (5 gallon) surge tank
- C air filter
- D air temp. thermocouple
- E thermocouple leads to Brown potentiometer
- F air to engine carburetor
- G absolute mercury pressure gage
- H Meriam micromanometer, in-H<sub>2</sub>O

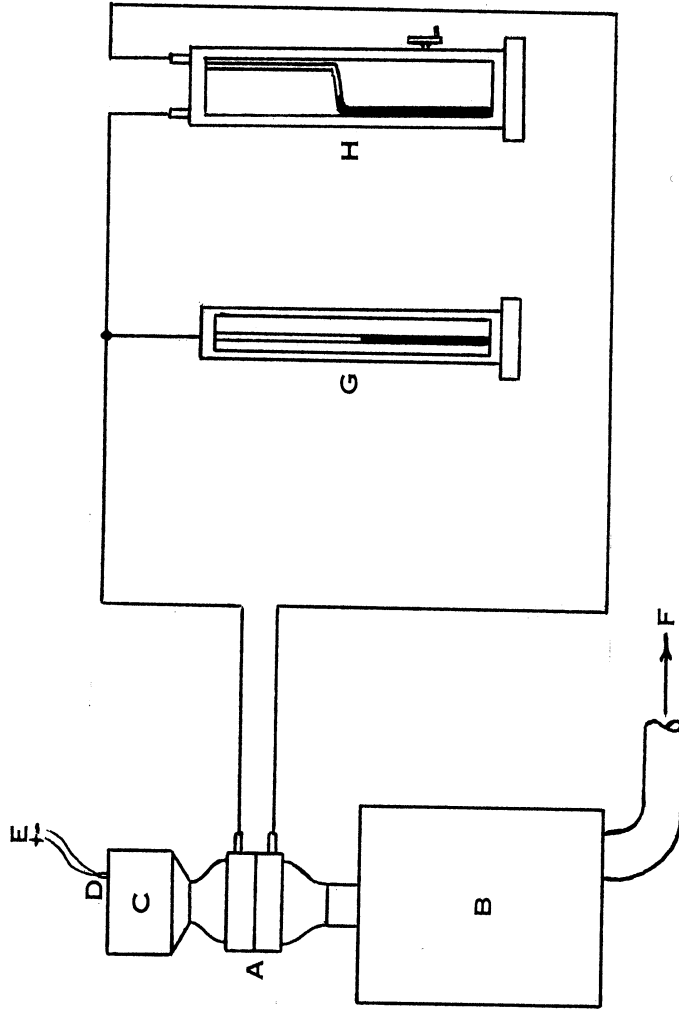


FIG 12-AIR RATE MEASURING SYSTEM

- A 6 gallon fuel tank
- B Bendix 12 v fuel pump
- C fuel burette
- D 148.4 ml volume
- E electronic timer (.001 sec increments)
- F thermatouple for fuel temp.
- G fuel to engine carburetor
- H thermocouple leads to Brown potentiometer

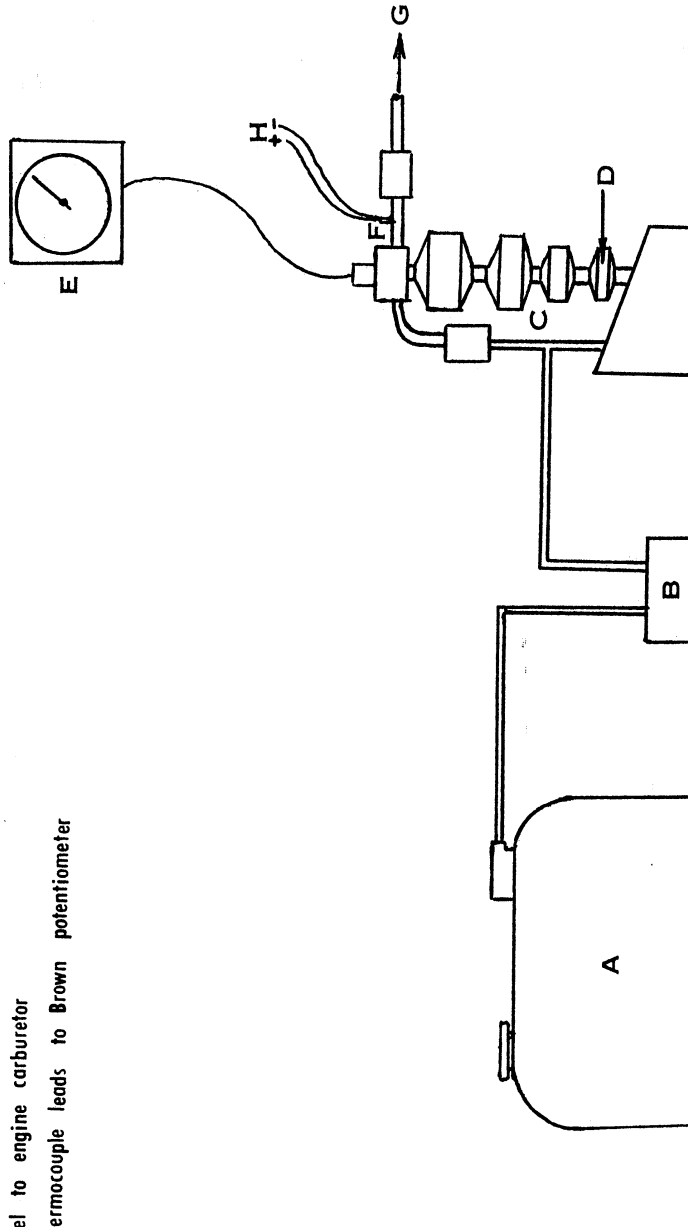


FIG 13—FUEL RATE MEASURING SYSTEM

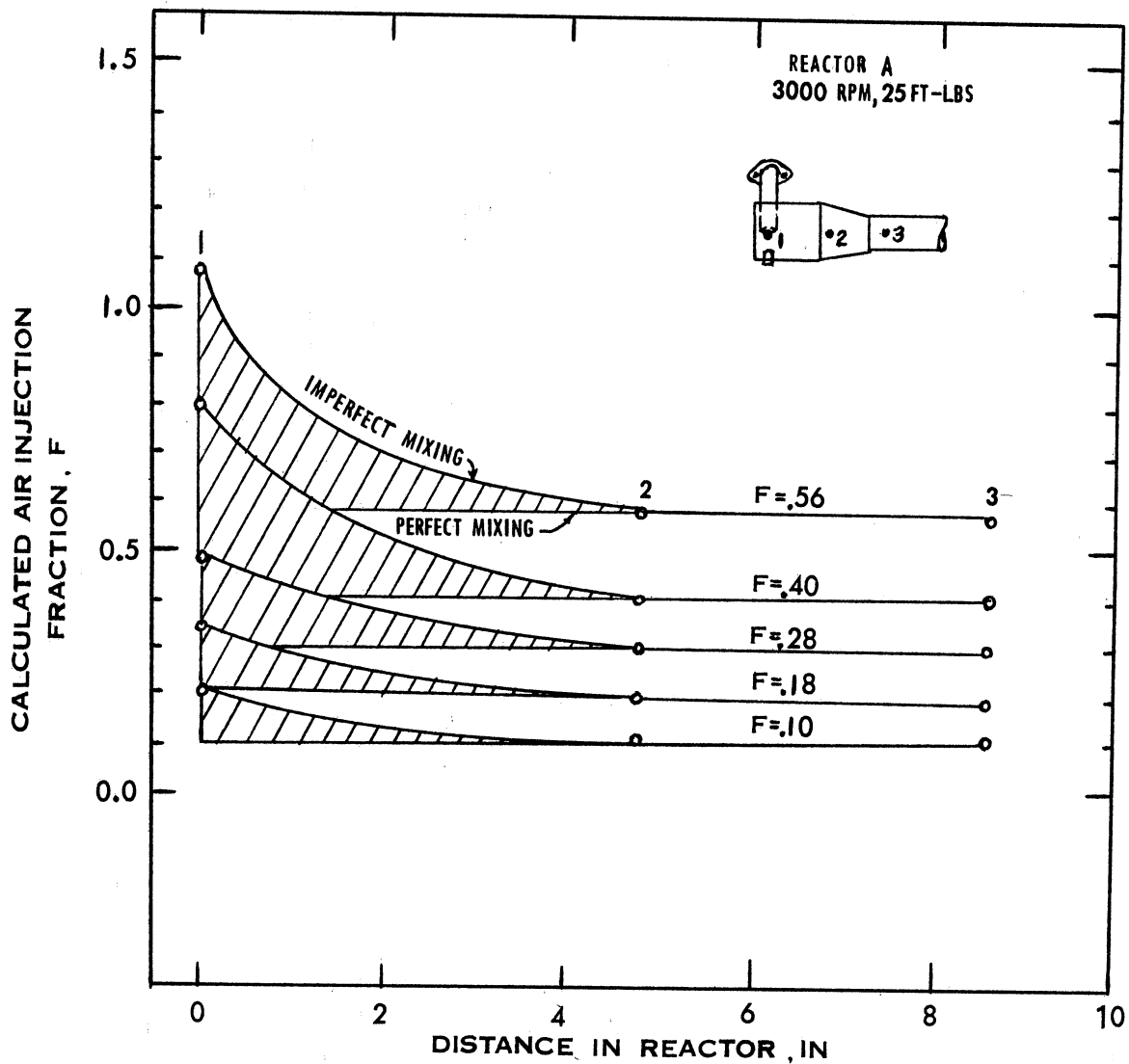


Figure 14a - Experimentally determined air injection fraction versus distance in the reactor. The shaded area suggests a region of imperfect mixing of injected air and exhaust.



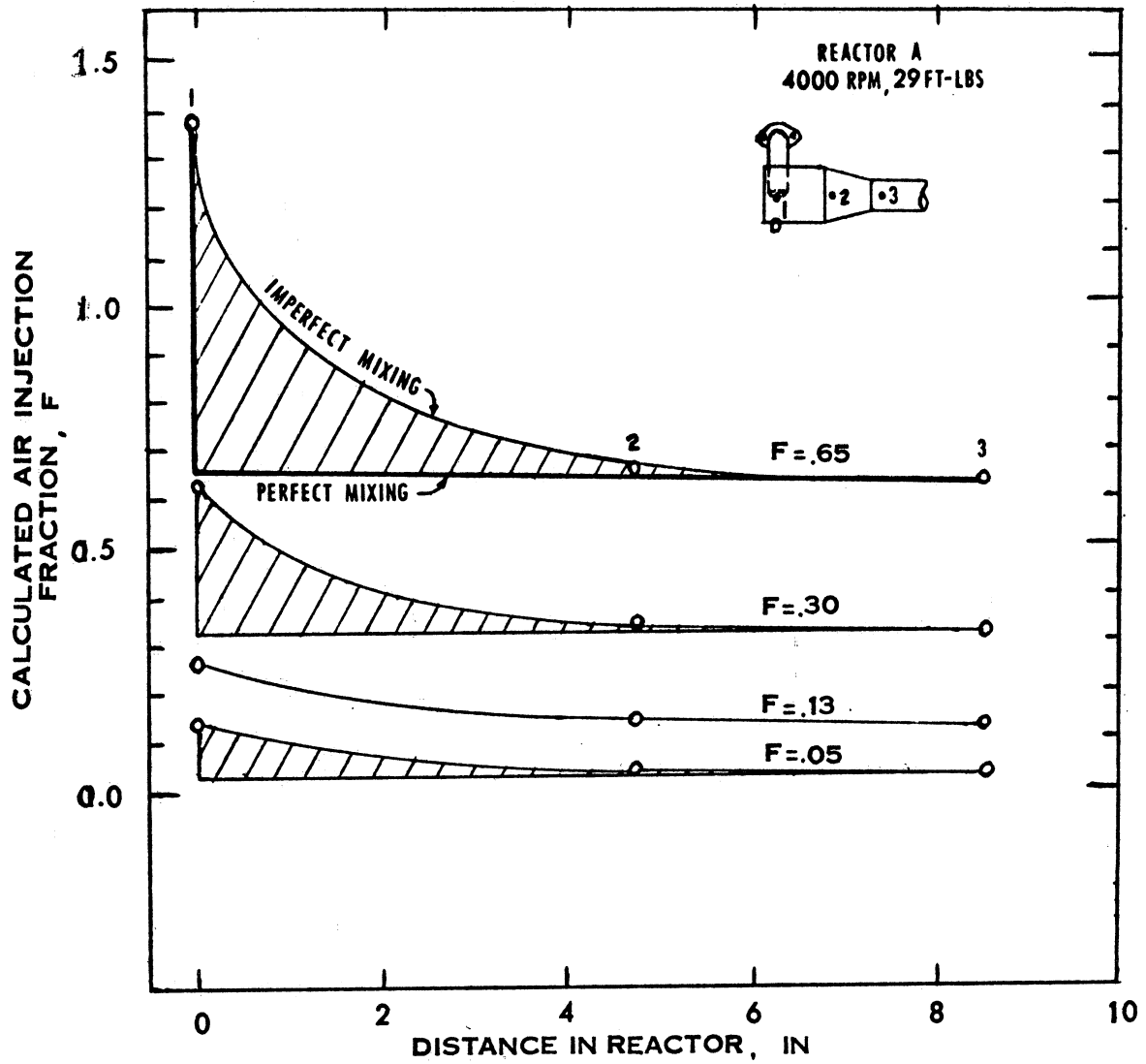
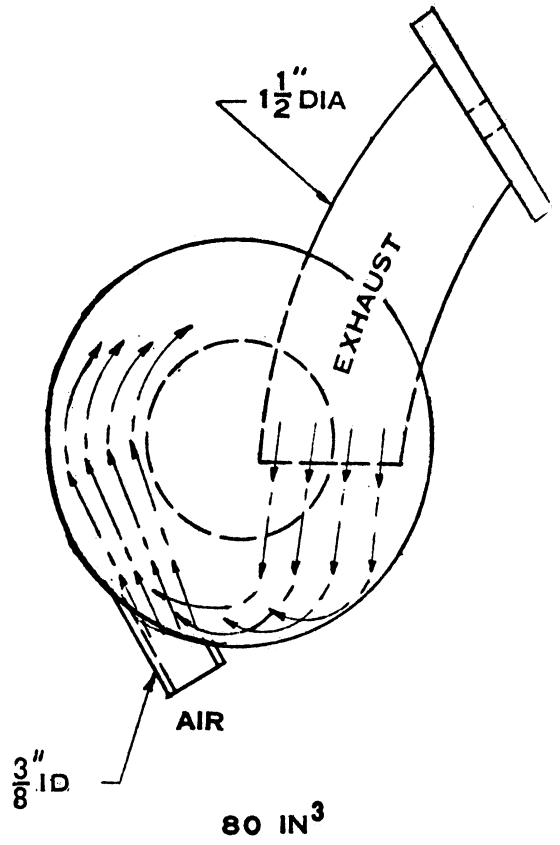
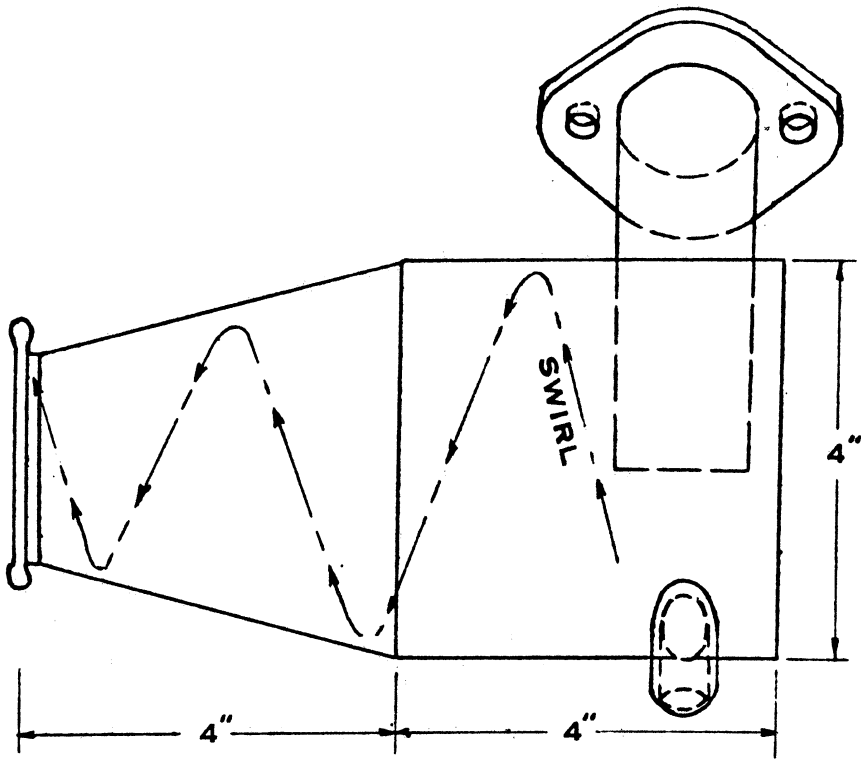
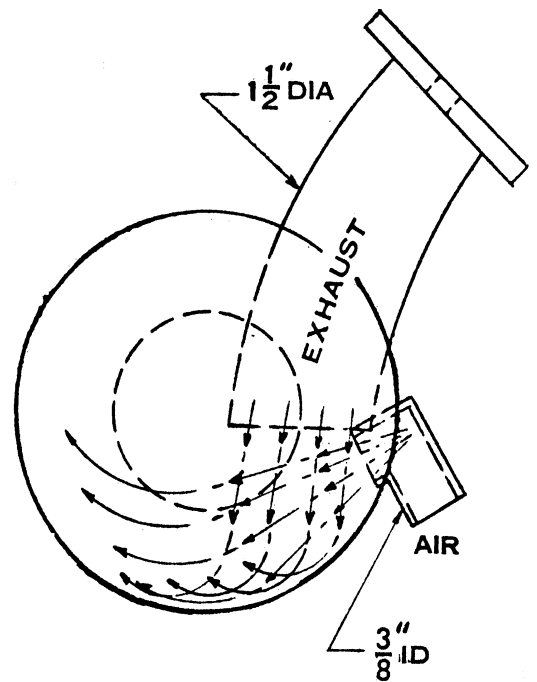
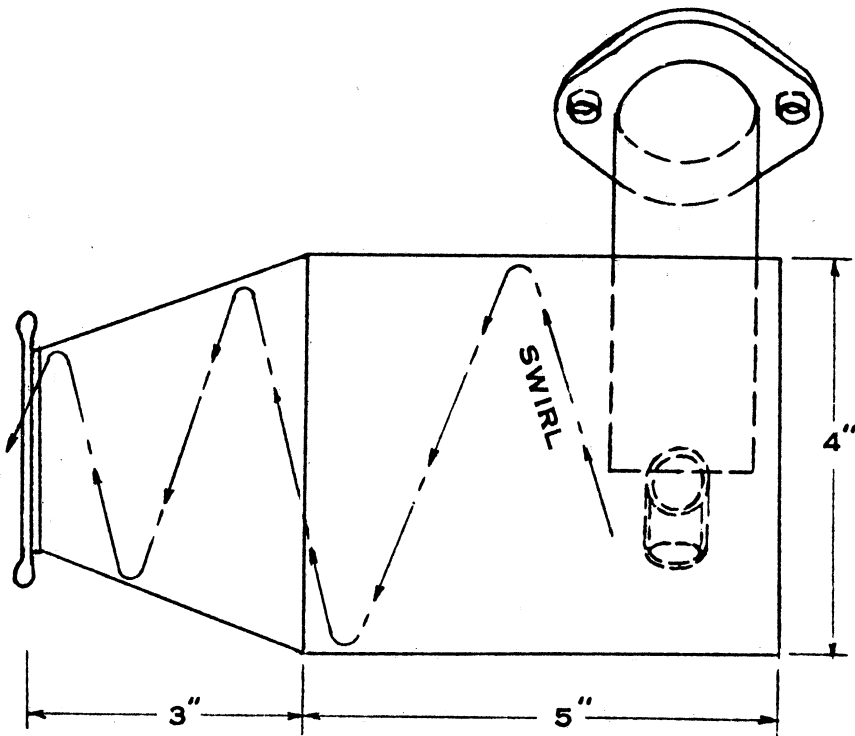


Figure 14b Experimentally determined air injection fraction versus distance in the reactor. The shaded area suggests a region of imperfect mixing of injected air and exhaust.



REACTOR A  
FIG 15



REACTOR B  
FIG 16

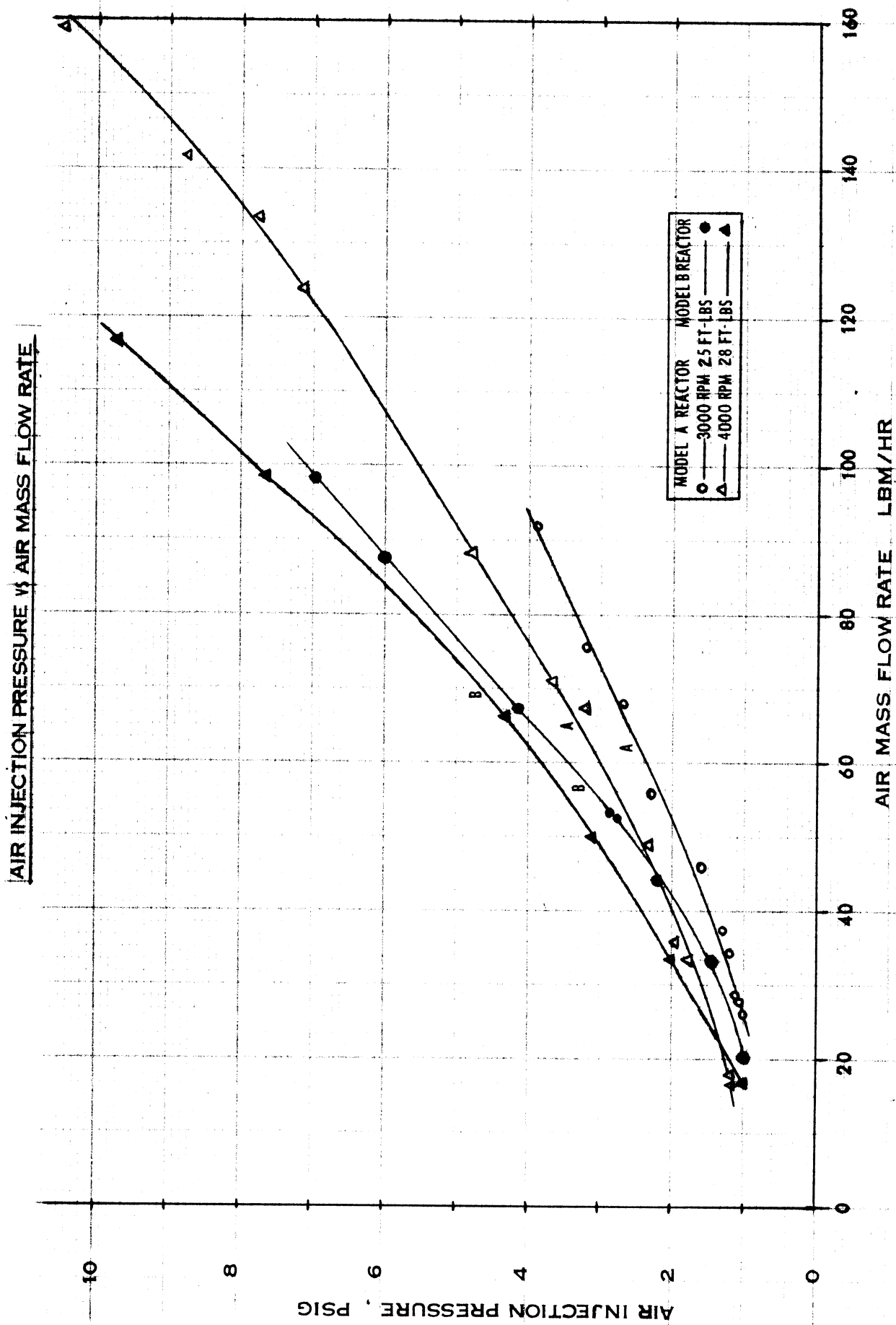


FIG 17

**CORRECTED CO VS AIR INJECTION FRACTION  
MODEL A REACTOR**

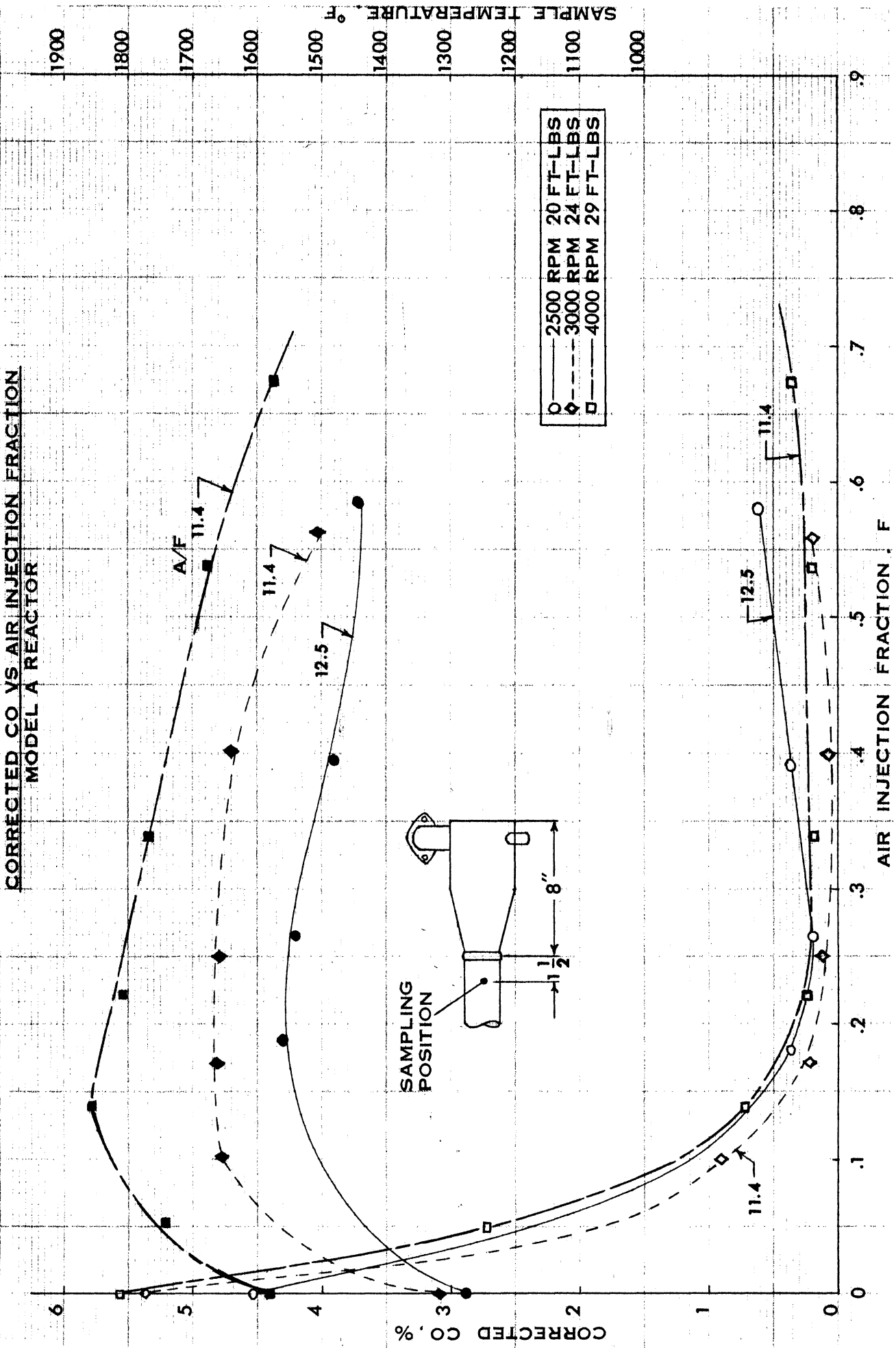


FIG 18

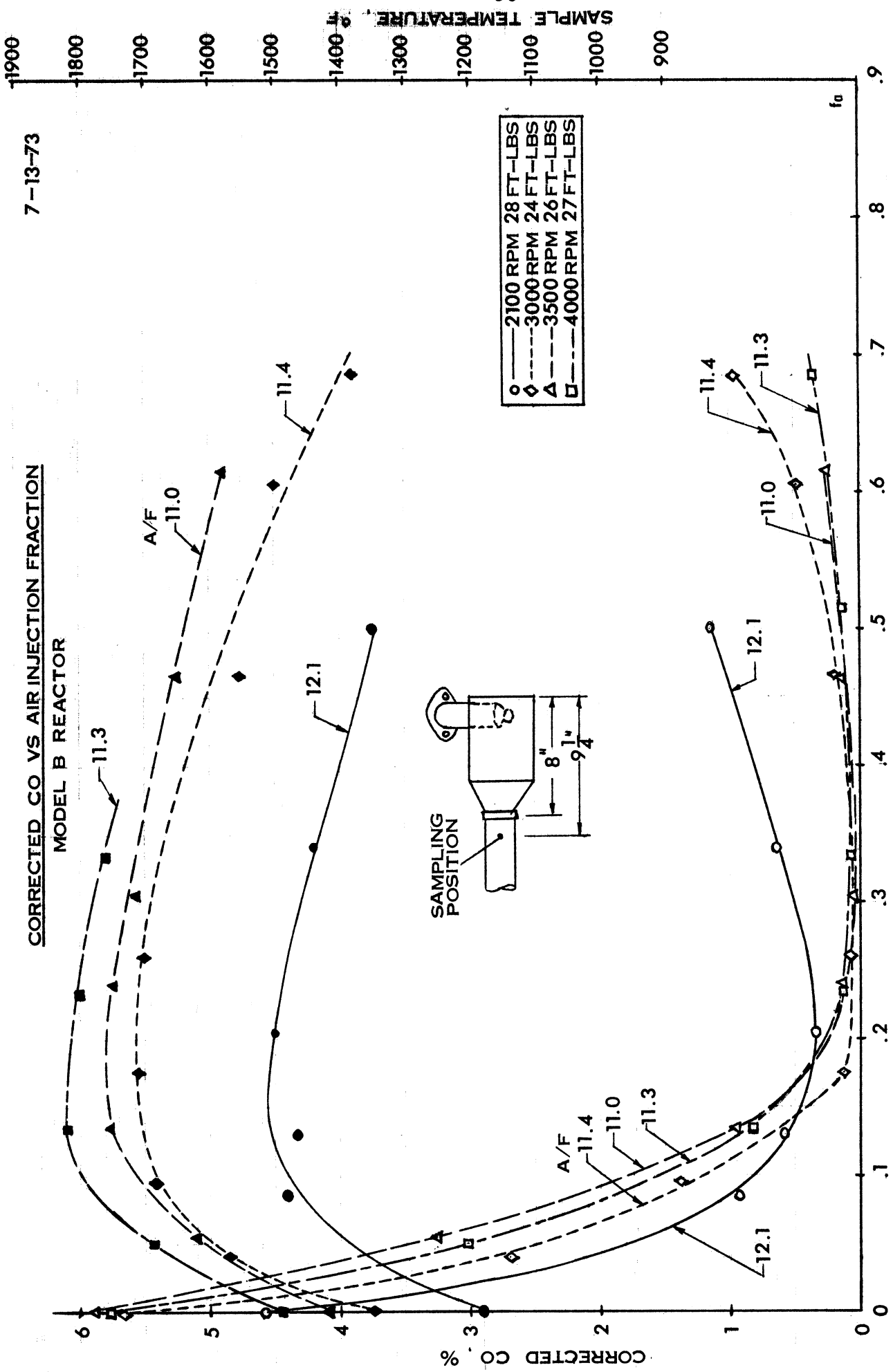


FIG 19

CORRECTED HC VS AIR INJECTION FRACTION  
MODEL A REACTOR

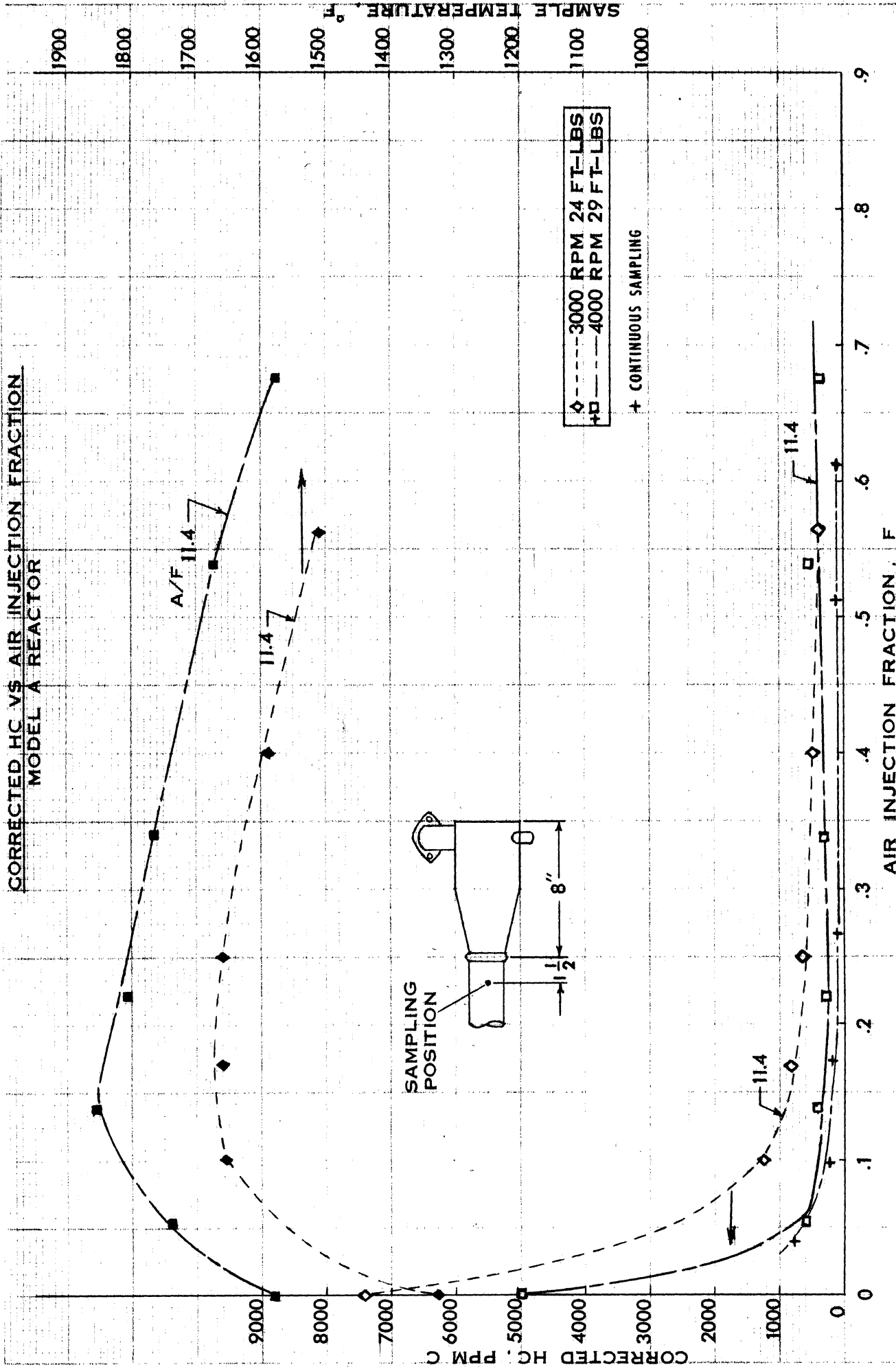
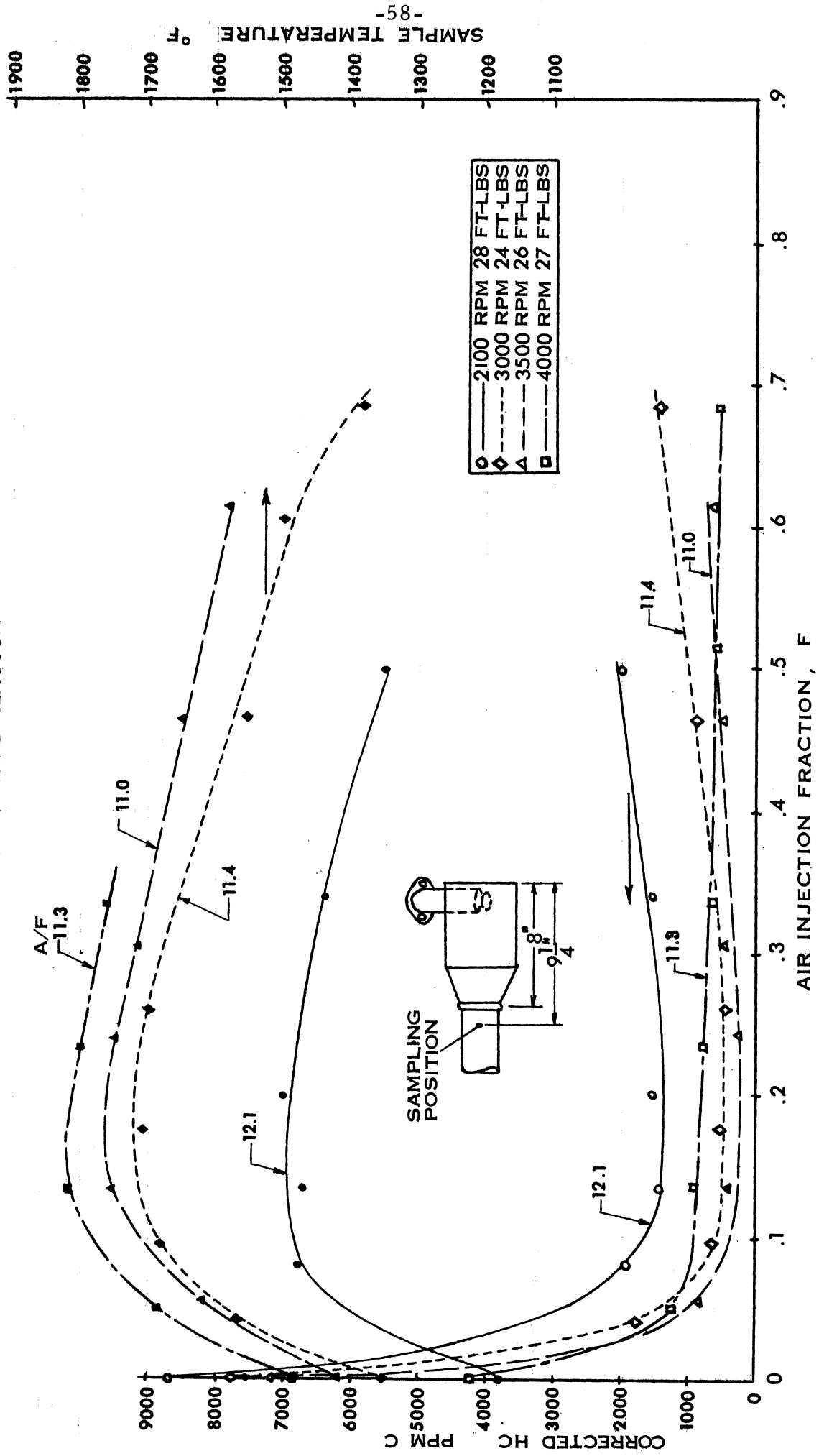


FIG 20

CORRECTED HC VS AIR INJECTION FRACTION  
MODEL B REACTOR

7-13-73



-58-  
SAMPLE TEMPERATURE °F

FIG 21

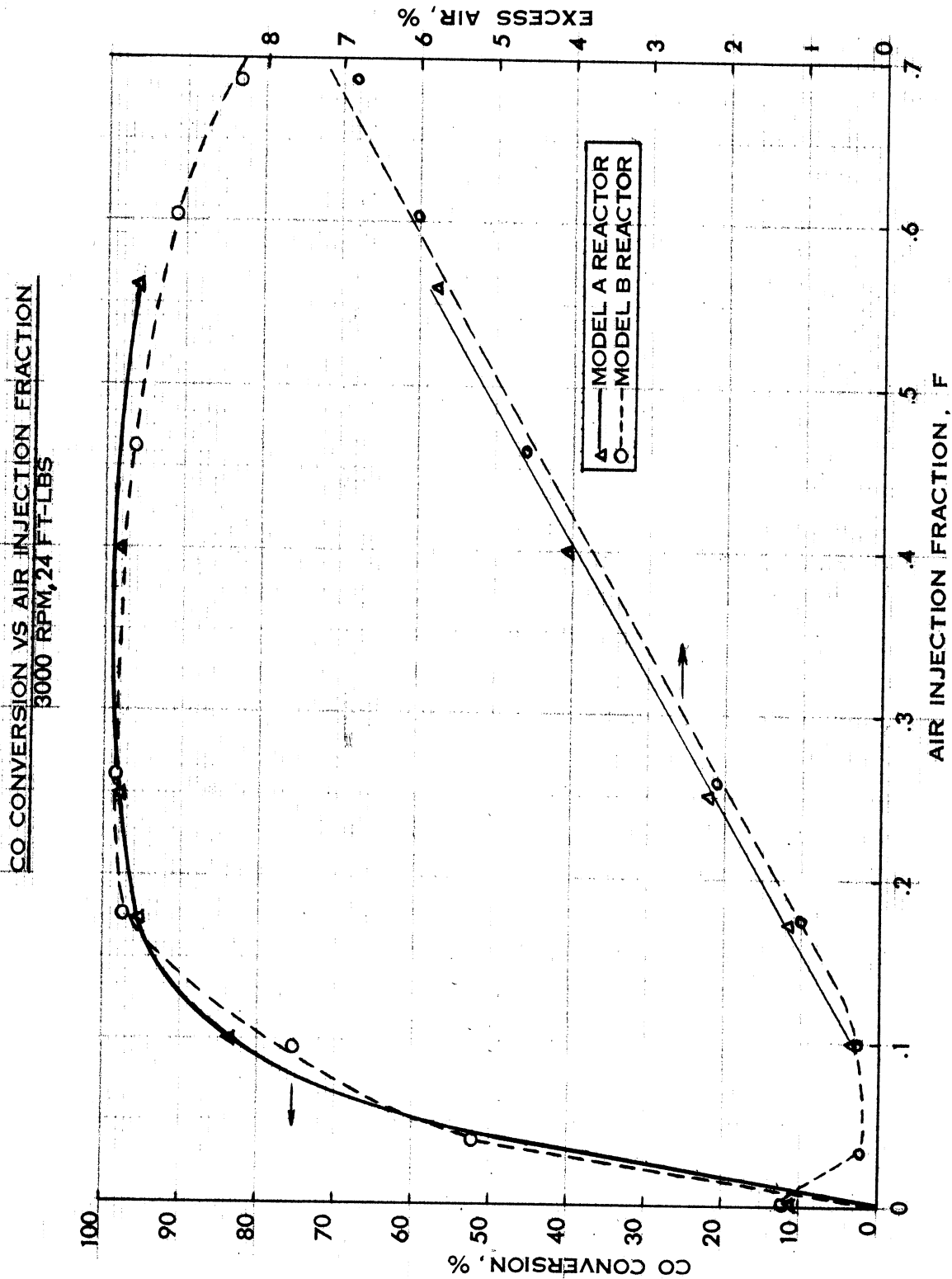


FIG 22



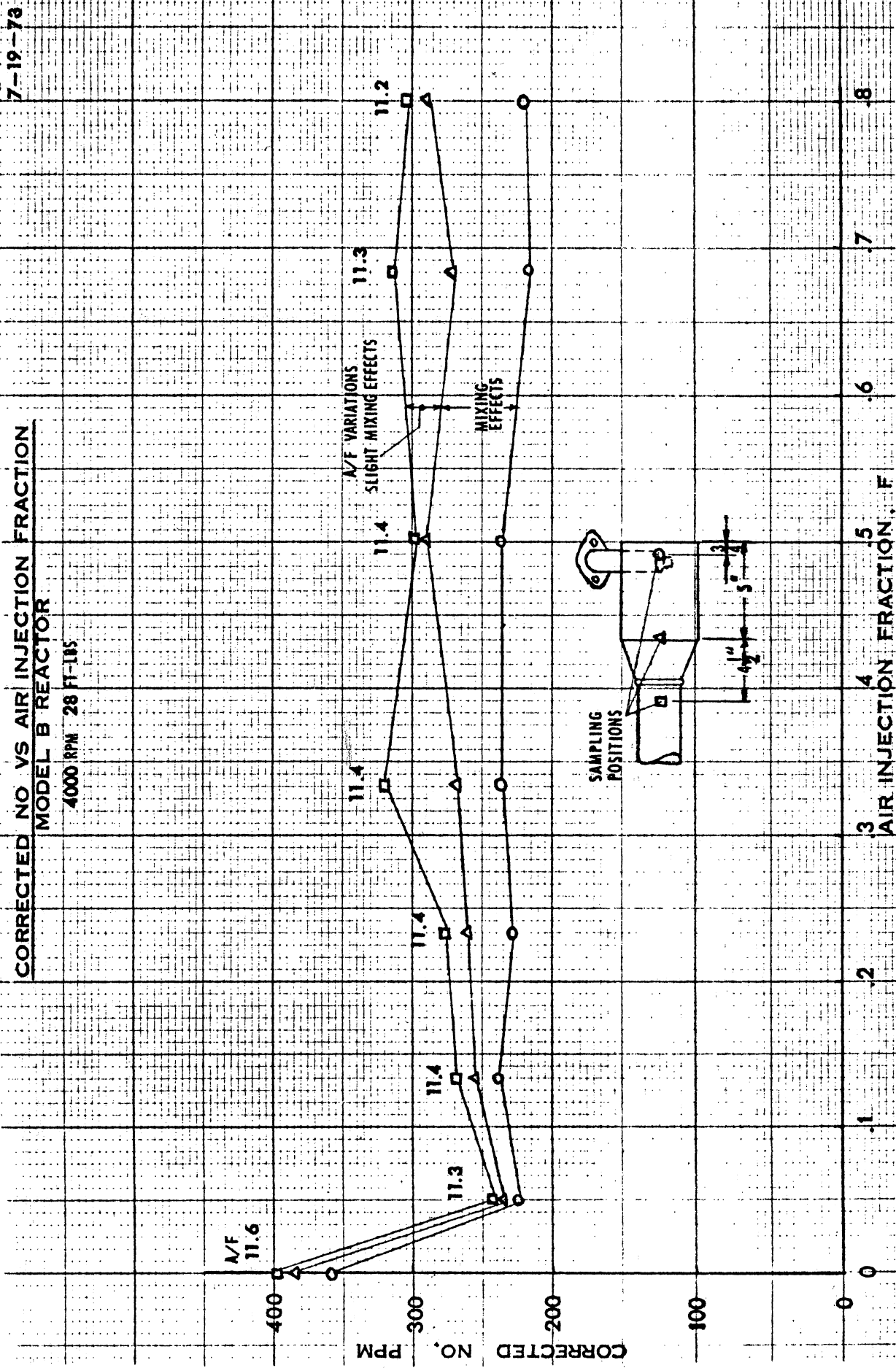
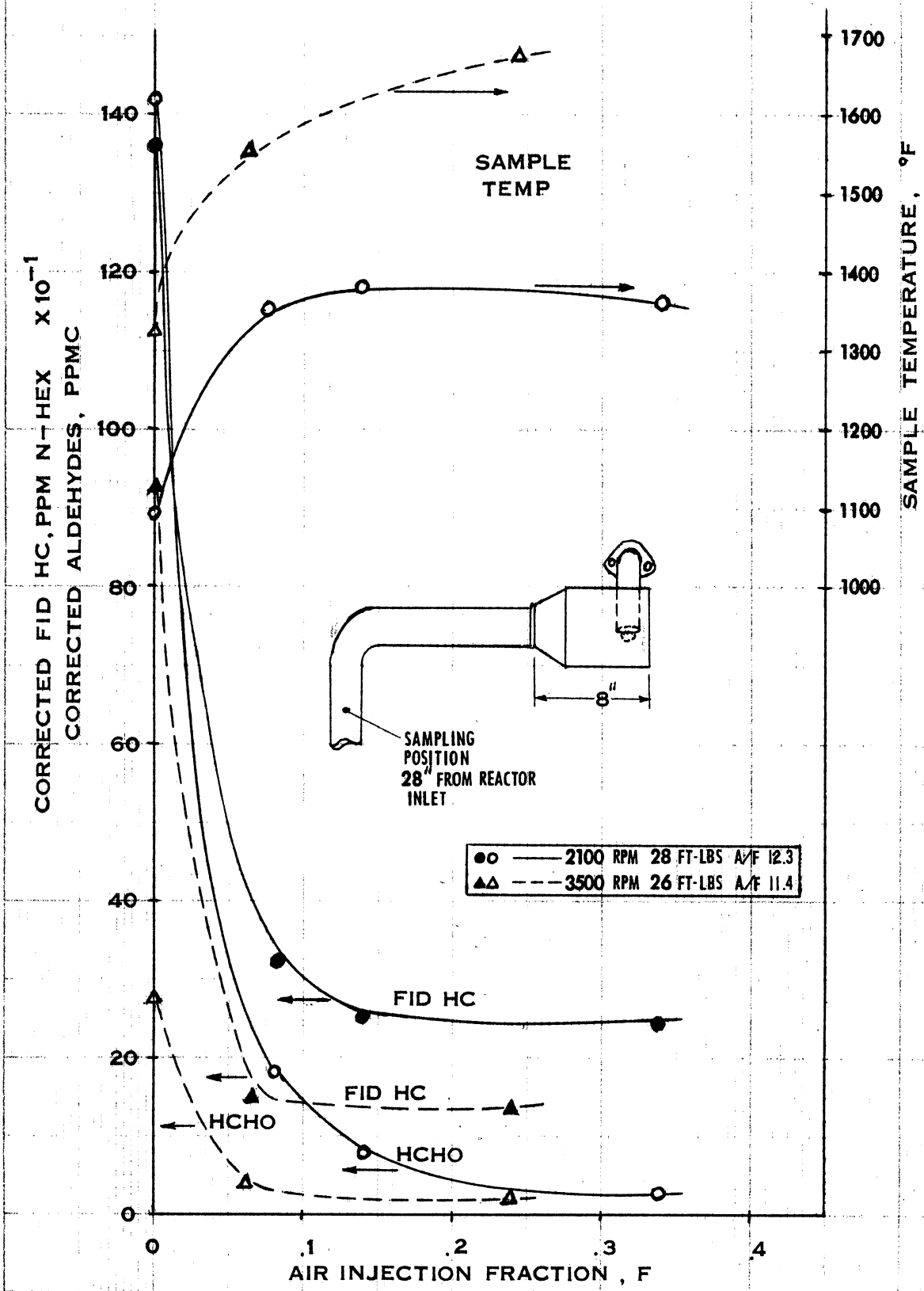


FIG 23

FIG 24

ALDEHYDE AND HC VS AIR INJECTION FRACTION  
MODEL B REACTOR



TEMPERATURES vs. REACTOR A/F

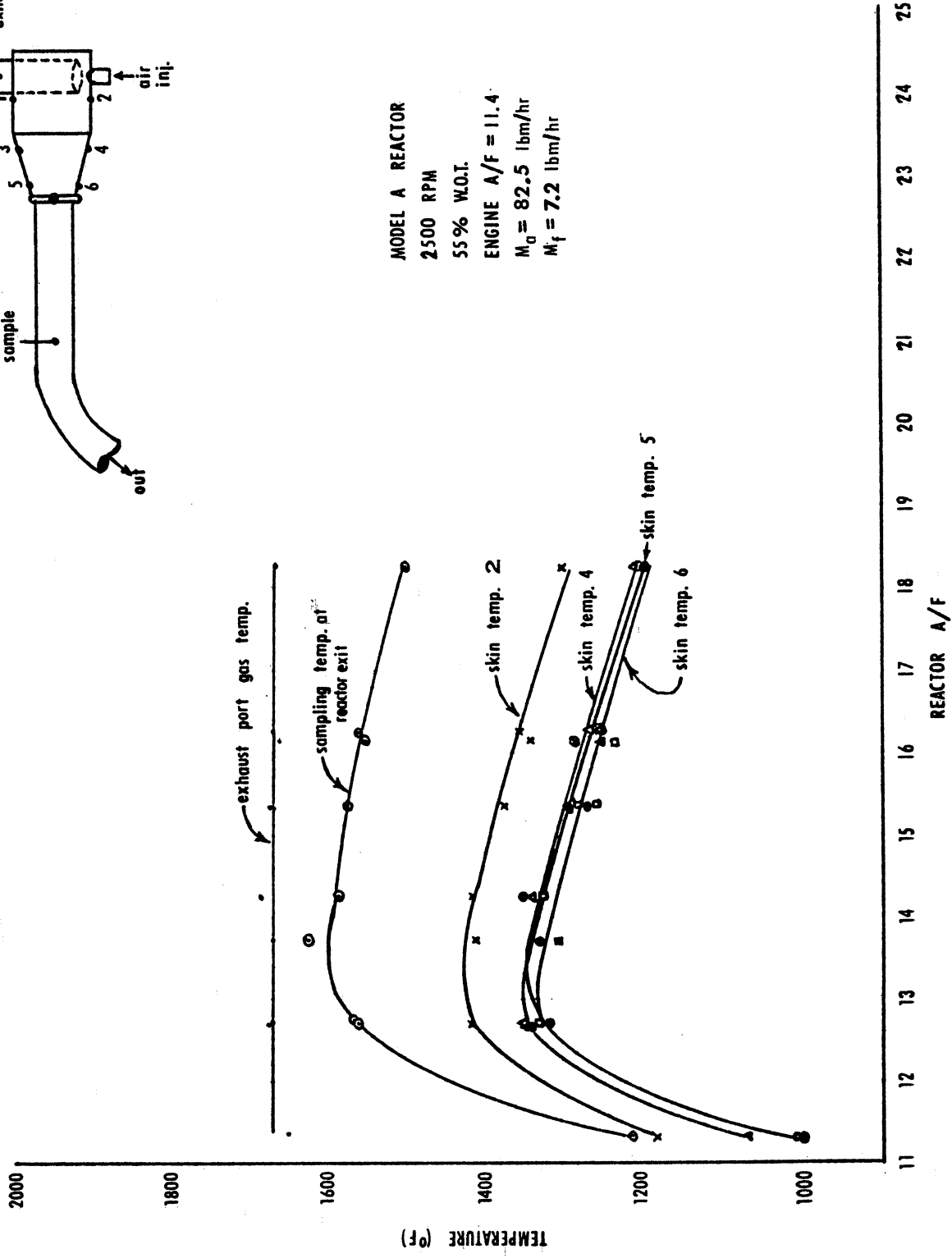
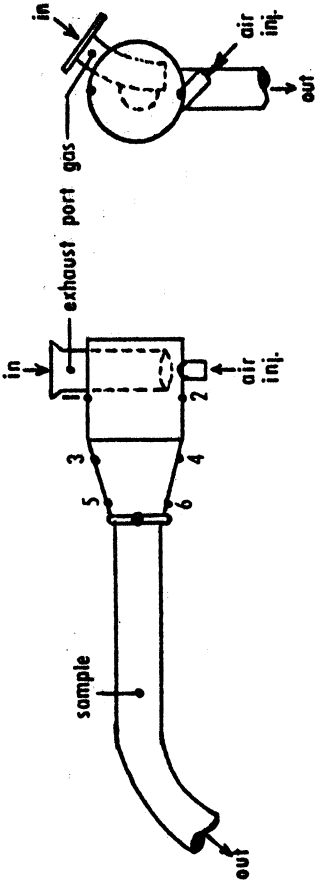


FIG 25



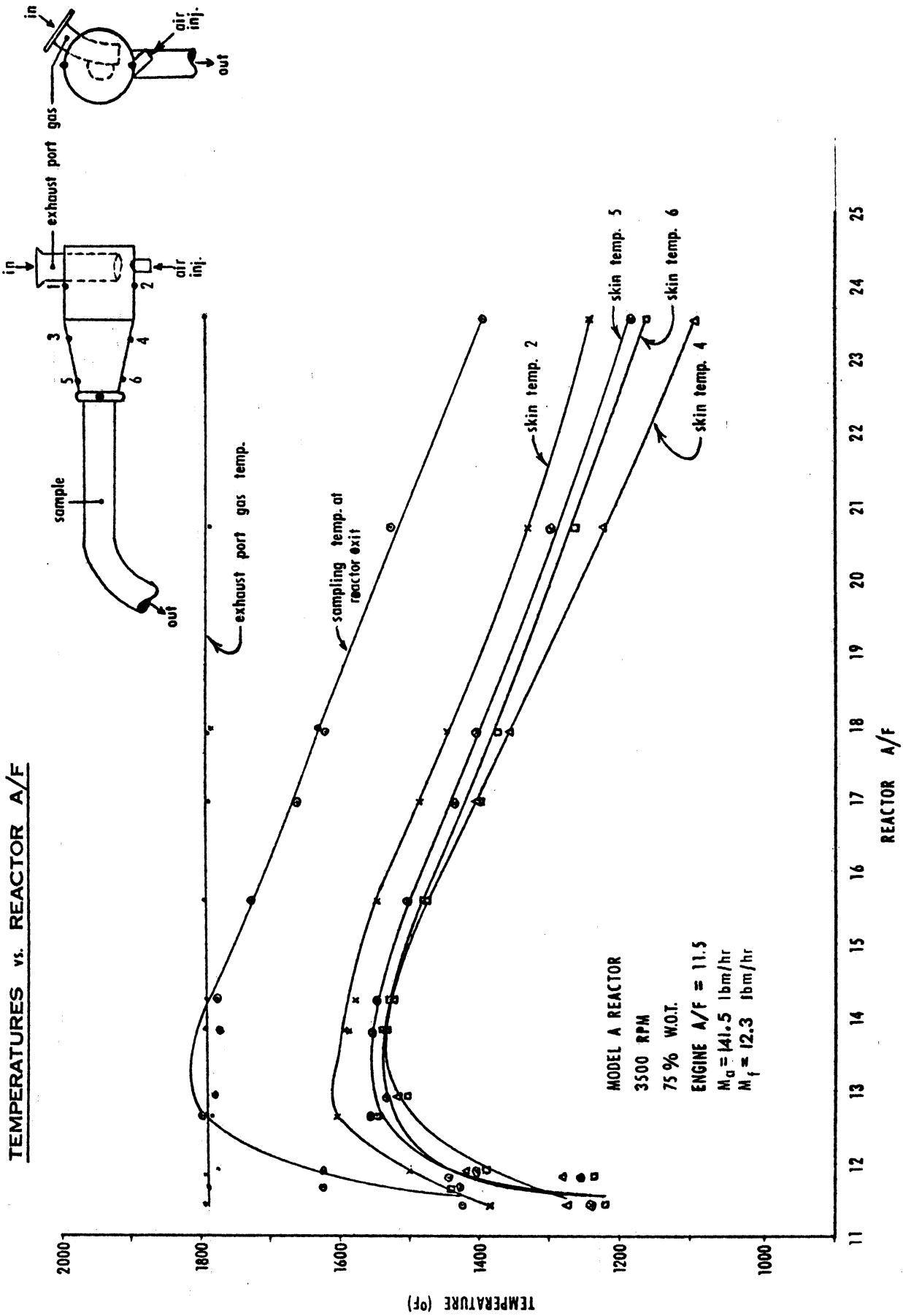


FIG 26

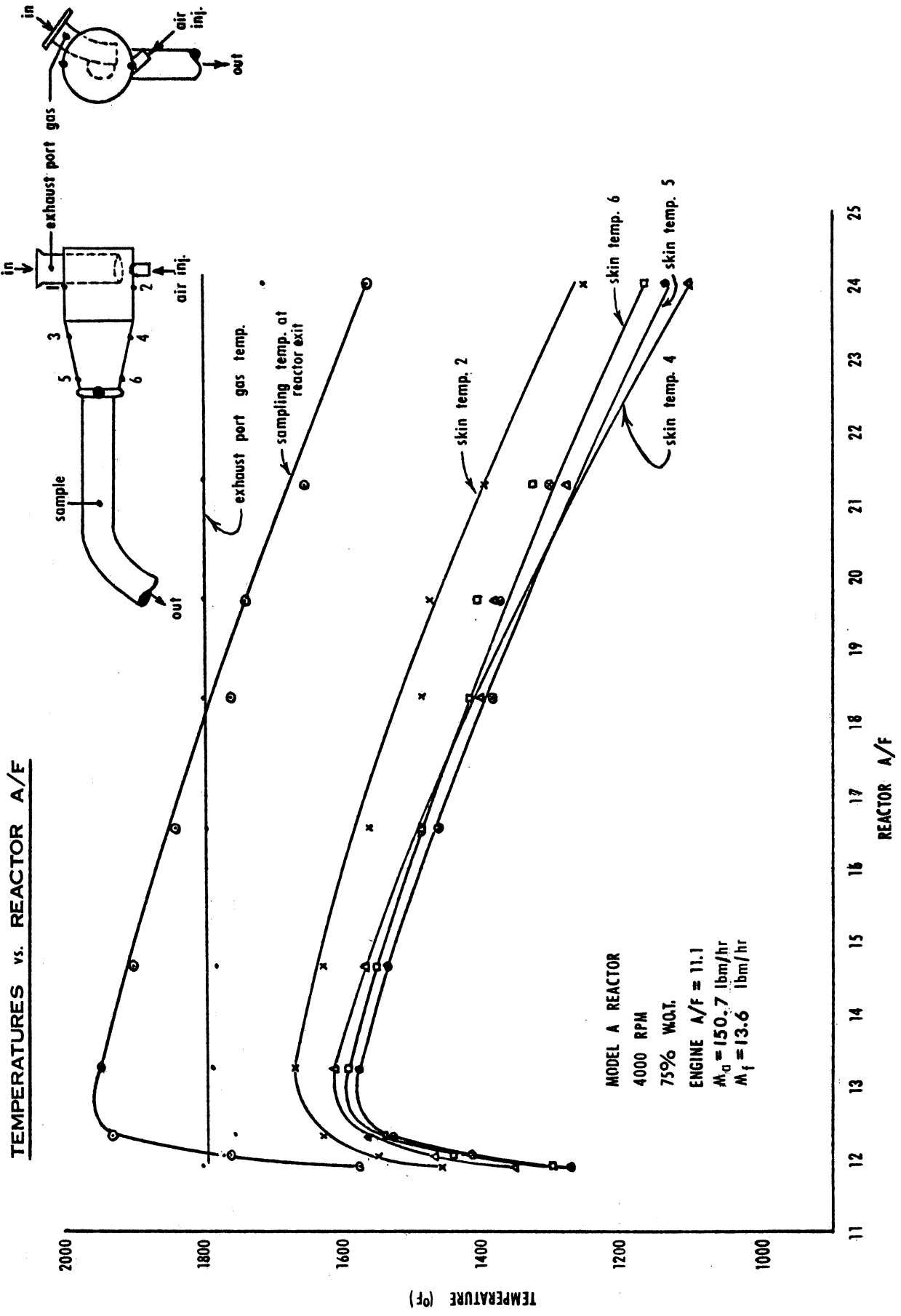


FIG 27

Appendix A

Data Expression

Emissions

Measured carbon monoxide, nitric oxide, hydrocarbon, and aldehyde emissions were corrected for air injection dilution according to the following equation:

$$\text{Corrected Value} = \text{Observed Value} \times \frac{C_o}{C_d}$$

where:  $C_o = \% \text{ CO} + \% \text{ CO}_2 + \frac{\text{FID HC in ppm C}}{10^4}$  in the undiluted exhaust.

$C_d$  = the same sum measured in the diluted exhaust.

The air injection fraction by volume on a dry basis, F (moles injected air/moles exhaust) is calculated by:

$$F = \frac{C_o}{C_d} - 1$$

The theoretical reactor air/fuel ratio is expressed analytically by the expression:

$$\text{Reactor A/F} = \text{A/F}_{\text{eng}} + F (1 + \text{A/F}_{\text{eng}}) \frac{\text{MW}_{\text{air}}}{\text{MW}_{\text{exh}}}$$

where:

F = air injection fraction

MW = molecular weight

Engine Performance

$$HP_{obs} = \frac{T \times N}{5252} \quad \text{where } T = \text{ft-lbs, } N = \text{rpm}$$

For w.o.t. condition:  $HP_{corr} = HP_{obs} \times C.F.$

$$C.F. = \frac{29.92}{(P_{atm})_{corr}} \left( \frac{T_{obs}}{520} \right)^{1/2}$$

where:  $(P_{atm})_{corr} = (P_{atm})_{obs} (\text{in-Hg}) \pm (\text{Temp C.F.}) - (\text{water vapor C.F.})$   
 $\pm (\text{elevation C.F.})$

$$T_{obs} = {}^{\circ}R$$

$$B_{mep} = 150.8 \frac{T}{64.4 \text{ in}^3} = 2.33 T; \quad T = \text{ft-lbs.}$$

Engine Air Rate

$$\rho_{\text{dry air}}^* = \frac{P}{RT} = \frac{P(144)(.491)}{(53.34)(T)} = \frac{1.325 (P_{atm})_{corr}}{T}$$

\*based on ideal gas assumption

where:  $(P_{atm})_{corr} = \text{in-Hg dry air}$

$$T = {}^{\circ}R$$

$$\dot{m}_a = \text{actual dry air mass flow rate} = (\rho_{\text{dry air}}^{\text{actual}}) \left( 60 \frac{\text{min}}{\text{hr}} \right) (\text{SCFM}) (P_{cf}) (T_{cf})$$

where: SCFM = volume flow rate determined from Meriam laminar flow meter

$$P_{cf} = \text{pressure correction factor} = \left( \frac{P_{atm})_{corr}}{29.92} \right)$$

$$T_{cf} = \text{temperature correction factor} = \left( \frac{530}{460 + {}^{\circ}F} \times \frac{181.87}{\mu g} \right)$$

Engine Fuel Rate

$$\text{Specific gravity of fuel} = \text{S.G.} = \frac{141.5}{131.5 + \text{API}_{\text{corr}}}$$

$\text{API}_{\text{corr}}$  = correct for increase in fuel temperature, add 1/10 API number for each degree fahrenheit that the fuel temperature is above the temperature at which the API reading was taken before each run.

$$\dot{m}_f = \text{actual fuel mass flow rate} = (\text{S.G.}) \left( \frac{60 \text{ min}}{\text{hr}} \right) \left( \frac{1 \text{ lbm}}{454 \text{ gm}} \right) (148.4 \text{ ml}) \left( \frac{1}{t} \right) = \frac{\text{lbm}}{\text{hr}}$$

t = fuel burette, duration time-min.

$$\text{BSFC} = \frac{\dot{m}_f}{\text{HP}_{\text{obs}}} = \frac{\text{lbm fuel}}{\text{hp} - \text{hr.}}$$

$$\eta_{\text{th}} = \text{Thermal efficiency} = \left( \frac{2545 \frac{\text{Btu}}{\text{hp-hr}}}{(19,100 \frac{\text{Btu}}{\text{lbm}}) (\text{BSFC})} \right) = \frac{.133}{\text{BSFC}}$$

The above expressions were programmed on a Hewlett-Packard 9820 for data reduction.



Appendix B

FID HC Parameter Optimization

Because the HC concentration at the reactor exit is generally very low, the operating parameters of the Beckman 109A FID were optimized for accuracy and equal sensitivity to the different hydrocarbon (HC) species in the exhaust. Since the flame ionization current is directly proportional to the sample-injection rate and the HC content of the sample, a high sample-injection rate was used. This allowed high meter attenuation to reduce the effect of background noise, which can be significant when measuring extremely low concentrations. While a high sample-injection rate is desirable, the interference from oxygen in the sample must also be considered.

Unfortunately, the response of the FID is dependent not only on the hydrocarbon content, but also on the amount of oxygen in the sample. Several investigators have found that oxygen in the sample can affect the accuracy of FID hydrocarbon measurement. This oxygen interference, or synergism, appears to be the result of several effects including, sample gas viscosity and flame reactions. Since the calibrating gas and sample gas are set at identical gage pressures, this implies their flow rates are equal. This is not exactly true unless the viscosities of the gases are the same. Oxygen can effect the sample viscosity which changes the regulated flow through the restrictor to the ionizing flame.

Investigation by D. M. Teague et al(6) indicate that at constant gage pressure, the gas flow rate decreases linearly with increasing oxygen

concentrations. It was also found that the flow of typical automotive exhaust (low oxygen concentration) is essentially the same as that of span gas (propane ( $C_3H_8$ ) in  $N_2$ ). But as the oxygen concentration in the exhaust increases, which occurs for example as air injection fraction increases, the viscosity effect can become significant.

Oxygen in the sample also effects the diffusion flame characteristics and may influence the degree of ionization of different organic carbon atoms. Precombustion reactions are suspected. The magnitude and direction of the oxygen effect appears to be related to HC structure.

At high burner air flow rates, the change in response appears to be related to the ease with which the respective HC is oxidized. Easily oxidized HC (such as acetylene) show large negative synergism\*, while oxidation resistant HC (such as methane) show the largest positive synergism.

Teague found that at a given sample and fuel rate, there appears to be an air flow rate that provides "zero" synergism for a broad band of oxygen concentrations (Figure A). This is especially desirable when the oxygen content of the sample varies over a wide range, such as when varying air injection fractions. The "zero" synergism air flow rate is relatively high which also minimizes any inaccuracy in the FID air pressure gage.

The use of He, instead of  $N_2$ , as a fuel diluent reduces the magnitude of the oxygen synergism, as shown in Figure B, and makes the diffusion air flow rate less critical. He has higher diffusivity and thermal conductivity

---

\*change in FID response. Negative synergism would be a lower reading than actual. Positive synergism would be a larger reading than actual.

which results in a lower energy density in the reaction zone, and therefore, a slightly lower response with the He diluent than with N<sub>2</sub>.

According to Teague, the following parameters are the best compromise between minimum oxygen synergism and least deviation from equi-response for various hydrocarbons.

Fuel mixture - 40% H<sub>2</sub>, 60% H<sub>e</sub>

Fuel flow rate - 122 cc/min (27 psig)\*

Diffusion air flow rate - 220 cc/min (16 psig)\*

Sample rate - 5-6 cc/min (~2 psig)\*

Teague's result using the recommended operating conditions are shown in Figure C. By use of this approach, the oxygen synergism effect in the present work is minimized, since the exhaust oxygen concentration with air injection (F = 0.0-.8) generally varies from .1-8% maximum.

The fuel and air capillaries of the Beckman 109A FID used in this reactor study had to be calibrated with a bubble flowmeter to determine the gage pressures necessary to operate at the parameters recommended by Teague. Since the original fuel capillary was designed for 40% H<sub>2</sub> - 60% N<sub>2</sub>, it had to be recalibrated to account for the viscosity difference of the 40% H<sub>2</sub> - 60% H<sub>e</sub> fuel. Since no diffusion air flow rate curve was available from the manufacturer, the air capillary also had to be calibrated. The two calibration curves are shown in Figures D and E. The sample capillary flow rates were also checked and found to be comparable to that specified by the manufacturer.

---

\*The gage pressure on the FID used in the present work to obtain the recommended flow rates.

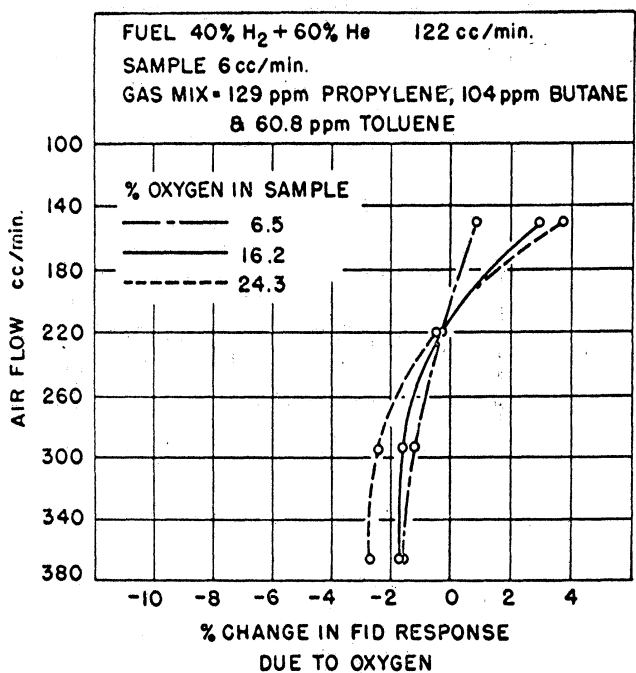


Figure A - Effect of diffusion air flow on oxygen synergism; oxygen content varied, recommended operating conditions.

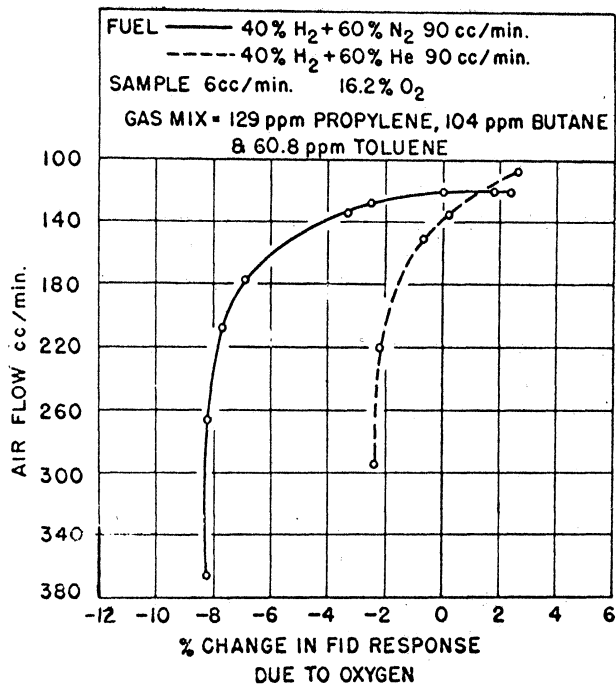


Figure B - Effect of instrument fuel composition on oxygen synergism.

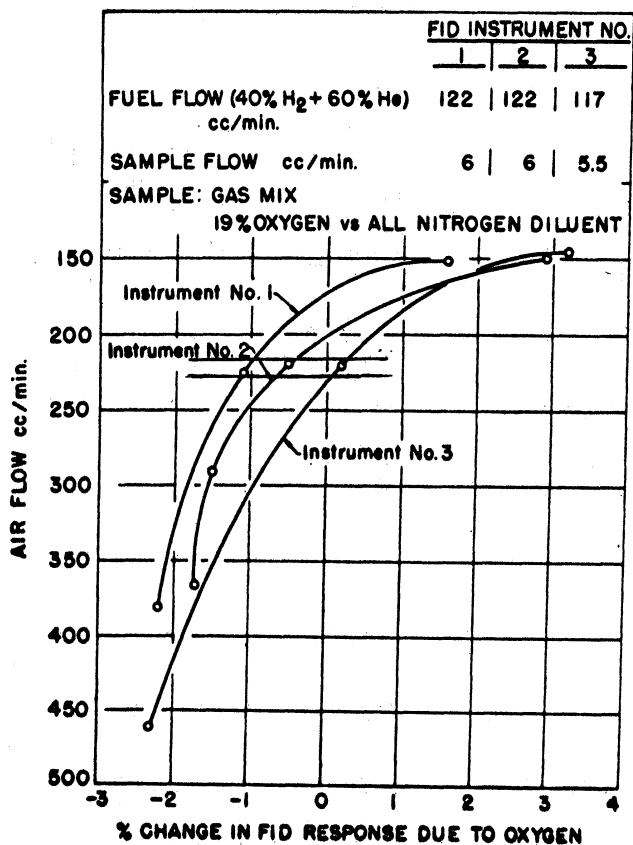
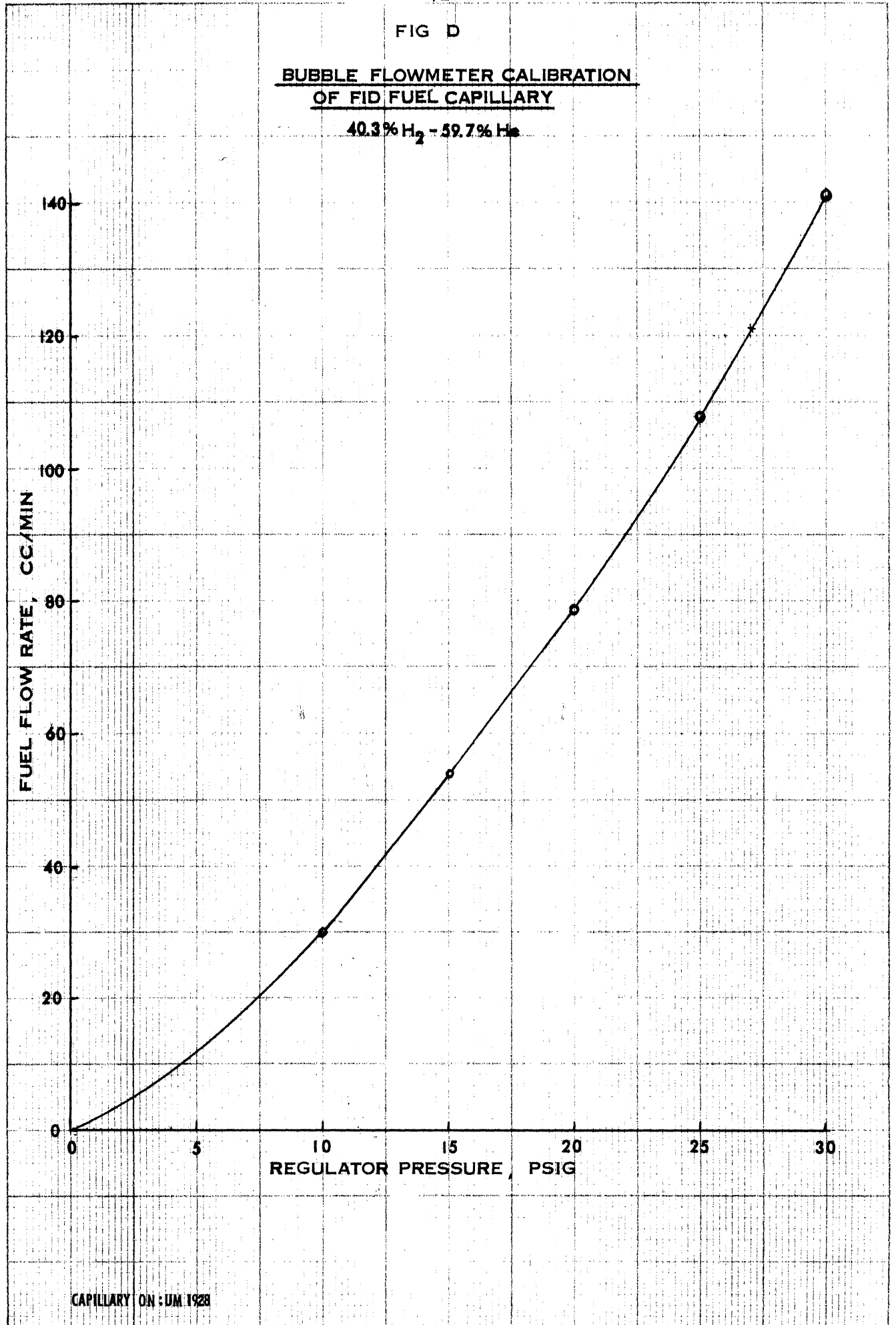


Figure C - Error in hydrocarbon measurement due to oxygen in the sample. Comparison of three FID instruments.

FIG D

BUBBLE FLOWMETER CALIBRATION  
OF FID FUEL CAPILLARY

40.3% H<sub>2</sub> - 59.7% He

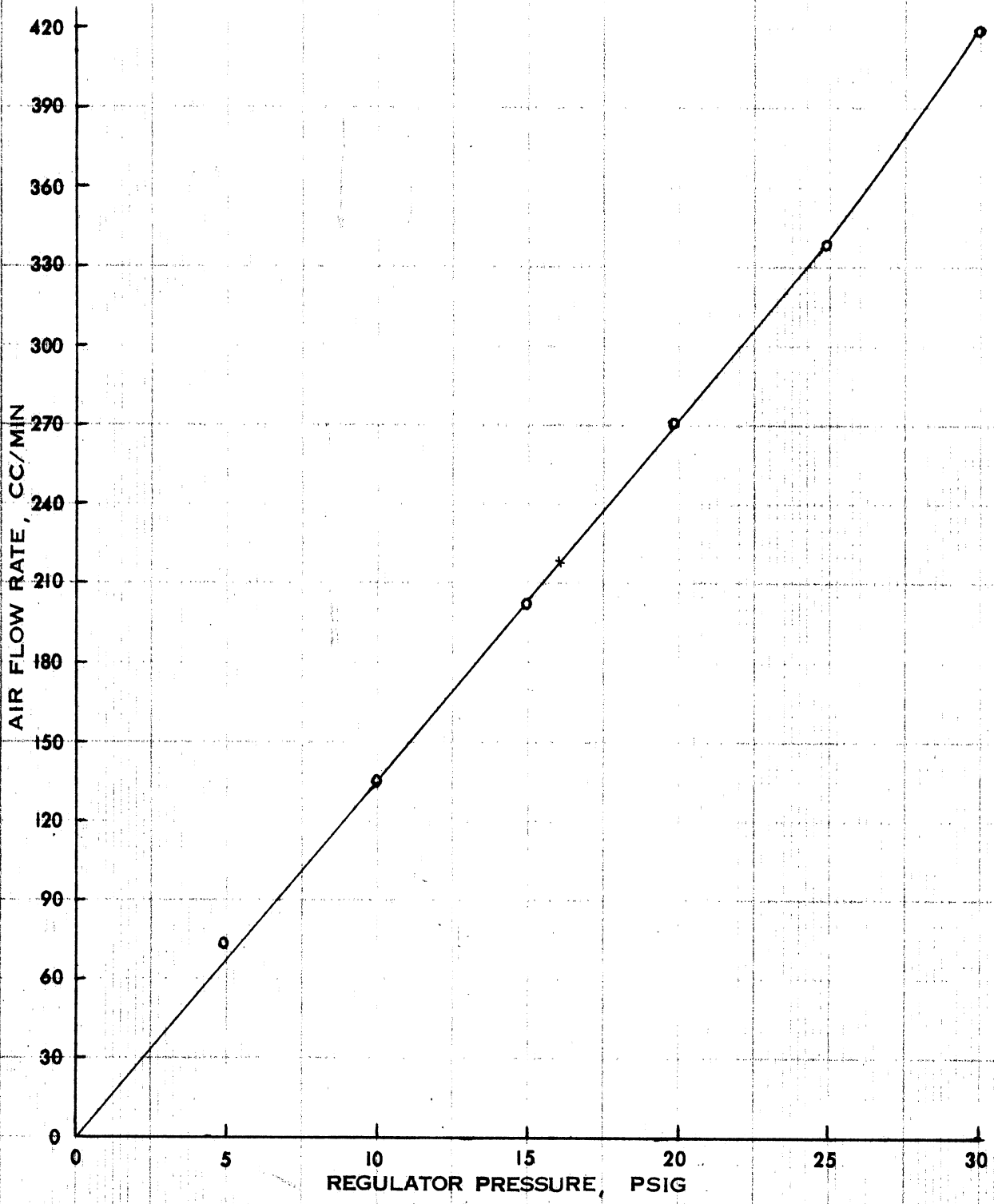


CAPILLARY ON : UM 1928

12 X 20 TO THE INCH 338-41  
KODAK SAFETY FILM

FIG E

BUBBLE FLOWMETER CALIBRATION  
OF FID AIR CAPILLARY



CAPILLARY ON : UM 1928

PHASE II

TRANSIENT PERFORMANCE OF THE MODEL A REACTOR

	<u>Page</u>
Foreword	76
1. Warm-up Performance	77
I. Introduction	77
II. Conclusions	78
III. Engine Operating Characteristics	79
IV. Test Equipment	82
A. Exhaust Gas Sampling and Analysis	82
B. Temperature Measurement	84
C. Secondary Air Injection	84
V. CO Conversion vs. Air Injection Fraction	85
VI. Warm-up Procedure	88
VII. Warm-up Test Results	89
2. Transient Deceleration and Idle Performance	93
I. Introduction	93
II. Conclusions	94
III. Deceleration Test Procedure	95
IV. Deceleration and Idle Test Results	95



Foreword

The steady-state evaluation described in Phase I demonstrated reactor performance at relatively high speeds and loads. The object of this phase of testing was to determine the transient cold start and warm-up idle, as well as transient deceleration performance. These tests required the installation of the Model A reactor in the OMC snowmobile. The centrifugal clutch used in this vehicle limits normal engine operation to one of two basic modes, (1) medium to full throttle, high-speed operation, and (2) idle. Mode 1 does not contain any low speed, low-load operation, a regime where reactor performance would be poor. Therefore, reactor performance in Mode 1 can be evaluated on the basis of the steady-state results of Phase I. Mode 2 (idle) plus warm up and transient deceleration performance are reported below.

During the first warm-up test, it became obvious that the major responsibility for keeping the engine running falls upon the operator, who must manually overcome variations in engine speed and keep the engine running. Attempting to conduct a controlled scientific experiment, where one parameter is varied while the others are held constant, appeared to be extremely difficult, and ultimately proved impossible. Unlike the automobile with its sophisticated carburetion, the snowmobile idle mixture adjustment and the throttle had to be manually varied to keep the engine from stalling. Even when warm, the engine "idled" erratically and the air-fuel mixture varied considerably.

As a result, the warm-up tests were not repeatable, with several tests being terminated by engine stalling. While most of the results followed a similar trend, individual results depended on variations in engine performance during the test and the agility of the operator. In discussing the results of the warm-up, deceleration, and idle tests, qualitative terms such as "stable" and "unstable" CO conversion will be used frequently to evaluate reactor performance. To avoid confusion, "stable" CO conversion will be defined as - less than 5% variation in CO conversion during a given period of time.

## 1. Warm-Up Performance

### I. Introduction

In the OMC snowmobile installation, thermal reactor transient performance was essentially related to the questions, "Will the reactor light-off at idle and once lit, will it remain so?" To answer these questions, a modified Model A reactor installed on a production OMC snowmobile was tested using a start-up procedure similar to the Federal Motor Vehicle Cycle. (The Model A reactor was described in Phase I and is shown in Fig. 15.)

Four test series were run using manually controlled air injection mass rates of 24%, 27%, 30%, and 33% of engine exhaust rate. For each test series the engine was pre-set to 1500 rpm with 6% exhaust CO, a condition previously found to provide the most stable idle.

The following procedure was used for all warm-up tests. Prior to each test, the warmed-up engine was adjusted to the pre-set idle condition

and then the vehicle was allowed to "soak" at 65-68°F for at least 12 hours. The engine was then cold-started and allowed to idle. Manual mixture adjustments were made as necessary to hold a relatively constant exhaust CO level. The following five variables were recorded by strip chart recorders: exhaust port temperature, exhaust port CO and CO<sub>2</sub> concentration, reactor exit temperature, and reactor exit CO concentration. Reactor exit O<sub>2</sub> was recorded manually at selected time intervals.

Three test series using secondary air mass rates of 24%, 27%, and 30% were successfully completed. The test series using 33% air injection was not completed due to repeated engine stalling.

## II. Conclusions

1. It was not possible to conduct a carefully controlled cold-start test because of the erratic starting and warm-up characteristics of the engine. The operator must continuously adjust the choke and idle mixture to keep the engine running, which causes a wide variation in test results.
2. The engine speed (1,500 rpm) and air-fuel mixture (5.5-6% CO) which provided the "best" idle also resulted in reactor "light-off" with CO and HC conversions of 65% or better.
3. Best "light off" conversion was obtained with air injection mass rates between 24-30% of the exhaust mass rate.
4. After the engine achieved a stable idle at 1500 rpm and 5.5-6% CO, ( $\approx 3.5$  min), the reactor CO conversion efficiency gradually increased until it reached an unstable level of between 65 and 85% after  $\approx 6.5$  minutes.

This may be contrasted to higher load steady-state CO conversions of nearly 100%.

5. To achieve repeatable cold-starting and fast repeatable reactor light off, a better production carburetor is required, one which can provide:

- (a) repeatable idle CO content during warm-up
- (b) a stabilized idle CO level of 5.5-6.0% CO consistently

6. Heating the injected air at idle should hasten light off and broaden the successful reactor operating range.

### III. Operating Characteristics of the OMC Rotary Engine as Installed in the Snowmobile

To establish the typical operating characteristics of the engine as installed in a production vehicle, engine speed and intake vacuum were measured "on the road" for a variety of driving modes. The vehicle tachometer was used to measure engine speed, and a vacuum gage was installed to measure the intake pressure downstream of the carburetor. The vacuum gage was calibrated with a mercury manometer. The gage response was linear with a constant error of  $\pm 1$  in. Hg. (see Fig. 1). With the tachometer and vacuum gage, any engine condition could be defined and simulated on the dynamometer test engine.

Using the production exhaust system, baseline idle emissions, engine speed, vacuum, and air consumption were measured. The results are summarized in Tables 1 and 2. At the manufacturer's recommended

Table 1  
 Characteristics of the OMC Engine at Various Idle Conditions

Engine Speed RPM <sup>2</sup>	Intake Vacuum in. Hg	Air Consumption (dry) lbm/hr.	Exhaust Port Emissions				
			% CO	% CO <sub>2</sub>	% O <sub>2</sub>	HC ppm n-hex	NO ppm
1000	10	17.6	7.0-7.4	7.5-7.9	3.0-3.4	1300-1325	222-237
1200	11.5	19.7	5.4	10.1	2.0	750	236
1500	12.	23.6	7.1	8.6	2.0-2.1	720	250
1500	12.	24.9	6.9	9.4	1.6	720 <sup>3</sup>	250
1600	12.2	25.0	5.6	10.1	1.3-1.4	660	264

Table 2  
 Idle Mixture Adjustment

Exhaust CO at Recommended Idle Speed <sup>1</sup> , 1200 rpm
Lean stable idle adjustment - 4.0% CO
Rich stable idle adjustment - 6.5% CO
Best idle adjustment - 5.5 - 6.0% CO
Choke had no significant effect on exhaust CO

- (1) warmed-up engine
- (2) using snowmobile tachometer
- (3) reading slowly decreasing with time

idle speed of 800-1200 rpm, our engine idled erratically and stalled unless the throttle was feathered continuously. It was concluded that the idle speed would have to be increased to provide a stable idle during warm-up and deceleration testing. An idle speed of 1500 rpm with the idle mixture adjusted to provide 5.5-6% exhaust CO ensured a relatively stable idle. Although the manufacturer suggested that idle speeds in excess of 1200 rpm may render the neutral control inoperative, the neutral control functioned properly at idle speeds up to 1800 rpm.

To determine when the centrifugal clutch would engage the drive train, the snowmobile was taken into an open field adjacent to the University of Michigan Automotive Laboratory and tested. It was found that engagement began at 2800-3000 rpm, 4-5 in. Hg. intake vacuum when the vehicle was operated in deep, dry grass. As the clutch engaged, the exhaust CO concentration ranged from 6 to 7%, while the intake vacuum decreased from 11 to 4 in. Hg. According to OMC, the carburetor delivers a relatively constant 6-7% exhaust CO throughout the engine operating range.

During prolonged idling, the carburetor became leaner as the engine warmed-up, causing the exhaust CO to decrease from 6% to 3.5%. At these leaner mixtures, the idle became unstable. Since the choke was found to have no significant effect on the idle exhaust CO concentration (at least not at the ambient temperature experienced, 60-70°F), no attempt was made to maintain a constant idle CO by varying the choke. The idle mixture screw was adjusted instead.

#### IV. Test Equipment

##### A. Exhaust Gas Sampling and Analysis

A modified Model A reactor (shown in Fig. 2) was installed in the snowmobile and instrumented for transient testing. The vehicle installation with exhaust sampling and analysis system is shown schematically in Fig. 3. Gas analysis and temperature measurement techniques are outlined in Tables 3 and 4.

With the exception of the reactor inlet thermocouple and the Mexa 300 NDIR CO analyzer, the analysis equipment used for the warm-up test was the same as that used for steady-state testing in Phase I.

A non-quenching 1/4" stainless steel sample probe and shield thermocouple were installed in the reactor inlet pipe. The probe had 12, 3/32" dia. holes and was selectively positioned to sample the exhaust gas at various positions across the diameter of the reactor inlet pipe, 3 in. downstream of the exhaust port. Because of relatively low exhaust temperatures (below 1250<sup>o</sup>F) at idle, a water-cooled quenching probe was not used. A specially shielded Platinum-Platinum, 13% Rhodium thermocouple was placed perpendicular to the sample probe to measure the average engine exhaust temperature.

To analyze the reactor exhaust, a special exhaust elbow was designed to accommodate the transverse water-cooled sample probe and shielded immersion thermocouple used in the steady-state testing (Phase I, Fig. 9b).

The reactor inlet CO concentration which ranged from 3-7% was measured with a Mexa 300 NDIR CO analyzer. The analyzer's accuracy

Table 3

Gas Analysis Techniques

<u>Exhaust Specie</u>	<u>Technique</u>	<u>Manufacturer</u>	<u>Range</u>
	<u>Reactor Inlet</u>		
Carbon monoxide	NDIR <sup>1,2</sup>	Horiba Ltd. Mexa 300	0-10%
Carbon dioxide	NDIR <sup>1,2</sup>	Beckman Inst. Model 315A	0-15%
	<u>Reactor Exhaust</u>		
Carbon monoxide	NDIR <sup>1,2</sup>	Beckman Inst. Model 315A	0-10%
Oxygen	Amperometric	Beckman Inst. Model 715	0-25%

Table 4

Temperature Measurement

Reactor Inlet and Exhaust

Platinum-Platinum, 13% Rhodium shielded thermo couples  
with Westronic M11D2 recorder<sup>3</sup>

- 
1. NDIR - nondispersive infrared
  2. Calibration gases checked by Orsat
  3. Provided and calibrated by Walker Research



was checked with calibration gases of 2.02, 4.9, and 8.2% CO and was found to be within  $\pm 2\%$  of the scale reading. The Texas Instrument Strip Chart Recorders, connected to the output of the exhaust CO and CO<sub>2</sub> and reactor CO analyzers, were calibrated before each test.

While instantaneous oxygen measurement was not possible with the Beckman analyzer used in the test, readings of O<sub>2</sub> at the reactor exit were recorded manually at 10 second intervals.

#### B. Temperature Measurement

Shielded Platinum-Platinum, 13% Rhodium thermocouples were used to measure engine exhaust and reactor temperatures. A specially shielded thermocouple was built for the reactor inlet, while the immersion thermocouple used in Phase I testing was used to measure reactor core and exit temperatures. Both exhaust and reactor temperatures were recorded simultaneously on the Westronic temperature recorder provided and calibrated by Walker Research.

Because the reactor inlet pipe had a relatively cold surface, especially during start-up and idle, a thermocouple with a cup-shaped shield was built to minimize temperature errors due to radiation losses. The platinum-rhodium wires were inserted through a ceramic insulating core and packed in a 3/16" diameter 304 stainless-steel tube. The thermocouple bead (junction) was kept as small as possible to minimize response time.

#### C. Secondary Air Injection

For metering injected air, the critical orifice flow cart described for the steady-state testing was also used for this phase of testing. Unfortunately, the secondary air flow rates at idle were so small (between 1.4-

2.5 cfm) that the orifice had to be operated in the non-critical region.

A 100 cfm Merriam laminar flowmeter and micro-manometer were available to calibrate the orifice in the non-critical region. However, because the secondary air flow was near the lower limit of the laminar flowmeter, the orifice calibration and, consequently, the measured air injection quantity is accurate within  $\pm 10\%$ . The air injection flow readings (cfm) were used as approximate set points and to provide a general check of the air injection fraction  $F'$ , which was calculated from the exhaust and injection air mass flow rate. (Note:  $F$  is the air injection fraction calculated from a carbon balance of the diluted and undiluted exhaust).

#### V. CO Conversion vs. Injection Fraction

Before conducting warm-up and deceleration tests, it was necessary to determine CO conversion as a function of secondary air flow for the chosen idle condition. To reduce the number of variables affecting CO conversion at idle, kinetic limitations were minimized by completely insulating the reactor with 1 in. of Kao-Wool. This provided the maximum reactor temperature and, therefore, the maximum CO conversion obtainable at a given engine condition. With the engine fully warmed up, the engine speed and reactor inlet CO concentration were held constant at 1500 rpm and 6% respectively, while the secondary air flow was varied over a wide range. CO conversion, reactor exhaust temperature, and  $O_2$  concentration in the reactor exhaust were measured at several pre-determined air flow rates.

To minimize hysteresis effects, measurements at each air flow rate were first taken by increasing the air flow in consecutive steps and then rechecking each point several times in random order. The CO conversion range for each injection fraction is shown in Fig. 4.

Stable CO conversion, in excess of 90%, was obtained with injection fractions,  $F'$ , between .27 and .48. For  $F'$  less than .27, conversion was relatively stable but mixing limited, while for  $F'$  greater than .48, CO conversion became unstable due to the cooling effect of the excess secondary air. Theoretically, with 6% CO, a stoichiometric mixture in the reactor is achieved with about 11% air injection (on a wet basis).

For  $F'$  between .27 and .48, CO conversion was stable and ranged between 93 and 99%+. The reactor exit temperatures in this range were between 1480-1525°F, while reactor core temperatures were probably even higher. At these temperatures, kinetic limitations would be minimal, with good mixing.

Below  $F' = .27$ , CO conversion appeared to be mixing limited. Despite the 1500°F reactor exit temperatures and 3.5-4.2% excess  $O_2$  in the exhaust, CO conversion was low. If the exhaust and secondary air had been well mixed, these conditions should have produced 95%+ CO conversion. Based on this experimental result, our conclusion is that the exhaust products and secondary air were poorly mixed under engine idle flow conditions.

To estimate the degree of mixing, the reactor Reynolds number was calculated by modeling the reactor as a large pipe. It is well known

that turbulence in pipes is predicted by the Reynolds number ( $R_e$ ). Mixing is expected to be good when flow is turbulent or transitional ( $R_e > 2,000$ ) and poorer when flow is laminar.

$$R_e = \frac{\rho V d}{\mu} = \frac{4 \dot{M}}{\pi \mu d}$$

where:  $\dot{M}$  = lbm exhaust/hr.

$d$  = diameter of tube (reactor), ft. = 4/12

$\mu$  = absolute viscosity, lbm/ft-hr.

$\rho$  = density of air, lbm/ft<sup>3</sup>

At 1500 rpm idle:  $\dot{M} = 27$  lbm/hr. and  $T = 1500^{\circ}\text{F}$ . Assuming the exhaust gas has the properties of air,  $\mu = .108 \frac{\text{lbm}}{\text{ft-hr}}$ .

$$R_e = \frac{4(27) 12}{\pi (4.0) .108} = 955$$

With air injection of  $F^1 = .5$  ( 50% increase in flow), the Reynolds number would be only about 1450, which is still considerably less than 2000. The above calculations support the conclusion that reactor turbulence and mixing are poor at this low idle flow rate.

Under these circumstances, air injected into the reactor inlet pipe, whose diameter is 1-1/2 inches, may mix well with the exhaust (on a micro-scale) since the Reynolds number of the combined flow in the pipe would exceed 3000. However, the inlet pipe may be too short to allow mixing across the entire diameter. Injection into the reactor inlet should pose no back pressure problems at idle, but would require a switchable air system for operation at higher loads.

Between  $F' = .27$  and  $.48$ , CO conversion is stable and in excess of 95%. The reactor exit temperatures range from 1500-1525°F, while the excess  $O_2$  increases linearly until  $F' = .48$ , where CO conversion begins to fall and becomes unstable.

As  $F'$  increases beyond  $.48$ , the cooling effect of the secondary air causes unstable CO conversion and eventually extinguishes the reaction. The reactor exit temperature decreases steadily from 1475°F at  $F' = .48$  to 1425° at  $F' = .53$  and finally at  $F' = .56$ , the temperature varies erratically between 1200-1300°F. The erratic variations in temperature and CO conversion are probably due to intermittent localized "light off" in elements of gas, which are extinguished when subsequently mixed with a large volume of relatively cool air.

From this test, two major conclusions can be drawn for reactor performance at idle (1) stable CO conversion in excess of 95% can be realized for a reasonably broad range of air injection fractions, and (2) the optimum CO conversion appears mixing limited, requiring at least 4.7% excess  $O_2$ . For speeds above 2000 rpm, half to full load, the excess  $O_2$  for optimum CO conversion was only 1.5-2.0%.

#### VI. Warm-Up Procedure

Since no information on any future snowmobile emission legislation was available, a start-up procedure similar to the Federal Motor Vehicle Cycle was used to evaluate the warm-up performance of the modified Model A reactor on the OMC snowmobile. With the engine fully warmed up, the idle

speed and idle mixture were pre-set to 1500 rpm and 6% CO. The snowmobile was then "soaked" for a minimum of 12 hours at 65-68°F.

The following procedure was used for all cold-start tests: with the engine in neutral, brake on, choke pulled out, and air injection\* pre-set, the primer was pushed twice, then the ignition was turned on. If the engine failed to start, the primer was pushed once more and the engine was cranked again. Once the engine started, only the idle mixture was adjusted to maintain the desired inlet CO concentration, or to keep the engine from stalling. This procedure was used in four test series using air injection rates of 24, 27, 30, and 33% of engine exhaust mass flow. The air injection was turned on when the engine started and was manually adjusted to maintain a constant mass flow rate.

#### VII. Warm-Up Test Results

The test series for 24, 27, and 30% air injection were successfully completed. But, based on the engine variations encountered during this testing, the test series for 33% air injection was abandoned, after the engine stalled during three consecutive tests.

Test results clearly indicated that a prescribed start-up procedure similar to the Federal test cycle is not representative of snowmobile operation in the hands of the consumer. Even at the higher pre-set idle speed and an ambient temperature of 70°F, the engine idled erratically and stalled if left unattended. Contrary to the automobile, the operator is mainly responsible for keeping the snowmobile engine running. In actual

---

\*In this research the injection air was from the building supply, not from a vehicle pump.

use, start-up and idle at sub-freezing temperatures may pose even more severe problems.

Reactor "light-off" was governed by the length of time required for the engine to reach a stable idle. Instead of being dependent on the thermal capacity and heat losses of the reactor, time to "light-off" was mainly a function of engine variations and operator corrections. Experimental data from two warm-up tests (24 and 30% air injection) are shown in Figs. 5, 6, and 7. The temperature trace for warm-up test 1 (Fig. 6) is representative of the engine exhaust temperature behavior observed in all the tests, except for the temperature increase after 6 minutes which is primarily due to leaning of the air-fuel mixture. As the engine exhaust temperature approached its stabilized value of about 1225°F (after 3.5 minutes), CO conversion increased steadily. If the carburetion were sophisticated enough to warrant cold-start evaluation of this vehicle, the 3-minute point would probably correspond to the "start-up" point. In that case, the reactor would probably achieve maximum efficiency within 3 minutes, compared to 6.5 minutes for this test.

Despite the major engine variations from test to test, all the reactor CO traces followed the same basic three-stage pattern. The three-stages could be classified as (1) no CO conversion, (2) unstable linearly increasing CO conversion, and (3) unstable maximum CO conversion. These stages, shown in Fig. 8, were primarily dependent on the engine exhaust temperature, which is a function of the engine A/F ratio. During the first three minutes of each test, a mixture ratio corresponding

to 6-7% exhaust CO was required to keep the engine from stalling. As a result of this rich operation, the exhaust temperature was well below the 1225°F obtained at the pre-set idle condition of 1500 rpm, 6% CO. On the average, it took approximately 1.5 minutes before the exhaust temperature even reached 1000°F,\* and almost four minutes before it reached the steady-state temperature for that particular air-fuel ratio. Once the exhaust temperature stabilized near 1200°F, the engine operated smoothly at the desired 5.5-6.0% CO and the reactor CO level began to decrease.

The CO concentration did not drop instantaneously, but decreased gradually resulting in a constant reactor temperature increase as shown in Fig. 6 between 3.5 and 6 minutes. The sudden increase in CO conversion and reactor temperature that is typical of "light-off" (luminous CO oxidation) was not observed in any of the warm-up tests. On the average, unstable CO conversion of 65-85% with a reactor exit temperature of 1300-1350°F, and 4.5-5.0%\*\* excess O<sub>2</sub> was observed. The insulated reactor tests (Fig. 4) exhibited a CO conversion of 73-93% with about 4% excess O<sub>2</sub> and a reactor exit temperature of 1500°F, for comparable air injection rates of 24-30%, ( $F' = .22-.26$ ).

Several modifications could be made to reduce reactor "light-off" time. Since reactor conversion efficiency at idle is primarily dependent on the reactor inlet temperature, the gas temperature at the reactor inlet can be increased by (1) reducing the length of the reactor inlet pipe and (2) by

---

\* When interpreting the first minute of Fig. 6, the thermal inertia of the thermocouple shield must be considered.

\*\* For Fig. 7, warm-up test 3. In Test 1, the excess O<sub>2</sub> is considerably higher due to the leaner mixture after 6.5 minutes.



pre-heating the secondary air. The former is far more practical. The modified A reactor used in the snowmobile had an extra long inlet pipe to facilitate installation. The inlet pipe length could be reduced by as much as 50%, which would reduce the heat losses between the exhaust port and reactor inlet. While the temperature increase would be small, in the idle temperature range (1200-1225°F), a small increase has a major effect on CO conversion. Pre-heating the secondary air would require some sort of heat exchanger and possibly a switchable injection system for high speed operation. It is doubtful that the air could be heated sufficiently since the exhaust system is relatively cool during the critical period following start-up.

## 2. Transient Deceleration and Idle Performance

### I. Introduction

After observing that the reactor would "light off" from a cold start within a given period of time, which was primarily dependent on "engine behavior", the question now became, "Will the reactor remain ignited during deceleration?" Unlike the cold-start test, the deceleration and idle tests closely simulated actual snowmobile operation.

Because the centrifugal clutch limits the engine to two basic modes: idle and moderate to full load, high speed operation, the reactor inlet gas temperature changed abruptly from 1500°F+ to 1200°F+ during deceleration, and back to 1500°F+ upon acceleration. For maximum CO and HC conversion, the reactor must remain ignited during deceleration and idle until the engine is put under load again.

To simulate the most adverse conditions for maintaining high CO and HC conversion, the engine was abruptly decelerated from the minimum operating speed and load, the clutch engagement point. This resulted in the lowest reactor temperature prior to deceleration. If 90%+ CO conversion could be maintained during this worst case deceleration, it is expected that the reactor will operate efficiently during deceleration from operating points with initially higher reactor temperatures.

The engine was decelerated from 3000 rpm, 6-7 in. Hg. intake vacuum, (at which point the reactor was "lit"), to 1500 rpm. Following the deceleration, the engine was allowed to idle for at least 5 minutes while the exhaust CO concentration and air injection rate were held constant.

The following idle combinations were tested:

<u>Reactor Inlet CO</u>	<u>Air Injection Mass Rate</u>
6%	27%, 32%, 35%
4.8%	32%
3.8%	32%, 35%

## II. Conclusions

While the deceleration tests were fairly repeatable, maintaining a constant engine exhaust CO at idle was still a major problem. Based on the deceleration tests completed, the following conclusions are drawn:

(1) When decelerating to idle from the worst reactor operating point, best CO conversion was obtained with a 1500 rpm idle speed, 5.5-5.8% exhaust CO with 29-33% air injection.

(2) Reactor inlet temperature is the most critical variable affecting optimum CO conversion during idle after deceleration.

(3) With idle mixtures leaner than 4.8% CO, CO conversion is unstable and may vary from 35-60%.

(4) CO conversion at idle could be improved by reducing the length of the reactor inlet pipe, pre-heating the injection air, or by diverting the cooling air from the cooling jacket, if one is used.

### III. Deceleration Test Procedure

The following procedure was used for every deceleration test.

With the snowmobile brake on, the engine was maintained at 3000 rpm, 6-7 in. Hg. intake vacuum until the reactor stabilized at 95% + CO conversion, then the throttle was closed. During deceleration, the secondary air was simultaneously reduced to the desired idle flow rate. The engine was then allowed to idle for a minimum of 5 minutes, while the exhaust CO and air injection rate were manually held constant. Exhaust temperature, exhaust CO and CO<sub>2</sub> concentration, reactor core temperature, and reactor exit CO concentration were recorded by strip chart recorders. The oxygen concentration at the reactor exit was manually recorded at 10 second intervals. The same sampling and analyzing system described in the warm-up tests was used. (see Fig. 3).

### IV. Deceleration Test Results

Of all the exhaust CO and air injection rate combinations tested (which were 6% CO with 27, 32, 35% air, 4.8% CO with 32% air, and 3.8% CO with 32 and 35% air), the test series with 6% exhaust CO exhibited best results.

Best CO conversion was repeatedly obtained when decelerating to a pre-set idle of 1500 rpm, 5.5-5.8% exhaust CO with 29-33% air injection. Even with this optimum air rate stable CO conversion was extremely sensitive to engine exhaust temperature. With exhaust temperatures above 1220°F, CO conversion was stable, but when the temperature dropped below

1200<sup>o</sup>F, the CO conversion became variable even with the optimum air injection rate.

Reactor inlet temperature during idle is the most critical variable affecting optimum CO conversion after deceleration. Unfortunately, the rich mixture (5-6% CO), required to maintain smooth engine idle limits the exhaust temperature to only 1200-1225<sup>o</sup>F. As a result, the secondary air must be carefully controlled to minimize its cooling effect, yet be of a sufficient amount to provide excess air to compensate for imperfect mixing and give good conversion efficiency.

Unlike the steady-state operation where optimum CO conversion could be maintained over a wide range of injection fractions, the secondary air had to be held within  $\pm 7\%$  of the optimum air flow during the deceleration tests. This corresponds to a range of only 0.05 F',\* compared to a range of 0.2-0.3 F for steady-state operation. Figure 4 indicates that by minimizing the reactor heat losses (in this case - insulating the reactor) optimum CO conversion was maintained over a broader range of .15 F'.

Increasing the reactor inlet temperature or possibly pre-heating the injected air would have the same effect as reducing heat losses. As previously mentioned, the reactor inlet temperature could be increased, without increasing the engine exhaust temperature by simply shortening the reactor inlet pipe. In an actual vehicle installation, the reactor will probably require some type of cooling jacket. If the cooling air were shut off during the idle mode, the jacket with a layer of stagnant air could

---

\*For the deceleration tests air injection fraction, F' was calculated from secondary air mass flow measurements as opposed to the carbon basis used in the steady-state testing calculations.

act as insulation to reduce reactor heat loss. Pre-heating the secondary air would definitely insure good CO conversion efficiency during long idle periods, but would require a switchable air injection system.

The best CO conversion results obtained are shown in Fig. 9. Despite the large variations in exhaust CO between 1/2 and 2 minutes after deceleration, once the engine exhaust CO concentration stabilized around 5.8%, stable CO conversion in excess of 90% was achieved. After 3 minutes, the exhaust temperature was between 1225-1230°F while the reactor core temperature remained above 1500°F. This compares with exhaust and reactor exit temperatures of 1225 and 1525°F, respectively for the insulated reactor with the same air injection fraction and 6% inlet CO (Fig. 4). Despite the lower reactor core temperature, due to reactor heat losses, the uninsulated reactor maintained stable CO conversion as long as the exhaust temperature was above 1220°F.

In order to bracket the optimum air injection range, deceleration tests with 27%, ( $F' = .25$ ) and 35% ( $F' = .33$ ) air injection rates were also conducted. As shown in Fig. 4,  $F' = .25$  is near the minimum injection fraction for stable CO conversion, while  $F' = .33$  would provide sufficient excess air to compensate for imperfect mixing. Although CO conversion was partially limited in both deceleration tests by low engine exhaust temperature, conversion was probably governed by insufficient air with 27% air and by the cooling effect of the excess air with 35% air.

Despite the 1500+°F reactor core temperature during the first 1-1/2 minutes following deceleration (Fig. 10), CO conversion was below 90%.

This suggests that CO conversion was limited by insufficient secondary air. Twenty seconds after the end of the deceleration cycle, the exhaust CO stabilized around 6% with a reactor core temperature of 1550°F. At this temperature, CO conversion should exceed 90% if sufficient air is present.

The reduced CO conversion may have been partly caused by the low exhaust temperature of 1190-1200°F which resulted from the slightly richer operation (6.3% CO) during the first 2.5 minutes. After four minutes, the average exhaust CO was reduced to 5.9% which resulted in a 10°F increase in the exhaust temperature. Even this slight reduction in exhaust CO and increase in exhaust temperature had a significant effect on CO conversion efficiency. The steady increase in reactor core temperature and decrease in reactor CO can be seen in Fig. 10 from 3 minutes on, as the exhaust CO decreased from 6.3 to 5.9%.

When the air injection rate was increased to 35%, ( $F' = 33$ ) the stable 90% + CO conversion efficiency deteriorated to 25-35%. Figure 11 shows that after 1.5 minutes, the exhaust CO remained fairly constant at 6% with an exhaust temperature of about 1200°F, which would normally result in at least 50%+CO conversion. But once the reaction is extinguished the cooling effect of the secondary air causes the reactor core temperature to decrease with time. Once the reactor core temperature decreased to less than 1100°F after 5 minutes, there was little possibility of "light off" occurring during the idle mode.

As previously mentioned, the engine exhaust CO decreased

as the engine became warm, which resulted in a rough idle with 3.8-5% exhaust CO. To determine what effect the lower reactor inlet CO, but higher inlet temperatures have on the CO conversion at idle, deceleration tests with exhaust CO concentrations of 4.8% and 32% air injection, and 3.8% with 32% and 35% air injection were conducted.

With 4.5-4.8% CO, the exhaust temperature increased to 1260<sup>o</sup>F (from 1225<sup>o</sup>F with 5.8% CO), but with 32% air, the CO conversion was only between 35-50%. Once the reactor cooled down from the initially "lit" condition, the reactor core temperature decreased to about 1100<sup>o</sup>F, while the exhaust temperature remained at 1260<sup>o</sup>F. It appears the only significant CO conversion occurred near the air injection port where the exhaust temperature was high. Apparently, the temperature increase from the oxidation of 1-2.0% CO in this region is not sufficient to overcome the cooling effect of the secondary air and the reactor heat losses.

Relatively stable, but non-repeatable, CO conversion of 70-80% was achieved with 3.8-4.0% reactor inlet CO and 35% air injection. The leaner mixture resulted in an exhaust temperature of about 1250<sup>o</sup>F. But when the injected air was reduced to 32%, to reduce the cooling effect of the excess air, the CO conversion decreased to 40-60%. Rough idling at this lean mixture (3.8% CO) caused considerable test-to-test variations, but generally the CO conversion was unstable and ranged between 40-80% with 32-35% air injection.

We conclude that exhaust concentrations of less than 4.8% CO result in non-repeatable CO conversion efficiencies of between 35-60%, with



occasional conversion of up to 80%. This leaner mixture also results in erratic engine idle.

A comparison of the temperature traces in Figures 10 and 11 illustrate how the exhaust temperature is affected by reactor temperature. The engine CO traces after 3 minutes for both tests are almost identical, yet the exhaust temperature with 35% air averages only 1175°F, while with 27% air averages 1210°F. This is not the result of an actual difference in exhaust gas temperature, but a difference in temperature in the area of the exhaust thermocouple. This temperature difference results from heat transfer to the area from a "hot" reactor, or heat transfer away from the area to a "cool" reactor. With a relatively constant exhaust CO (constant exhaust gas temperature), the exhaust area temperature follows the trend of the reactor core temperature.

As a result of this "feedback" effect, a 25°F increase in exhaust gas temperature may cause "light-off", which in turn raises the exhaust area temperature to further promote the "light-off". Similarly, if the reactor does not "light-off", the lower reactor temperatures decrease the temperature in the critical reactor inlet area, which reduces any chance of "light-off".

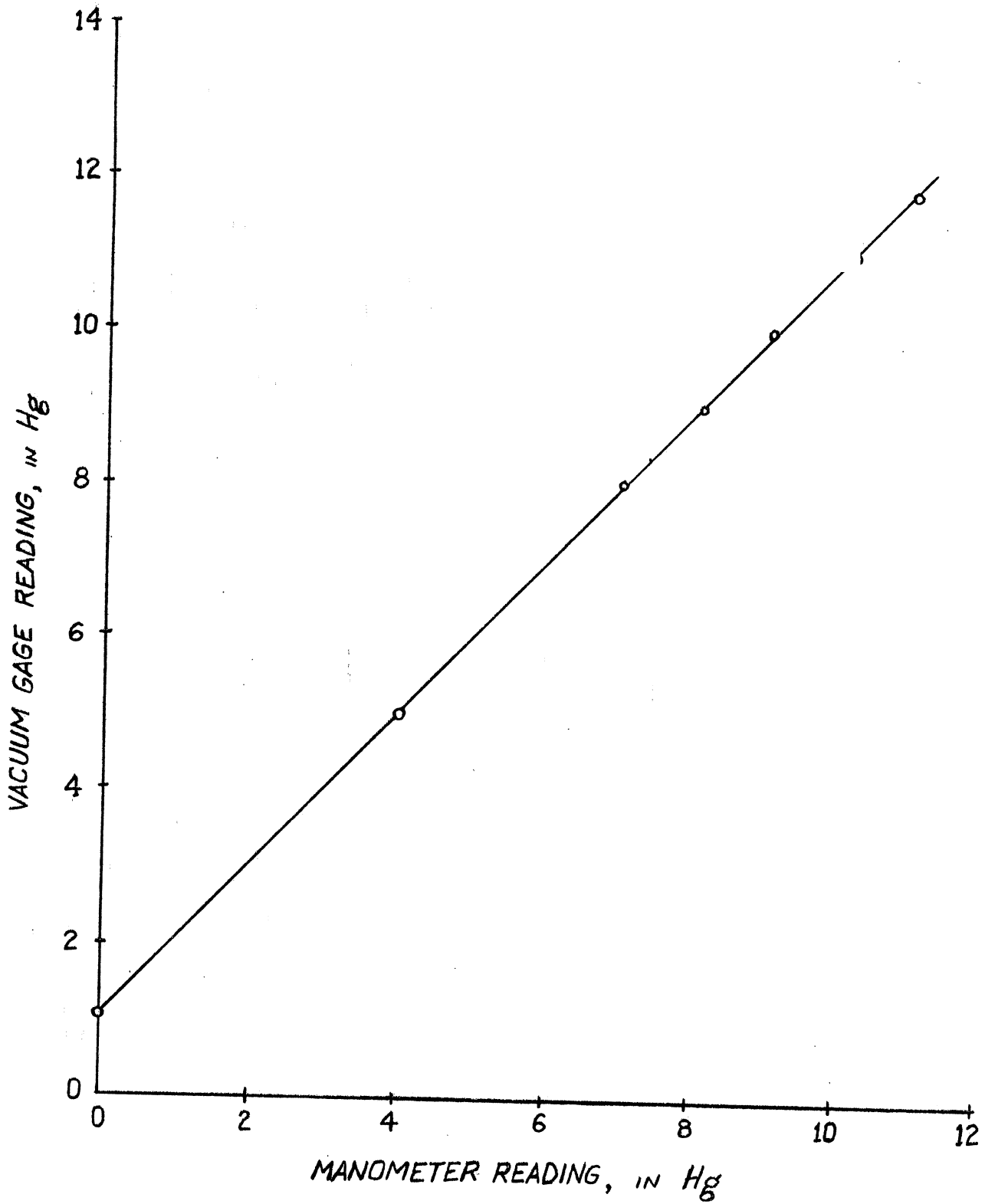


Fig. 1 - Calibration of Vacuum Gage installed on OMC Snowmobile

$V = 80 \text{ IN}^3$

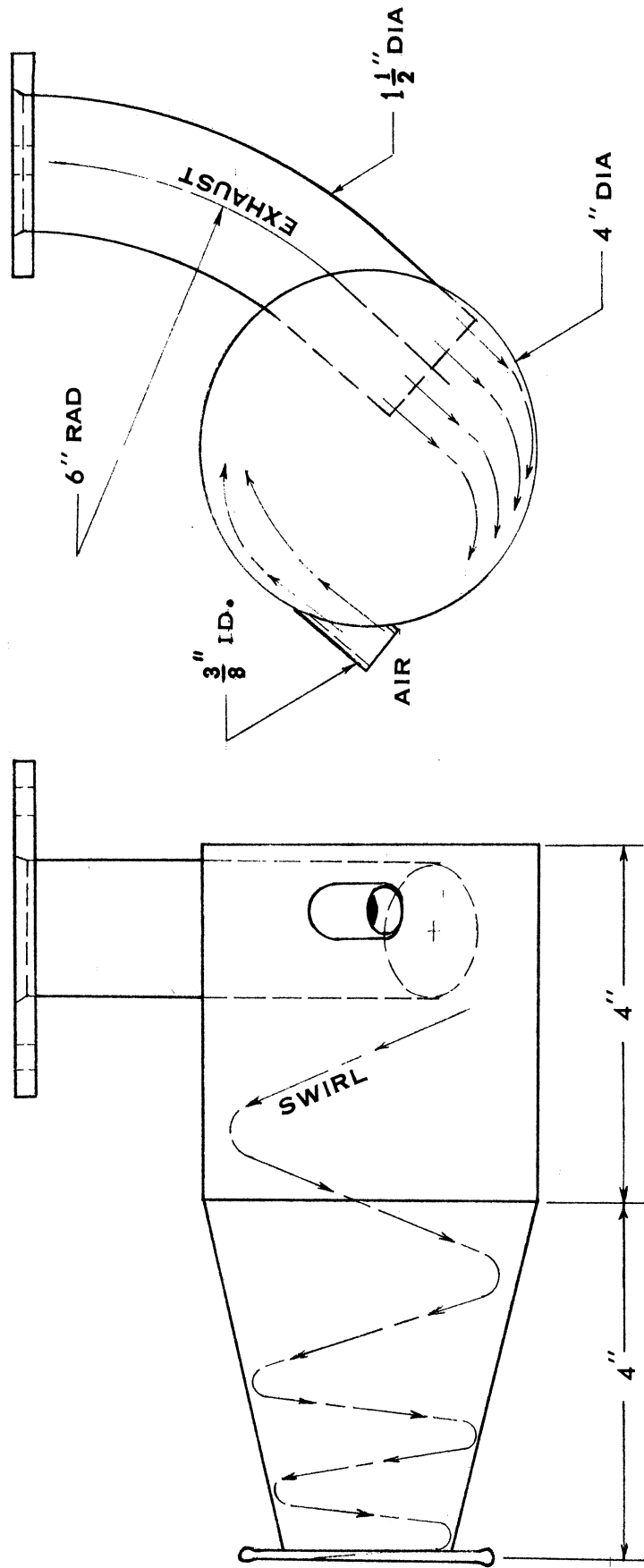


FIG 2 - MODIFIED MODEL A REACTOR

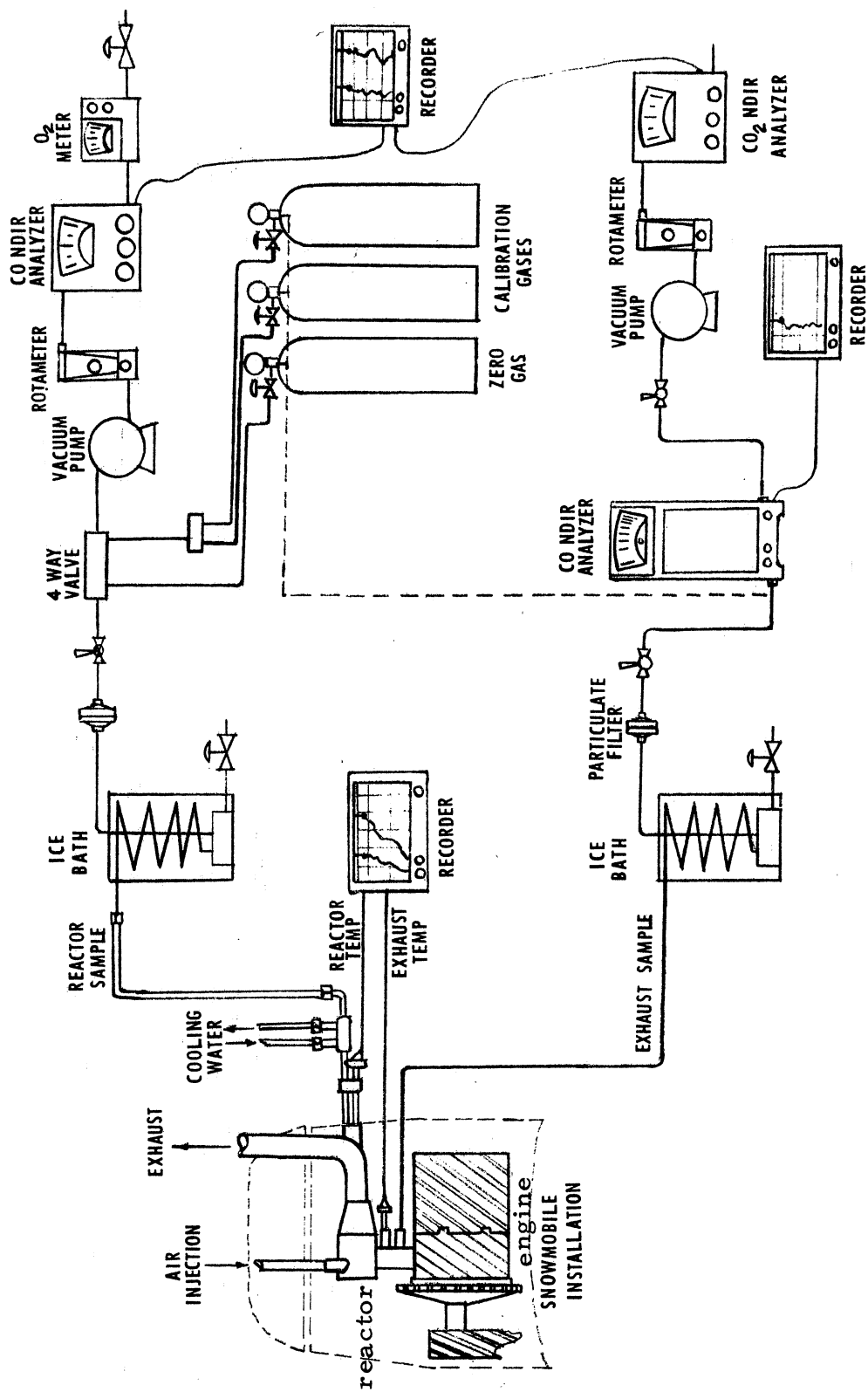


Fig. 3 - Schematic of exhaust gas sampling and analysis system used for testing transient reactor performance.

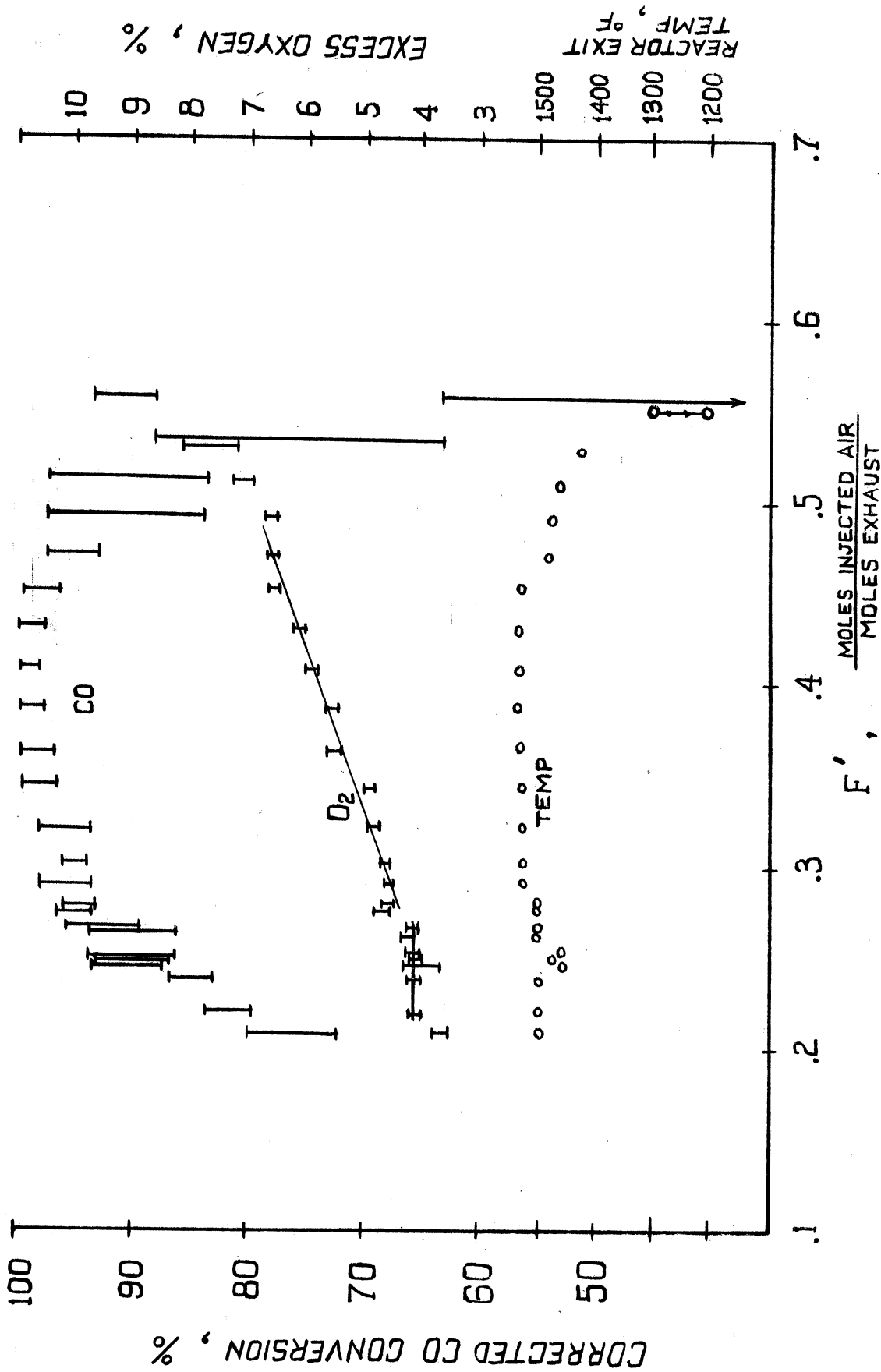
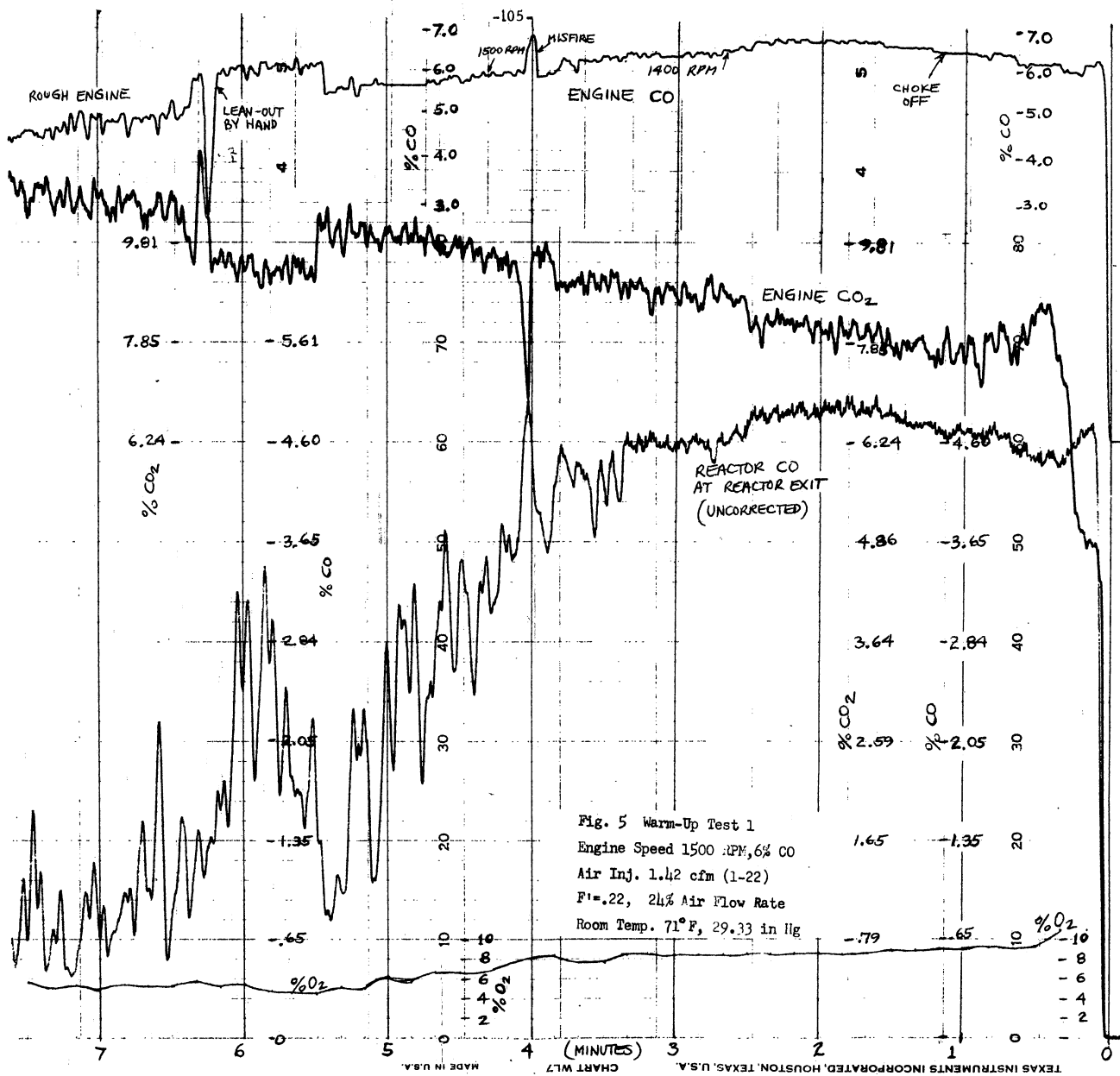


Fig. 4 - CO conversion vs.  $F'$  for modified Model A Reactor on OMC snowmobile at idle. Engine: 1500 rpm, 12 in. Hg. intake vacuum,  $\dot{m} = 25$  lbm/hr. Reactor: 6% CO in , inlet temperature = 1225°F. Reactor completely insulated with 1 inch of Kao -Wool.



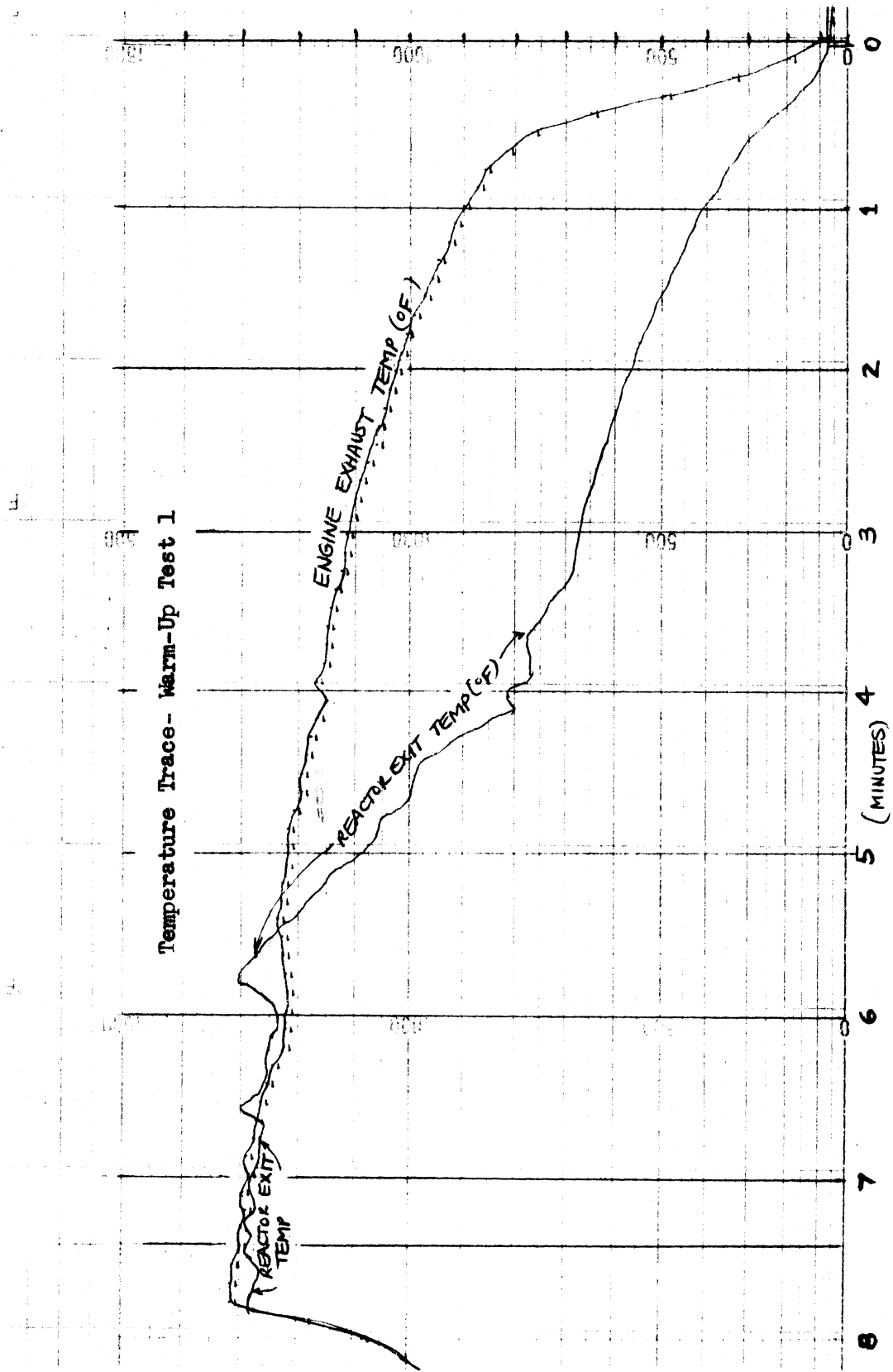
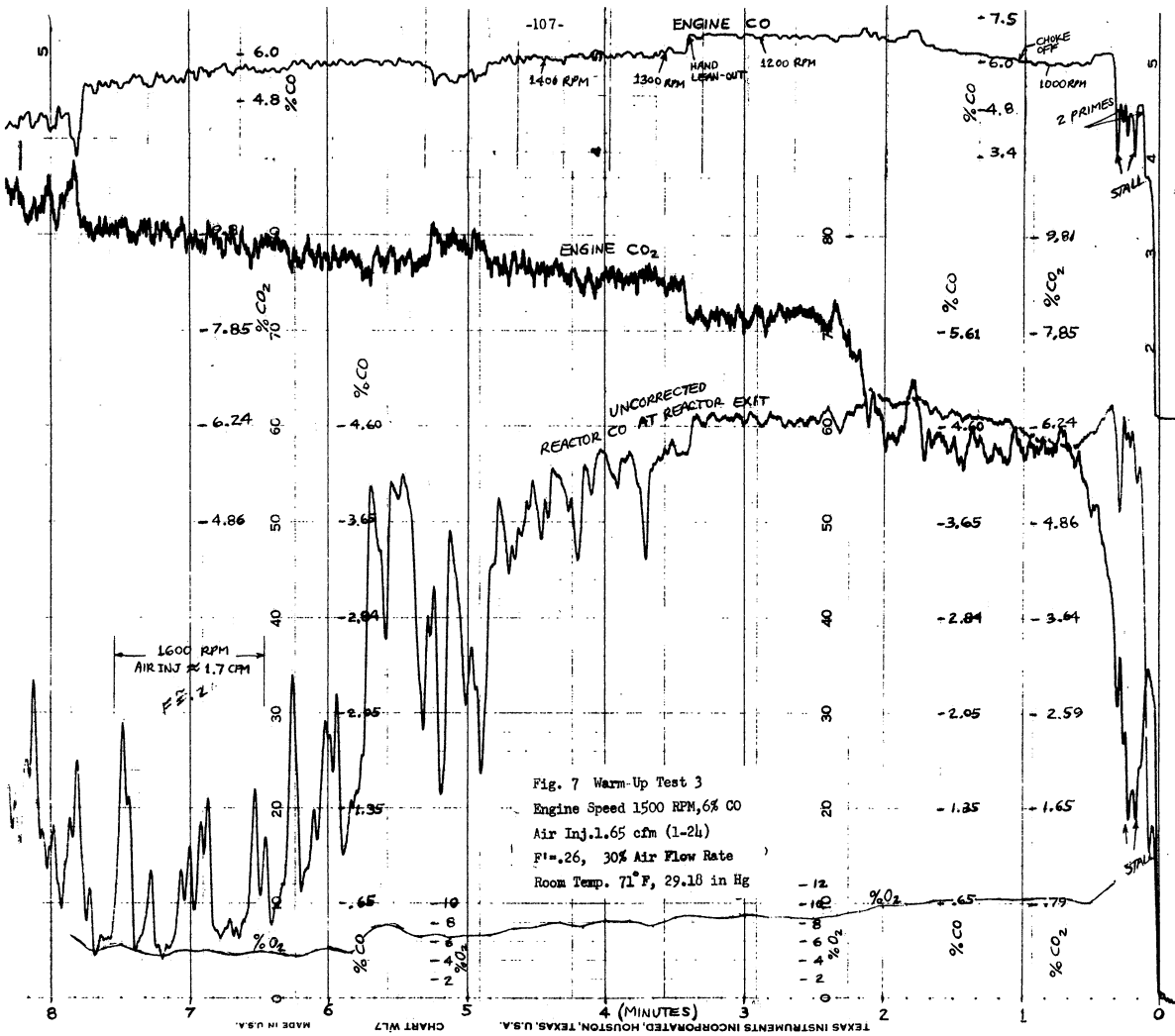


Figure 6





Typical CO Behavior During A Warm-up Test

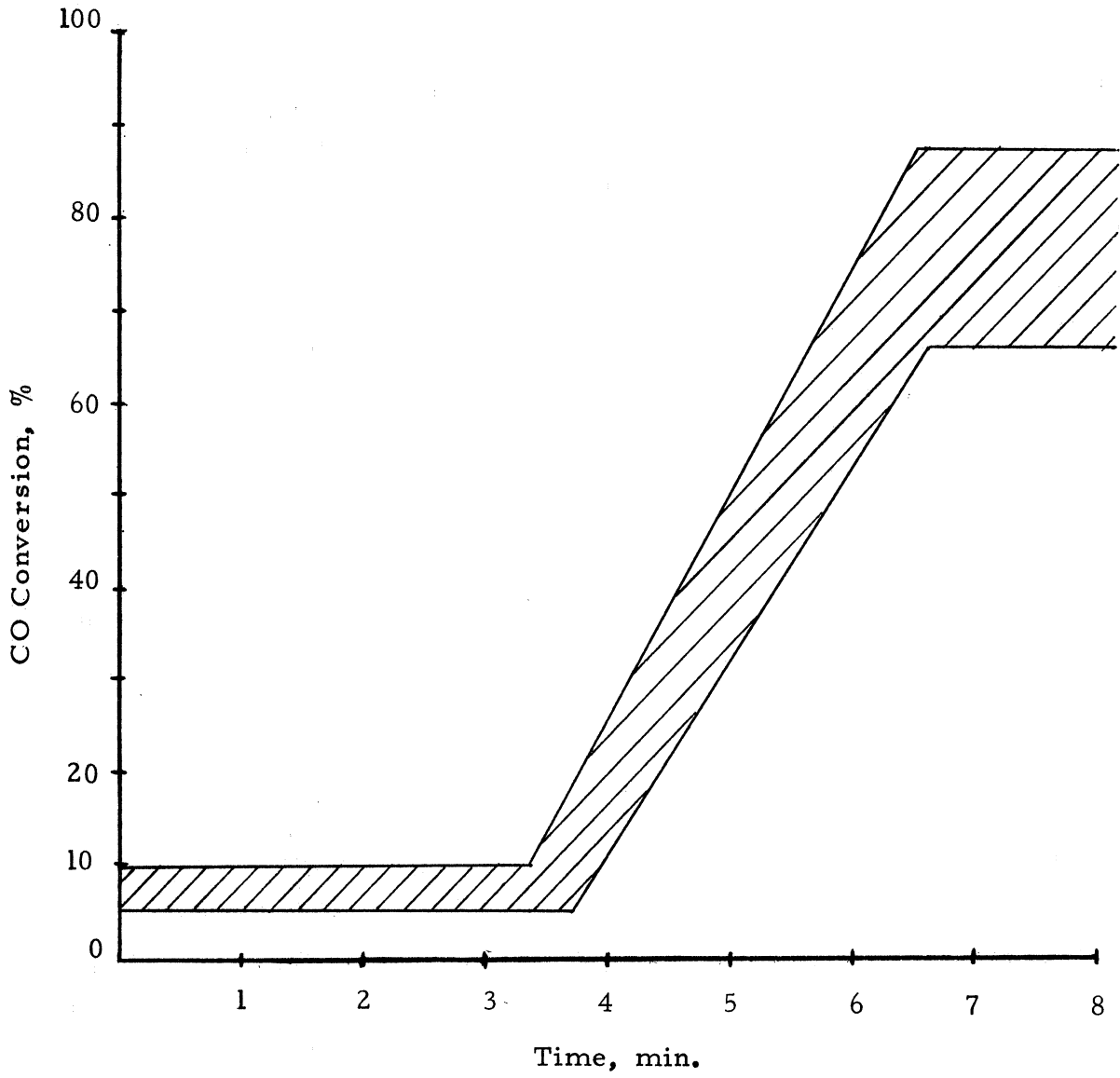
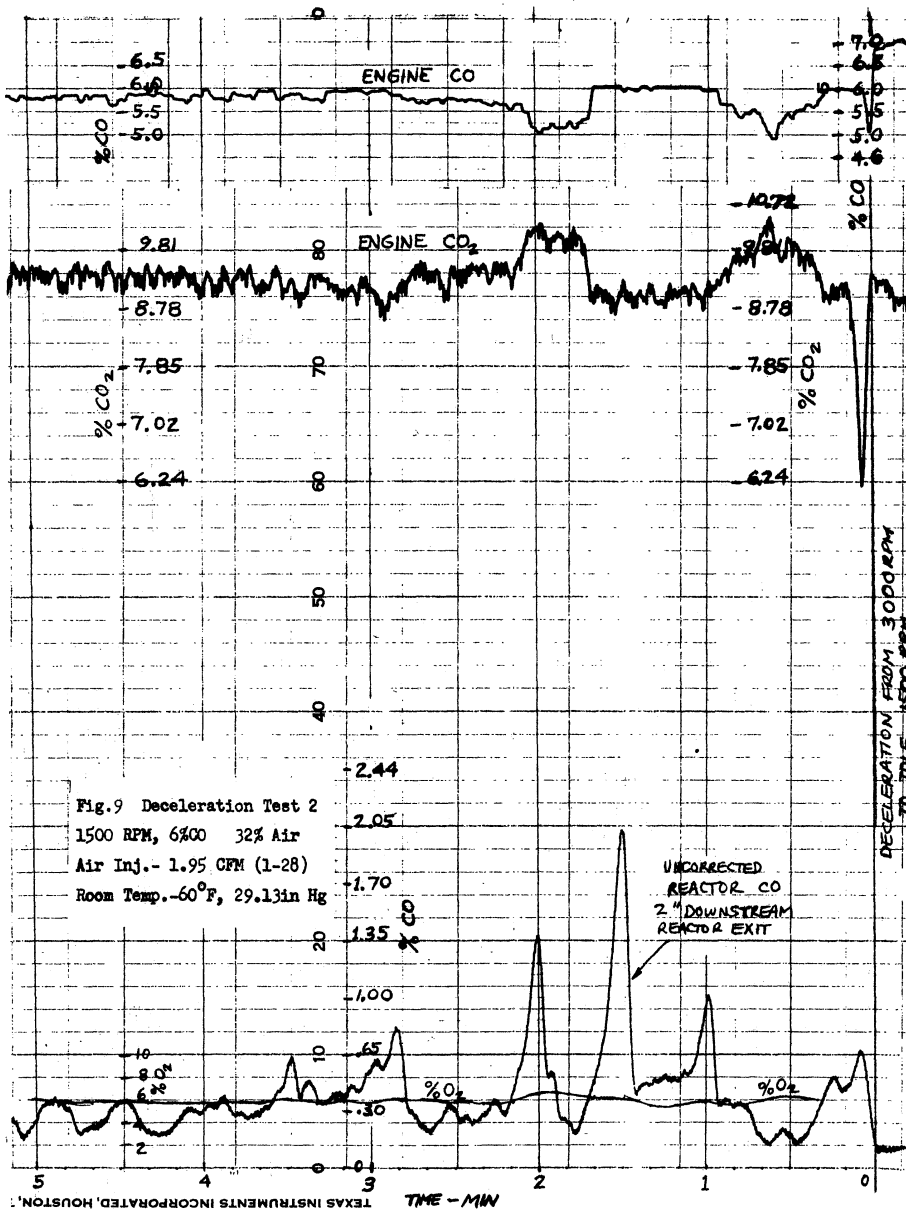
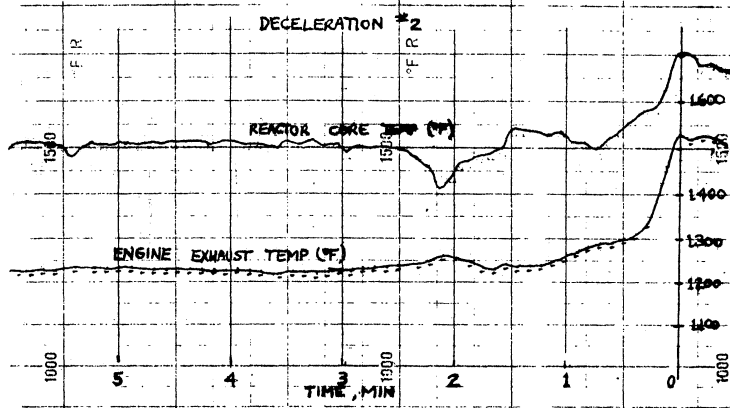
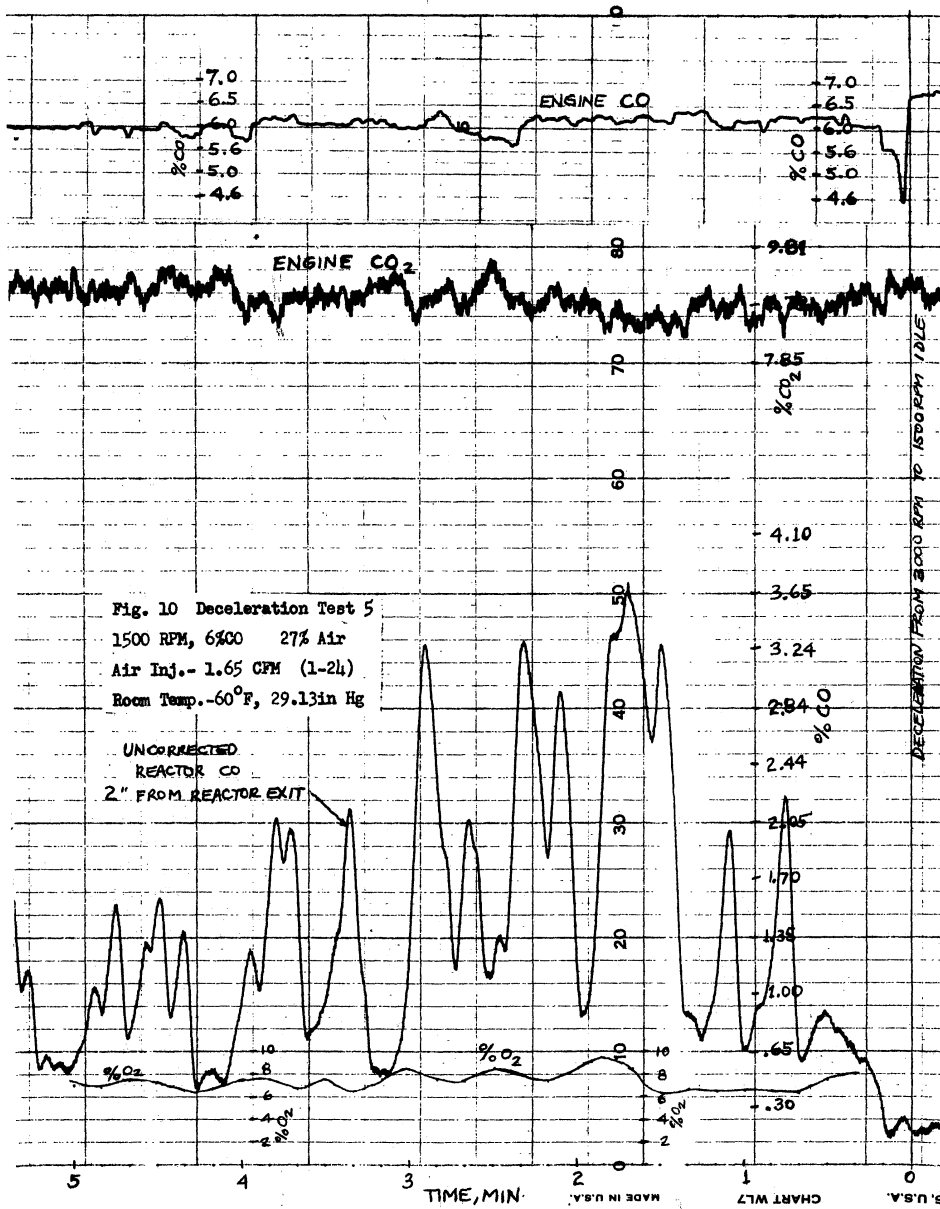
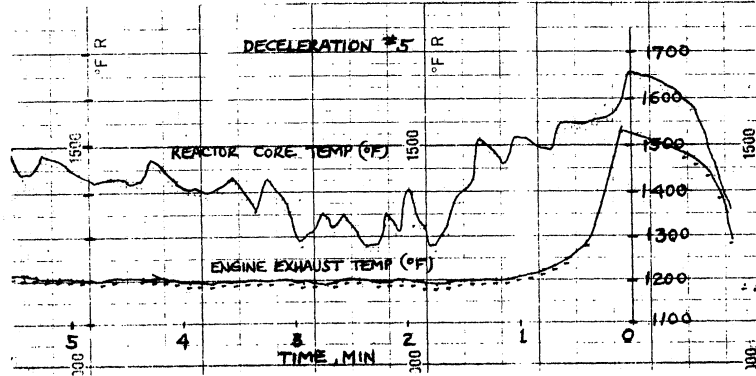


Figure 8





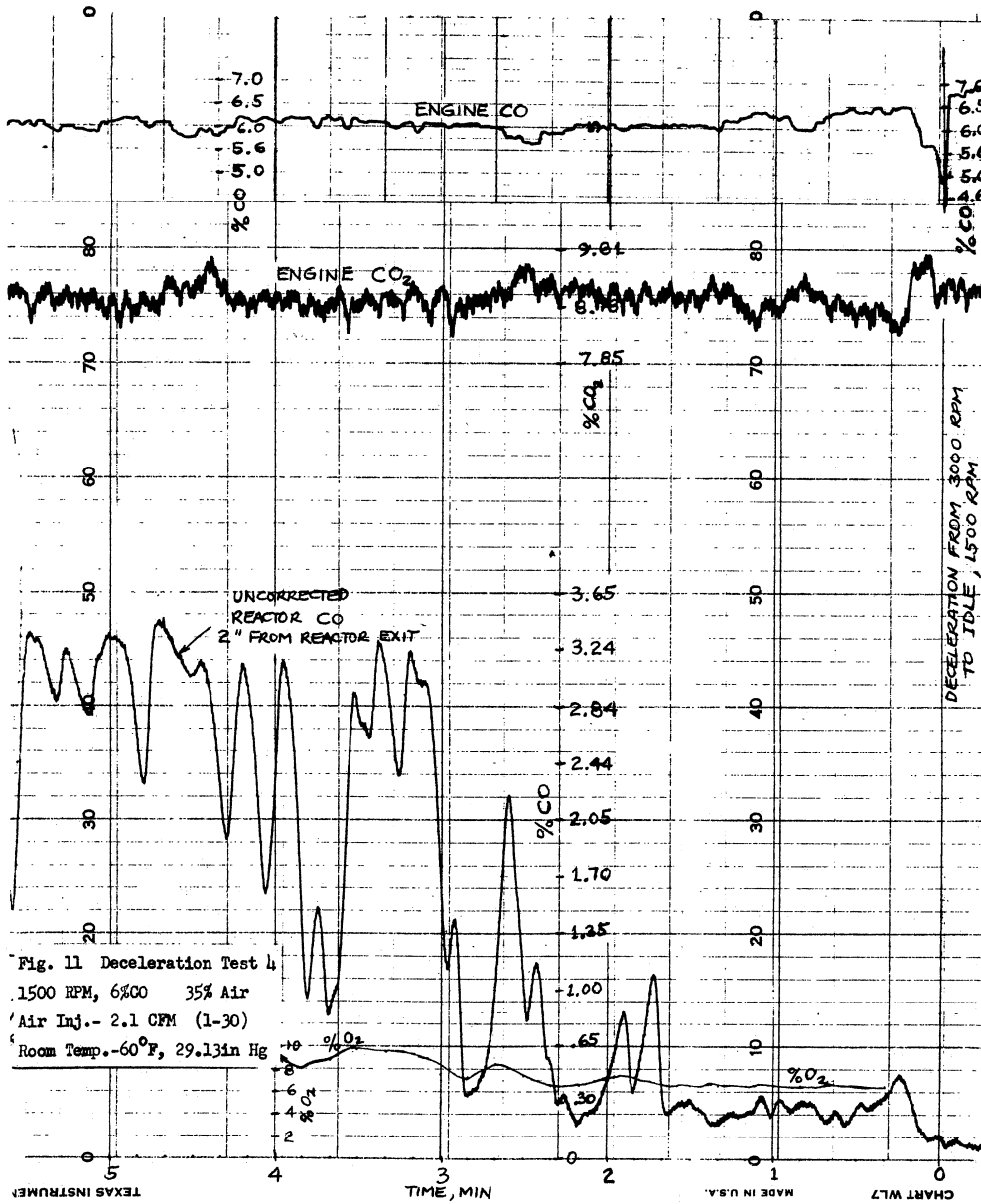
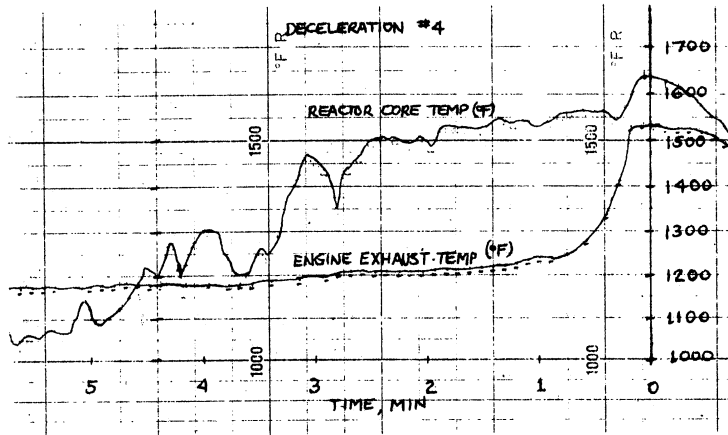


Fig. 11 Deceleration Test 4  
 1500 RPM, 6%CO 35% Air  
 Air Inj.- 2.1 CFM (1-30)  
 Room Temp.-60°F, 29.13in Hg

PHASE III

EFFECT OF VOLUME AND GEOMETRY VARIATIONS ON  
THE STEADY-STATE PERFORMANCE OF SIMILAR REACTORS

	<u>Page</u>
I. Introduction	114
II. Conclusions	115
III. Test Equipment	118
A. Low HC Sampling Circuit	118
B. Engine Exhaust Temperature Measurement	119
IV. Test Procedure	119
V. Discussion	120
A. Performance Comparison of the Various Reactors	121
B. Overall Performance Characteristics of Each Reactor	122
C. Performance Characteristics Within Each Reactor	124
D. Theoretical Design Considerations	128
1. UM-CRC Dynamic Patterns of Flow	128
2. Two-Stirred Tank Model	128
a. Theory	128
b. Comparison of Theoretical Predictions with Experimental Results	131
c. Computer Predictions	134
3. Concluding Remarks	135
VI. References to Phase III	136
Appendix	
A. Typical Engine Characteristics with Reactor and Secondary Air	158
B. UM-CRC Computer Program Development	159
Distribution List	167

## I. Introduction

The purpose of this final phase of testing was to determine the effect of moderate volume and geometry changes on the steady-state CO and HC conversion efficiency of the Model A reactor design. This information provides guidelines for designing reactor configurations that might be required for a given application or for manufacturability considerations.

Three variations of the A reactor were built and tested. These were termed reactors C, D, and E. Reactors C and D were cylindrical in cross-section, but had less volume than reactor A, while reactor E had approximately the same volume as A, but had an elliptical cross-section. The same air injection configuration and air nozzle size were used for reactors A, C, D, and E. The B reactor, which was discussed in Phase I, was similar to A except that it had a different air injection configuration. Specifications for the A, B, C, D, and E reactors are given in Table 1.

The steady-state performance of the C, D, and E reactors was tested at the same operating conditions and by the same procedure used to test reactors A and B in Phase I. Each reactor was tested at 3000 RPM, 24 ft-lbf and 4000 RPM, 27 ft-lbf, steady-speed and fixed throttle, while the air-fuel ratio was manually adjusted to maintain a constant CO and CO<sub>2</sub> input to the reactor. Exhaust gas temperature, CO, CO<sub>2</sub>, HC, NO, and O<sub>2</sub> concentrations were measured at the exhaust port and at various positions along the reactor centerline. With the exception of the "low HC" circuit and the shielded exhaust port thermocouple, the test equipment and exhaust analysis system used was the same as described in Phase I.

Analysis of the steady-state reactor conversion efficiency has been divided into three sections:

Comparison of CO conversion of the A, B, C, D, and E reactors as a function of air injection fraction at 3000 RPM, 24-ft-lbf, and 4000 RPM, 27 ft-lbf.

. HC and CO conversion and temperature for each reactor as a function of air injection fraction at 3000 RPM, 24 ft-lbf, and 4000 RPM, 27 ft-lbf.

. CO concentration and temperature at various positions along the centerline of each reactor (A, B, C, D, and E) as a function of air injection fraction at 3000 RPM, 24 ft-lbs.

Using the experimental data, a simplified theoretical model was developed, and the predictions from this model were compared to the experimental results.

## II. Conclusions

1. Under steady-state operation, 3000 RPM, 24 ft-lbs, reactors C, D, and E provided 90% + CO conversion for air injection fractions,  $F$ , between .15 and .45. Maximum CO conversion for these reactors was 95%.

2. At 4000 RPM, 27 ft-lbs, the smaller reactors, C and D, provided 90% + CO conversion for air injection fractions between .23 and .48.

The three larger reactors, A, B, and E, provided 95% + CO conversion over a wide range of injection fractions ( $F = .23$  to  $.55+$ ).

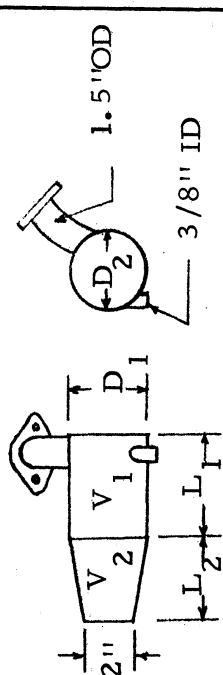
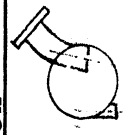
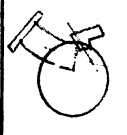

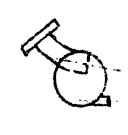



3. The A reactor provided the highest CO conversion, 97-99% +, over the widest range of air injection fractions of all the reactors tested. It is the best design.

4. Generally, HC conversion for the A, C, D, and E reactors exceeded 95% for air injection fractions between .1 and .4 at 3000 RPM, 24 ft-lbf and between .1 and .5 at 4000 RPM, 27 ft-lbf.

5. A two-stirred tank model predicts the experimental data reasonably well, but more data is needed at lower CO conversions to verify the model.

TABLE I

		Thermal Reactor Configurations						
Reactor	End View and Air Injection Position	D <sub>1</sub> (in)	D <sub>2</sub> (in)	L <sub>1</sub> (in)	L <sub>2</sub> (in)	V <sub>1</sub> <sup>3</sup> (in <sup>3</sup> )	V <sub>2</sub> <sup>3</sup> (in <sup>3</sup> )	V <sup>total</sup> (in <sup>3</sup> )
A		4	4	4	4	50	30	80
B		4	4	5	3	62	22	84
C		4	4	2	4	25	30	55
D		3.25	3.25	4	4	33	19.5	52.5
E		5.5	3	4	4	52	22.5	74.5

### III. Test Equipment

The same test equipment and exhaust analysis system (Fig. 1) used for the steady-state testing of Reactors A and B, (described in Phase I) was used to test Reactors C, D, and E. Two significant changes were made however, (1) a separate sampling circuit was added to measure the low HC concentrations downstream of the reactor, and (2) the chromel-alumel bayonet thermocouple used to measure engine exhaust temperature was replaced with a specially shielded platinum-platinum, 13% rhodium thermocouple.

#### A. Low HC Sampling Circuit

The error in HC measurement due to "hang-up" in the sample lines was minimized, if not eliminated, by the installation of a separate low HC sampling circuit. Since the air injection fraction was calculated from measurements of the diluted and undiluted exhaust, the raw exhaust and treated exhaust had to be alternately sampled through the same sampling and analysis system. This resulted in HC "hang-up" in the sample lines. With the separate "low HC" circuit shown by the dotted lines in Fig. 1, only the two feet of tubing between the 4-way valve and FID analyzer, was exposed to the raw exhaust. This short section of tubing was quickly purged when low HC concentrations were measured.

During calibration, the zero point for the low HC circuit was set by introducing dry N<sub>2</sub> into the sample line at the reactor probe. Using this technique, the background for the entire "low HC" sample line was zeroed-out.

## B. Engine Exhaust Temperature Measurement

The shielded platinum-platinum, 13% rhodium thermocouple designed and built for Phase II testing was used to measure engine exhaust temperature. This resulted in two improvements, (1) it reduced the error in temperature measurement due to the radiation losses observed with the un-shielded chromel-alumel thermocouple, and (2) it allowed the exhaust temperature to be printed out on the Westronics strip recorder along with the reactor temperature.

## IV. Test Procedure

All data were taken at steady-state, fixed throttle with constant CO and CO<sub>2</sub> input to the reactor. For each test point, the air-fuel ratio and secondary air were held constant. Temperature, CO, CO<sub>2</sub>, HC, NO, and O<sub>2</sub> oxygen concentrations were measured at the exhaust port using the "high HC" circuit, and then the same measurements were made in and downstream of the reactor using the "low HC" circuit. The "low HC" circuit was never exposed to untreated exhaust. Sufficient time was allowed for all readings to stabilize, and the exhaust port was sampled repeatedly to ensure the reactor input remained constant while measurements were made in and downstream of the reactor. This alternating sampling technique was used for each reactor position and air injection fraction tested.

Engine parameters including speed, load, temperatures, back pressure, air flow, and fuel flow were also measured during each run so that any variation in engine operation could be detected.

## V. Discussion

The data presented in Figures 2 thru 18 are intended to provide design guidelines for determining the best reactor configuration for a given application. Using these results, the designer can estimate the effect moderate volume and geometry changes would have on the conversion efficiency of the basic tangential-swirl reactor design. Some theoretical guidelines are also presented at the end of this discussion.

The experimental results are presented in three general groups:

- A. Performance comparison of the various reactors - Figs. 2 and 3 compare the CO conversion of the A, B, C, D, and E reactors as a function of air injection fraction.
- B. Overall performance characteristics of each reactor - Figs. 4 thru 13 show the HC and CO conversion and reactor temperatures for reactors A, C, D, and E as a function of air injection. HC and oxygen concentrations are also shown for reactors C, D, and E.
- C. Performance Characteristics within each reactor - Figs. 14 thru 18 show the CO concentration and temperature at selected points along the centerline of each reactor (A, B, C, D, and E) as a function of air injection fraction.

### A. Performance Comparison of the Various Reactors

All five reactors provided CO conversion of 90%+ over a wide range of air injection fractions (F). At 3000 RPM, 24 ft-lbf (Fig. 2) the C, D, and E reactors provided approximately the same maximum CO conversion efficiency ( $\approx 95\%$  at  $F = .25$ ), and maintained this level up to  $F = .38$ . For air injection fractions greater than .38, the CO conversion efficiency of the smaller C and D reactors (55 and 52.5 in<sup>3</sup>, respectively) decreased more rapidly than for the larger E reactor (74.5 in<sup>3</sup>).

This sharper decrease in conversion in the smaller reactors was caused by several interrelated factors, primarily decreased residence time and mixing, coupled with increased air injection cooling and lower heat losses. The decrease in residence time is thought to be the major factor. (It is beyond the scope of this research to predict the relative importance of each factor).

Reactors A and B provided CO conversion in excess of 95% between  $F = .17$  and  $.5$ . While both reactors achieved maximum conversions of 98%+, reactor A maintained a higher level over a wider range of air injection fractions. CO conversion began to decrease sharply for the B reactor beyond  $F = .45$ . This was previously discussed in Phase I (page 32).

While the difference in CO conversion efficiency between the A and B reactor for  $F > .3$  was small, it must be emphasized that there is a fivefold CO reduction between 95 and 99% conversion. This difference may become

significant if high air injection fractions are required to control reactor temperatures or if stringent emission standards have to met.

At 4000 RPM, 27 ft-lbf, (Fig. 3) the difference in CO conversion between the larger reactors (A, B, and E) and the smaller reactors (C and D) became more distinct. The A and B reactors were superior, with CO conversion of 98%+ for  $F > .3$ . Reactor E achieved 97% conversion at  $F = .27$  and maintained this level to at least  $F = .55$ . The maximum CO conversion for the A, E, C, and D reactors was directly related to their volume, with reactor A having the largest volume. Reactor B had a different air injection configuration which had a negative effect on the conversion efficiency.

The smaller C and D reactors achieved a maximum CO conversion of about 95% and maintained this level over a range of only  $F = .2$ . The minimum air injection fraction required for maximum conversion cannot be determined from Fig. 3, because there are insufficient data points in the region between  $F = .1$  and  $.23$ . For  $F > .4$ , the conversion efficiency of both reactors decreased rapidly.

Reactor volume (residence time) appears to have a major effect on the maximum CO conversion level reached, and the range of air injection fractions over which this level can be maintained.

#### B. Overall Performance Characteristics of Each Reactor

Figures 4 thru 13 show the CO, HC, temperatures, and excess oxygen for the A, C, D, and E reactors as a function of air injection

fraction at the two steady-state test conditions. These graphs will not be discussed in detail but have been included to provide a visual comparison showing the magnitude of the temperatures and exhaust concentrations that can be expected at 3000 and 4000 RPM, moderate load operation. However, these graphs illustrate some important points that should be mentioned.

Although the HC and CO conversion efficiencies of reactors A and B were discussed in Phase I-Figs. 18 thru 22, Fig. 4 was included to provide a comparison between the data taken with the original sampling system and the data taken with the improved sampling system. The data of Fig. 4 were obtained using the "low HC" sampling circuit, which gives a more accurate measure of the magnitude of the HC reduction. This data may be compared to the earlier data shown in Figs. 20 and 21 of Phase I. Although the B reactor was not retested using the "low HC" circuit, it is expected that the difference in HC conversion efficiency would be similar to that of the A reactor.

As expected, HC conversion was higher than CO conversion for reactors C, D, and E at the operating points tested (Figs. 5, 6, 8, 9, 10, 12). For the A reactor (Fig. 4), CO conversion was slightly greater than HC conversion, but both conversion efficiencies are so high that the remaining unconverted differences are difficult to judge. HC concentrations are typically reduced to 20-25 ppm, as shown in Figs. 7, 11, and 13. The magnitude of the reduction and air injection range over which this reduction can be maintained depended on the particular reactor design. Figures 7, 11, and 13 also show that the oxygen concentration increases linearly for air injection fractions greater than  $F = .1$ . At the air-fuel ratios used in these tests,



$F = .11$  would provide a stoichiometric mixture in the reactor. Thus, the linearly increasing oxygen is predicted from excess combustion air.

No temperature traces are shown for the C, D, and E reactors at 4000 RPM, 27 ft-lbs because the reactor thermocouples failed during these tests. For each reactor, the 3000 RPM, 24 ft-lb. tests were completed before beginning the higher speed tests. The thermocouples failed early in the 4000 RPM tests of the C and D reactors. Because of the high cost of making the 16", platinum-platinum, 13% rhodium thermocouples, no attempt was made to measure the temperature in reactor E at 4000 RPM.

The thermocouple did not fail during similar testing of the A and B reactors. All thermocouples were made from the same spool of wire and by the same procedure. Apparently, the temperatures and pressure pulses in the smaller reactors present a more hostile environment.

#### C. Performance Characteristics Within Each Reactor

The corrected CO concentration and temperature at various positions along the centerline of each reactor are shown in Figs. 14 thru 18. These graphs are a good indication of how effectively the volume of each reactor is utilized for CO conversion at the 3000 RPM test point.

A comparison of the CO concentration at position 1 in each reactor shows that with optimum secondary air more than 75% of the CO had been converted at this point in the A, B, and C reactors. But only about 50% of the CO had been converted at the same position in the E reactor. Measurements

taken at position 1 in the D reactor (not shown in Fig. 17) showed substantial scatter, which suggests that the mixing in this region was extremely poor.

In reactor A (Fig. 14), more than 90% of the CO had been converted at position 2 with F between .17 and .45. The final 7 to 9% reduction occurred in the tapered section and in the following 1-1/2 inch section of exhaust pipe. Additional measurements taken 10" downstream from the reactor exit showed CO and HC conversions of almost 100% for F between .25 and .40. The CO concentration curve for position 1 is dotted to indicate scattered data from a poorly mixed, lean mixture at this point. If the exhaust gas and secondary air were perfectly mixed, the dotted curve would be shifted to the left so that the first data point (at F = .2) would approach the first data points for positions 2 and 3 at F = .1. As would be expected, the maximum reactor temperature occurred between F = .1 and .2 (for positions 2 and 3). The stoichiometric reactor mixture is at  $F \approx .11$ .

The CO profile for the B reactor (Fig. 15) is similar to that for reactor A, except that the exhaust products and secondary air appear to be more uniformly mixed at position 1. This is based on the observation that the dotted CO concentration curve at position 1 almost coincides with the curves for positions 2 and 3. The decrease in CO conversion and reactor temperature at position 2 for  $F > .28$  suggests that with high air injection rates the reaction moves further downstream in the reactor.

In reactor C (Fig. 16), the CO concentration and temperature are almost constant at positions 1 and 2. No significant conversion occurred

between these two points, but it should be noted that these points are also relatively close together in this design. Again, the shifting to the right of the CO concentration curves for positions 1 and 2 suggests non-uniform mixing in these regions.

The D reactor's smaller diameter (3-1/4") appears to have an adverse effect on the mixing of exhaust gas and secondary air in the reactor inlet region. Temperature and CO measurements taken at position 1 (Fig. 17) showed substantial scatter, which indicated that mixing was extremely poor in this region. Judging from the slight shift between the position 2 and 3 CO concentration curves, the exhaust gas and air are fairly well mixed at position 2. As the air injection fraction is increased beyond .38, the CO concentration increased sharply.

The reactor inlet temperature for reactor D was about 50°F higher than for reactors B, C, and E. This was primarily caused by poor engine gas seals.

The most obvious feature of the E reactor (Fig. 18) is the very poor mixing at position 1. The extreme shifting of the CO concentration curve at position 1 relative to position 3 indicated excess air at position 1. The color of the reactor metal during the tests suggested that the majority of reaction in the elliptical section occurred in the lower half of the reactor. The exhaust is directed toward the bottom of the reactor where the metal glows dull red, while the secondary air flows to the top of the reactor where the metal is always dark. Apparently, considerable mixing does not occur until just ahead of the tapered section.

The minor diameter of the E reactor may be too small to develop good mixing near the reactor inlet. Mixing could be improved by changing the air injection angle. Pointing the air nozzle toward the bottom of the reactor where the exhaust enters should improve mixing in the reactor inlet region.

This experimental data (Figs. 4 thru 18) has been included to provide directional design information for modifying the basic Model A design for adaption to a particular vehicle package.

## D. Theoretical Design Considerations

### 1. UM-CRC Dynamic Patterns of Flow Model

Initial theoretical predictions of reactor performance were made using the existing UM-CRC Dynamic Patterns of Flow Computer Simulation. A number of improvements were made in the model some of which related specifically to prediction of Wankel engine reactor performance. These are summarized in Appendix B.

Calculations showed that the Model A reactor should be quite efficient (as it was) with CO conversion of 90% and HC conversion of 93% - run 1-10 of Appendix B. Actually the experimental reactor results showed better conversion in the upstream sections of the reactor than the computer predicted. Low estimated reaction rates and better mixing in the test reactor were thought responsible. Table II of Appendix B describes calculations with varying mixing and reactor volume.

Subsequently a simpler two-stirred tank model with improved kinetics was developed which is thought to more accurately fit the particular reactor designs of this program. It is discussed below.

### 2. Two-Stirred Tank Model

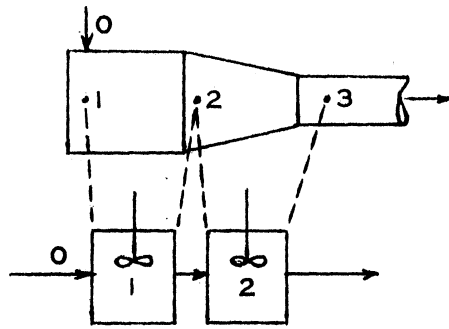
#### a. Theory

Based on the general design of the A thru E reactors, we have chosen a two tank continuously stirred system\* as a simple theoretical model. We believe a stirred tank Model is appropriate because the injected air is well mixed with the exhaust in the reactors tested. This two-stirred tank model

---

\*This model assumes continuously stirred tank reactors (CSTR). The test reactors could be best described as partially stirred tank reactors (PSTR) which approximate CSTR behavior.

is shown below.



Temperature and composition are assumed constant throughout each tank. The model assumes perfect mixing within each tank and no intermixing between tanks. While this model uses two tanks, separation of the actual reactor into two distinct reaction regions is only an approximation. A more detailed prediction would require a substantial amount of data along the length of each reactor and is not considered justifiable.

The design equation for a single stirred tank reactor is<sup>1</sup>:

$$X_{CO} = r_{CO} \frac{V}{(F_{CO})_0} \quad (1)$$

where:

$V$  = reactor fluid volume (in.<sup>3</sup>)

$(F_{CO})_0$  = molar flow rate of carbon monoxide,  $\frac{\text{moles CO}}{\text{sec.}}$

$X_{CO}$  = extent of CO conversion,  $1 - \left(\frac{\text{out}}{\text{in}}\right)_{CO}$

$r_{CO}$  = reaction rate of CO,  $\frac{\text{moles CO}}{\text{in}^3 \text{-sec.}}$

For two tanks in series, the design equation becomes:

$$X_{CO} = \frac{V}{(F_{CO})_0} [r_{CO1} f + r_{CO2} (1 - f)] \quad (2)$$

where:

the subscripts 1 and 2 refer to tanks 1 and 2

$f$  = the fraction of the total volume in tank 1

The following expression from reference 2, Final Report, pg. 53, was used to calculate the CO reactor rate:

$$r_{CO} = 1170 e^{-\frac{45,821}{\bar{R} T}} P_{CO}^{.386} P_{O_2}^{-.051} P_{NO}^{.145} \quad (3)$$

where

$\bar{R}$  = universal gas constant,  $1.987 \frac{\text{cal}}{\text{gm-mole-}^\circ\text{K}}$

$T$  = temperature,  $^\circ\text{K}$

$P$  = partial pressure, psi

In the above expression, the reactor pressure was taken to be 15 psia, NO was set at 300 ppm, and the value of the  $O_2$  term was assumed to be unity.\*

\*Assuming the  $O_2$  to be unity resulted in a maximum error of 5% with the air injection fraction used for the calculations.

Note that equations 1 and 2 predict that conversion efficiency is directly proportional to reactor volume and inversely proportional to CO molar flow rate. CO conversion is also directly proportional to the reaction rate which is a strong increasing function of temperature.

Theoretically, the CO concentration and temperature within a CSTR are uniform throughout. The values used in equations 2 and 3 were taken from Figs. 14 thru 18, and are summarized in Table 2. The temperature and CO concentrations in Table 2 were obtained by averaging the measurements at positions 1 and 2 in the reactor and using these averages as the values for tank 1 of the model. The values for tank 2 were obtained by averaging the measurements at positions 2 and 3. Tank 1 was assumed to contain this volume up to a cross-section at location 2 and Tank 2 the remaining volume.

Table 2 shows averages for temperature and composition of all data as well as data excluding reactor E, the elliptical reactor. The averages excluding reactor E are thought to be more meaningful since reactor E was poorly mixed and the accuracy of its temperature and composition data was questionable.

b. Comparison of Theoretical Predictions with Experimental Results

The CO conversion for each of the five reactors with optimum air injection was predicted from the two tank model and compared to the experimental results at 3000 rpm using the actual data for each reactor (Table 2). Figure 19 shows theoretical conversion fraction from Eq. 2 (solid line) versus the ratio of reactor volume to molar flow rate of carbon monoxide.



TABLE 2  
 Experimental Data for Simplified Theoretical Model  
 3000 RPM, 24 ft-lbf load,  $F \approx .25$

Reactor	$T_1$ $^{\circ}F$	$T_2$ $^{\circ}F$	$CO_1$ %	$CO_2$ %	$(F)_{CO_2}$ $\frac{\text{moles } CO}{\text{sec.}}$	$\frac{V(F)_{CO_2}}{\text{in}^3\text{-sec}}$ $\frac{\text{moles } CO}{\text{moles } CO}$	$f = \frac{V_1}{V_{\text{total}}}$	X Actual	X Predicted
A	1740	1700	0.7	0.2	$6.33 \times 10^{-5}$	$1.26 \times 10^6$	.73	.98	1.00
B	1770	1720	0.7	0.2	$6.58 \times 10^{-5}$	$1.28 \times 10^6$	.75	.98	1.00
C	1730	1710	1.2	0.7	$6.41 \times 10^{-5}$	$.86 \times 10^6$	.68	.94	1.00
D	1750	1675	1.2	0.5	$6.35 \times 10^{-5}$	$.83 \times 10^6$	.76	.98	1.00
E	1660	1550	1.5	0.4	$6.35 \times 10^{-5}$	$1.18 \times 10^6$	.70	.94	.85
Total Average	1730	1671	1.06	0.4	$6.40 \times 10^{-5}$		.72		
Average w/o Reactor E	1748	1701	.95	0.4	$6.42 \times 10^{-5}$		.73		

Actual test values of this ratio are indicated by the vertical dotted lines. Theoretical conversion is indicated by the x's and experimental conversion by the circles. The simplified model predicts complete CO conversion for reactors A, B, C, and D which is in substantial agreement with the experimental data in Table 2, but only 85% conversion for reactor E (see Fig. 19). The predicted conversion for reactor E is low because of the low measured temperatures resulting from poor mixing. In the E reactor the effect of increasing the temperature in each of the two tanks by 40°F is shown by the E' line. These temperatures may be more representative of the actual temperatures within the reaction zone and lead to 100% CO conversion. The difference in slopes for reactors A through D primarily reflect variations in temperature and, to a lesser degree, variations in CO concentration.

The slight differences in conversion efficiency between the theoretical predictions and actual data result from imperfect mixing of the exhaust and injected air in the reactor. Our model assumed perfect mixing which makes 100% conversion possible.

A comparison of the experimental results at 3000 rpm for the five reactors with some theoretical predictions is shown in Fig. 20. The experimental points are the values measured at positions 2 and 3 in Figs. 14 thru 18. The theoretical lines were calculated assuming a 40°F temperature difference between tanks 1 and 2, and a CO concentration of .95% in tank 1 and .4% in tank 2. The value of  $f$  was taken as .73. These values are representative of the "Average without Reactor E" in Table 2.

The limited data shown in Fig. 20 shows that the two stirred tank model, using the "Average without Reactor E" data, predicts the experimental results reasonably well. To verify the model requires some additional partial conversion data in the 20-80% region. Unfortunately, a reactor small enough, flow rate high enough, or temperature low enough to achieve data in this partial conversion range was never attained during our testing.

c. Computer Predictions

The model predicts that 100% conversion can be achieved at the given 3000 rpm reactor conditions with a volume of 40-45 in.<sup>3</sup>, assuming good mixing (see Fig. 20). Depending on the degree of mixing, the reactor volume may have to be increased somewhat, perhaps to 45-50 in.<sup>3</sup> to achieve maximum conversion without an increase in reactor temperature. According to this prediction, reactors C and D are just large enough to achieve maximum CO conversion at 3000 rpm, 24 ft-lbf.

Figure 19 shows that the operating point (the dashed vertical line) for Reactor A could be shifted to the left to  $V/(F_{CO})_O = .81$  and still achieve complete CO conversion. This corresponds to a reactor volume of 51 in.<sup>3</sup> at the given reactor conditions.

Figure 21 shows the performance predicted for the Model A and C reactors using the "Average without Reactor E" experimental values. A range of operating temperatures are plotted using a 50° F temperature difference between tanks 1 and 2. This graph suggests that temperatures above 1680° F are required to give high CO conversion at the 3000 rpm test

point for the A reactor, and temperatures above 1725°F, for the C reactor. At the 4000 rpm, test point reactor A requires above 1725°F, and reactor C above 1775°F. Actually, these are the minimum temperatures in each case.

For a given flow rate complete CO conversion can be achieved at lower reactor temperatures by shifting the vertical operating lines to the right, i. e., by increasing reactor volume. Figure 21 suggests that the A reactor is just large enough to be effective on this engine at 4000 rpm if temperatures are about 1700°F. A smaller reactor would require higher operating temperatures. Higher operating temperatures pose serious problems with thermal reactors and are undesirable. Even reactor A appears too small to achieve virtually complete conversion at 5000 rpm. With 1700°F temperatures 75% conversion may be possible.

### 3. Concluding Remarks

A two-stirred tank model appears to be reasonable for predicting the directional effects of varying volume, flow rate, temperature, and composition for a rotary engine reactor in which air is well mixed with exhaust, as in our designs. More experimental data at partial conversion is required to verify the model. On the other hand, for exhaust port air injection, or some other injection scheme where reactor mixing is poor, this simplified model will greatly overstate CO conversion and the UM-CRC Dynamic Patterns of Flow Model is expected to be better.

VI References for Phase III

1. Levenspiel, O., Chemical Reactor Engineering, Wiley & Sons, 1962, pg. 103.
2. Patterson, D. J., et al, "Kinetics of Oxidation and Quenching of Combustibles in Exhaust Systems of Gasoline Engines", Three Annual Reports to CRC, 1969-1972.

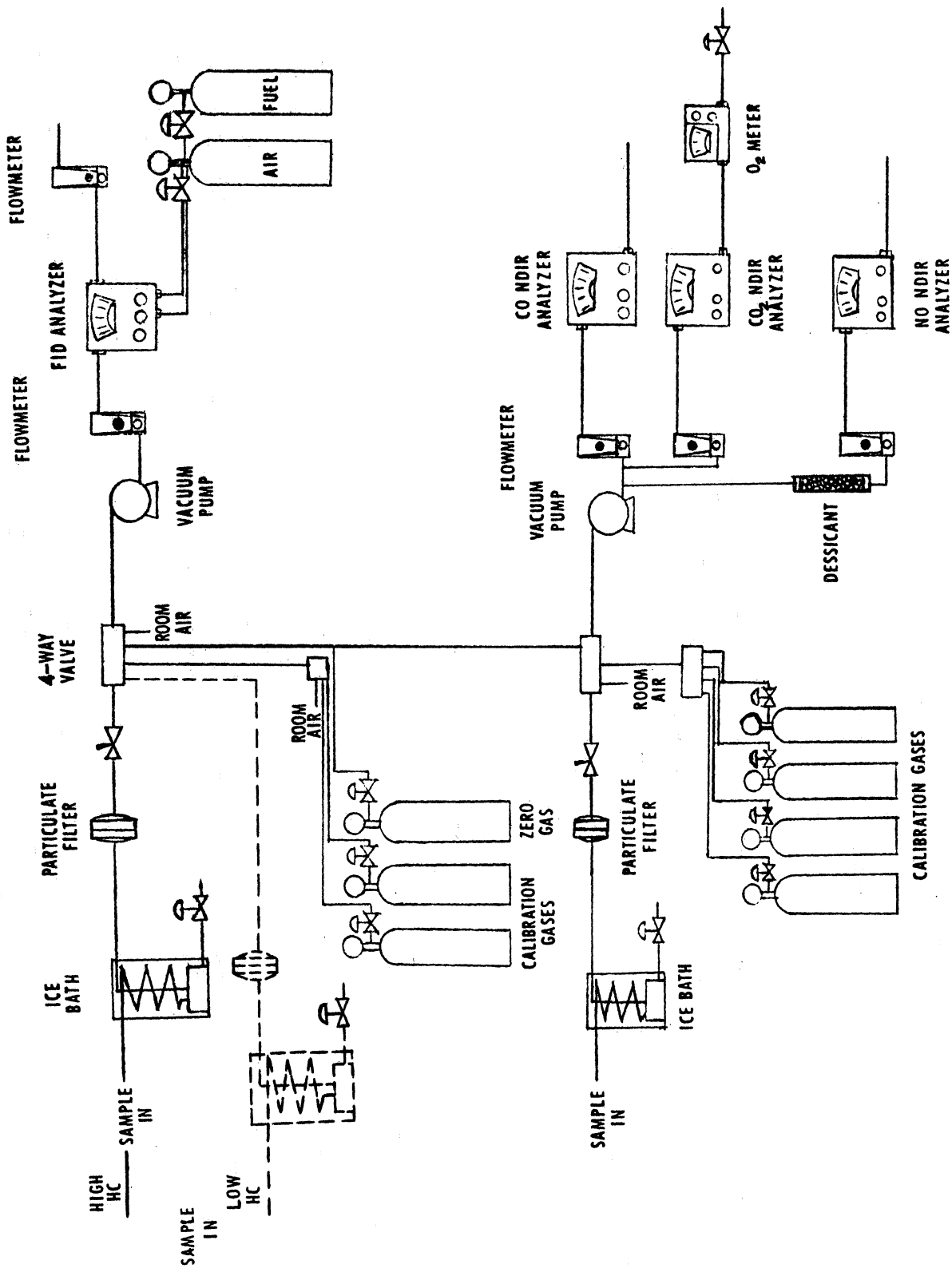


FIG 1 - SCHEMATIC OF ANALYTICAL SYSTEM

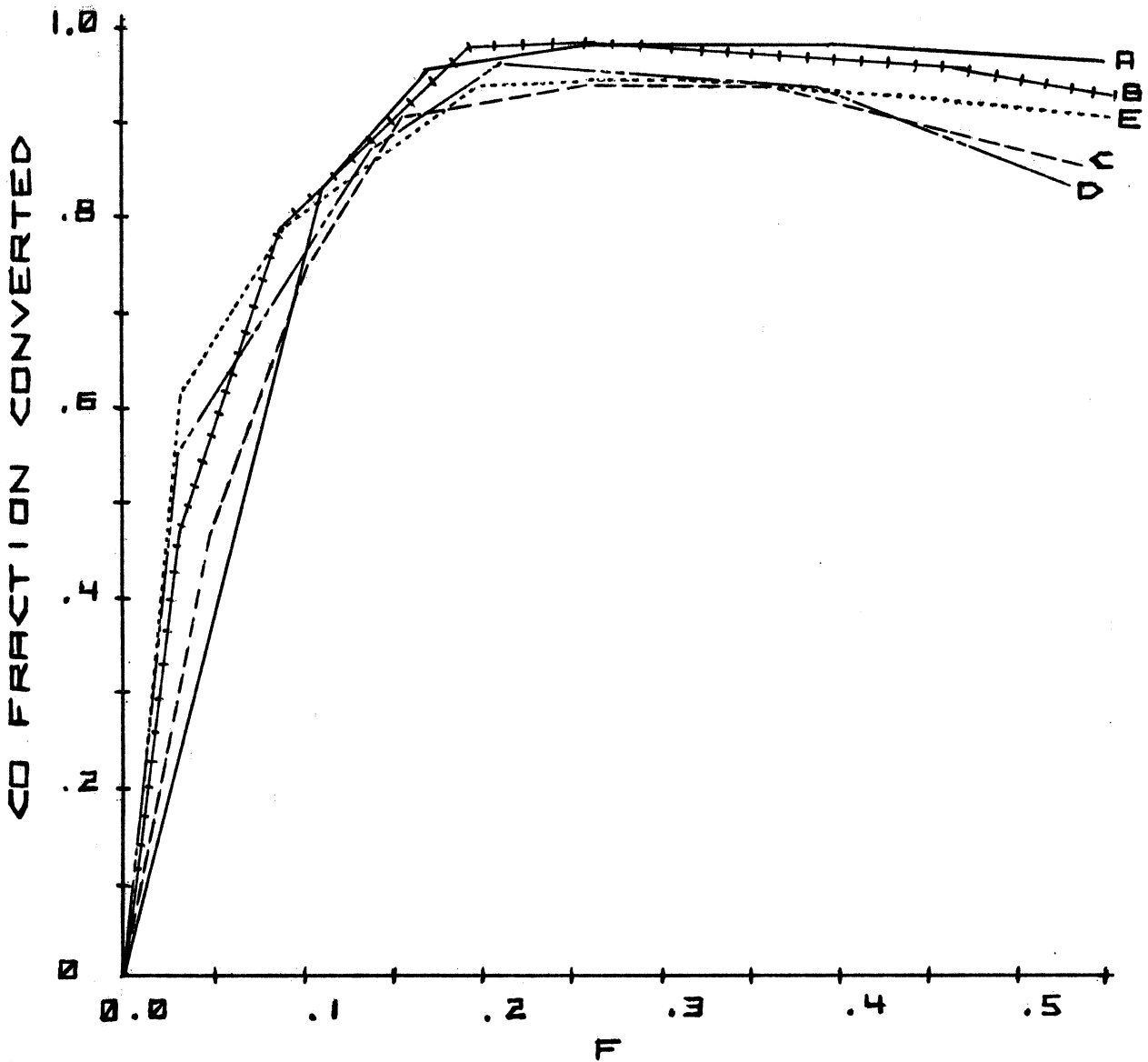


Fig. 2 - CO Conversion vs. Injection Fraction for all Reactors. Exhaust Sampled 1-1/2" Downstream of Reactor Exit. Engine - 3000 RPM, 24 ft-lbf. Reactor Inlet - 5.5 % CO.

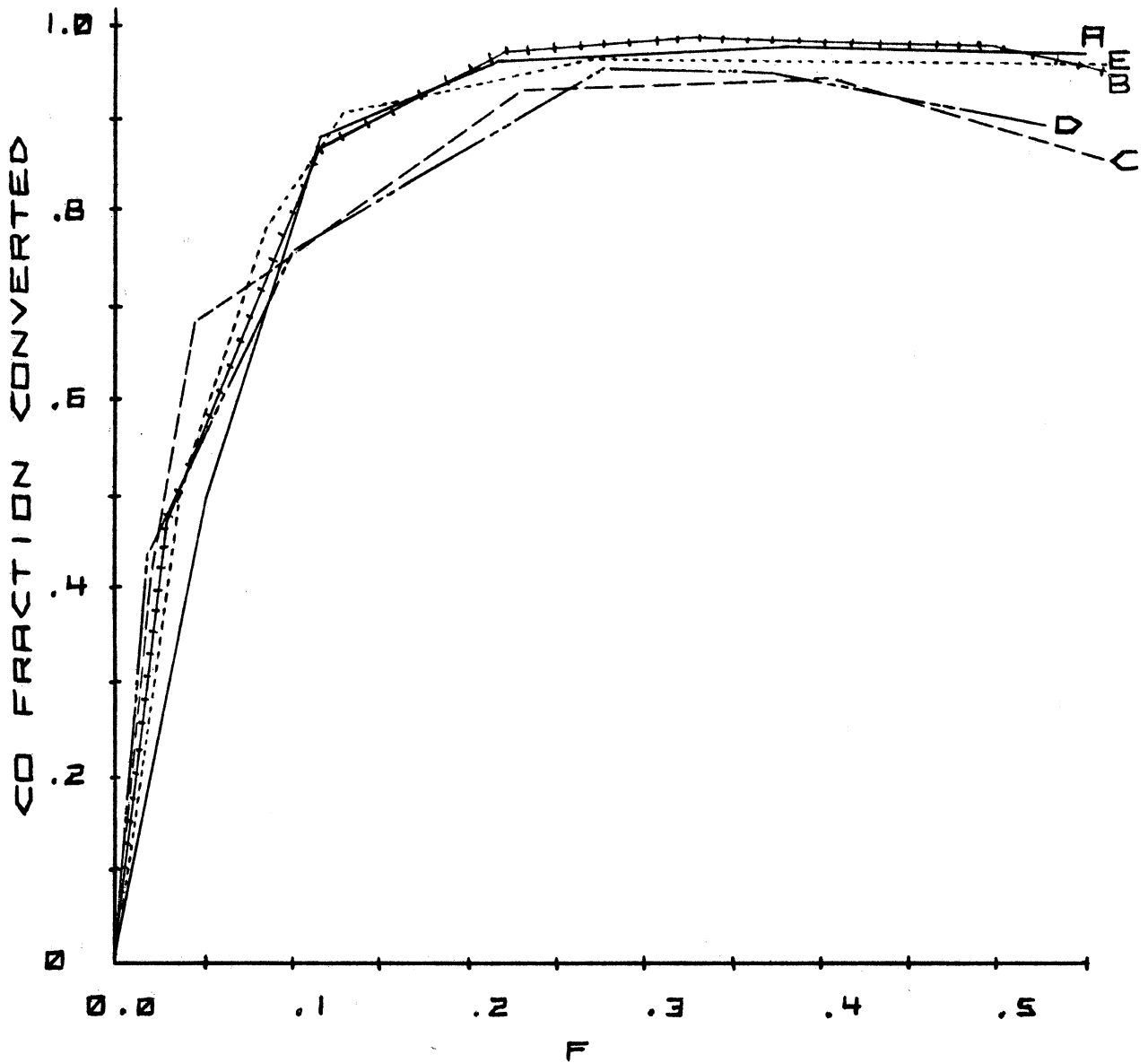


Fig. 3 - CO Conversion vs. Injection Fraction for all Reactors. Exhaust Sampled 1-1/2" Downstream of Reactor Exit. Engine - 4000 RPM, 27 ft-lbf. Reactor Inlet - 5.6% CO.



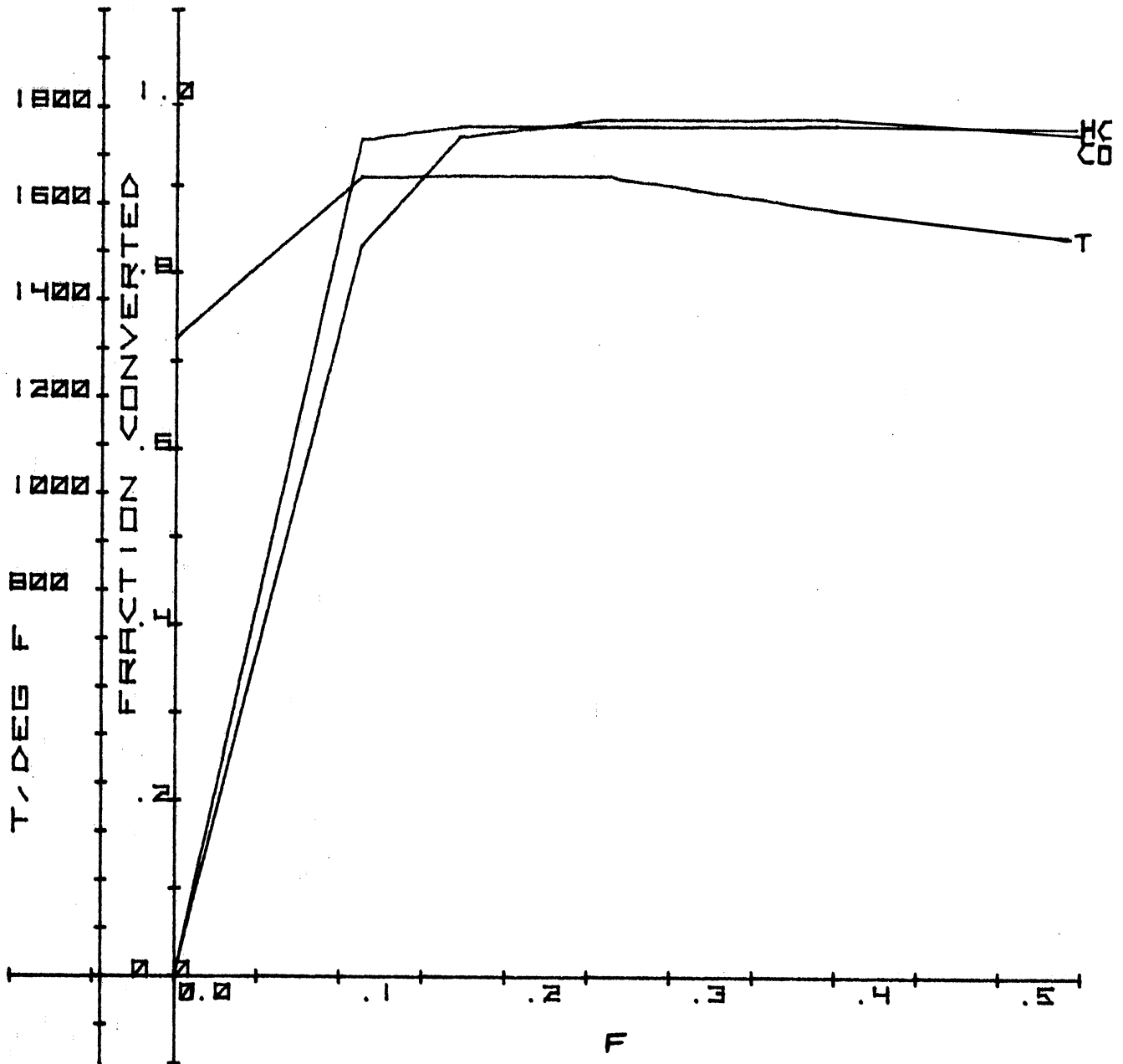


Fig. 4 - CO and HC Conversion and Reactor Temperature vs. Injection Fraction for Reactor A with Continuous HC Sampling. Exhaust and Temperature Measured 1-1/2" downstream of Reactor Exit. Engine - 3000 RPM, 24 ft-lbf,  $\dot{m} = 107$  lbm/hr,  $\dot{m}_f = 9.3$  lbm/hr. Reactor Inlet - 5.5% CO, 884 ppm n-hexane, 1638°F.

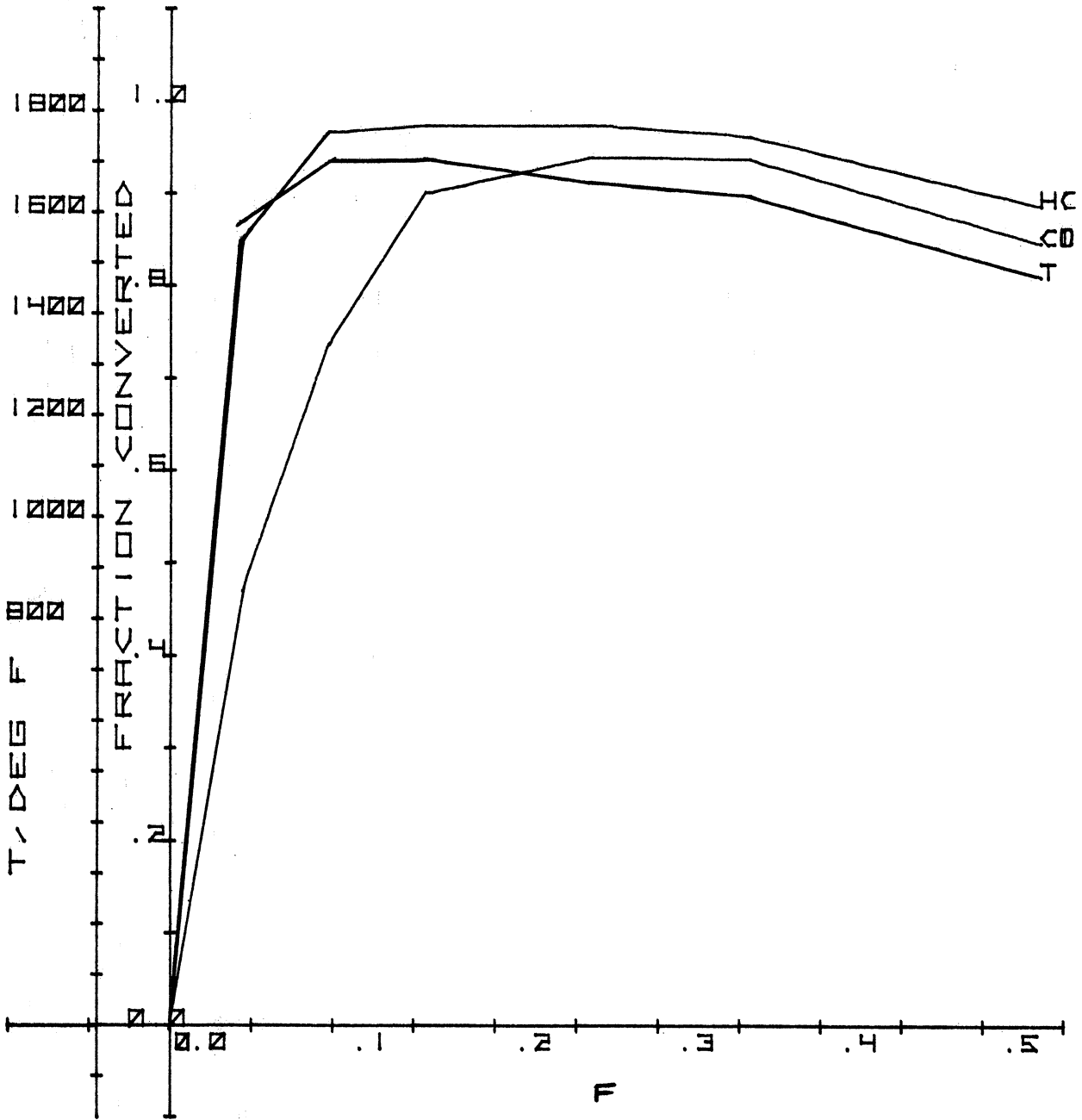


Fig. 5 - CO and HC Conversion and Reactor Temperature vs. Injection Fraction for Reactor C. Exhaust and Temperature Measured 1-1/2" Downstream of Reactor Exit. Engine - 3000 RPM, 26 ft-lbf,  $\dot{m} = 110$  lbm/hr,  $\dot{m}_f = 9.5$  lbm/hr. Reactor Inlet - 5.5% CO, 692 ppm n-hexane, 1615°F.

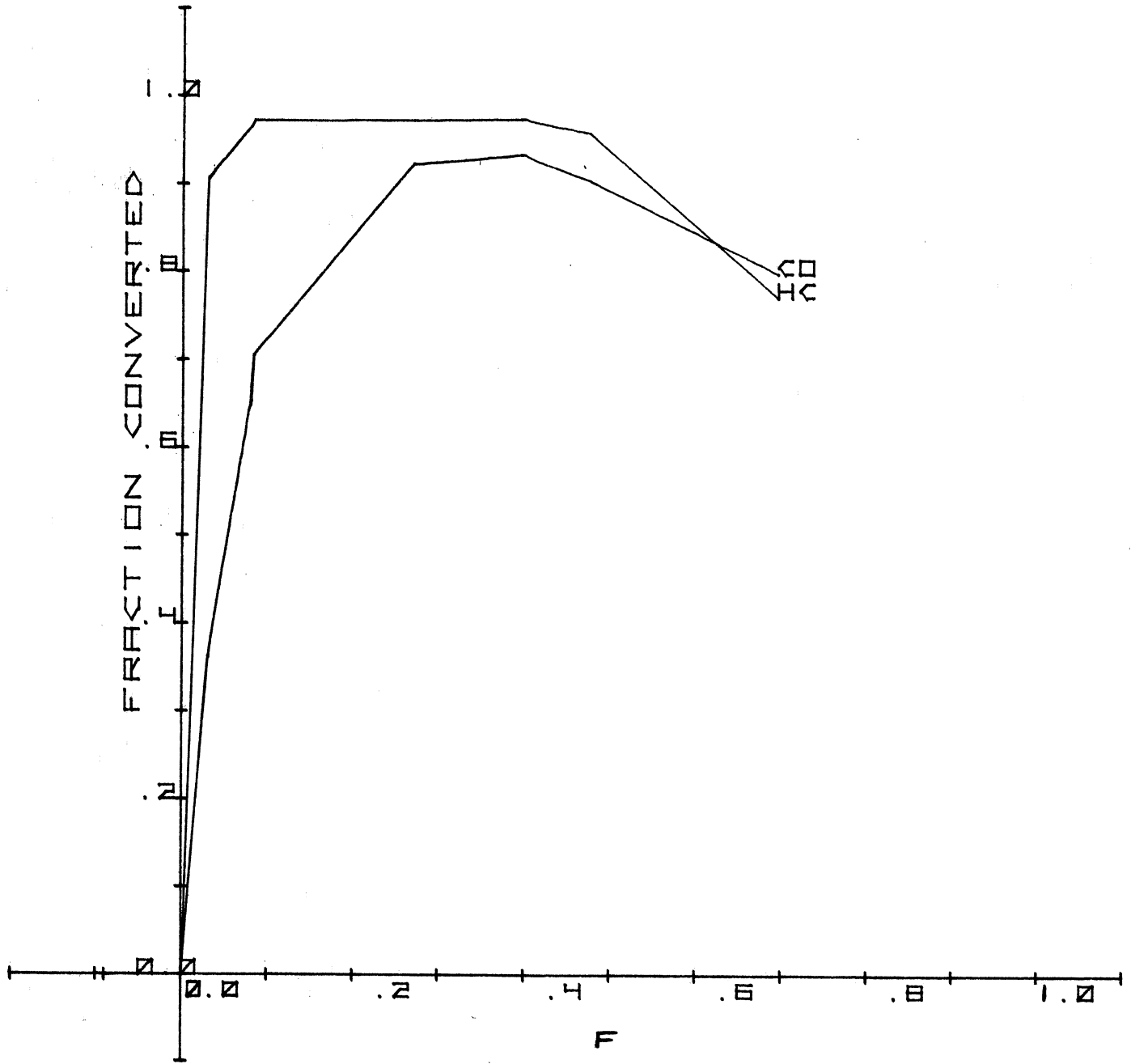


Fig. 6 - CO and HC Conversion vs. Injection Fraction for Reactor C. Exhaust Sampled 1-1/2" Downstream of Reactor Exit. Engine - 4000 RPM, 28 ft-lbf,  $\dot{m} = 170$  lbm/hr,  $\dot{m}_f = 14.5$  lbm/hr. Reactor Inlet - 5.6% CO, 690 ppm n-hexane, 1780°F.

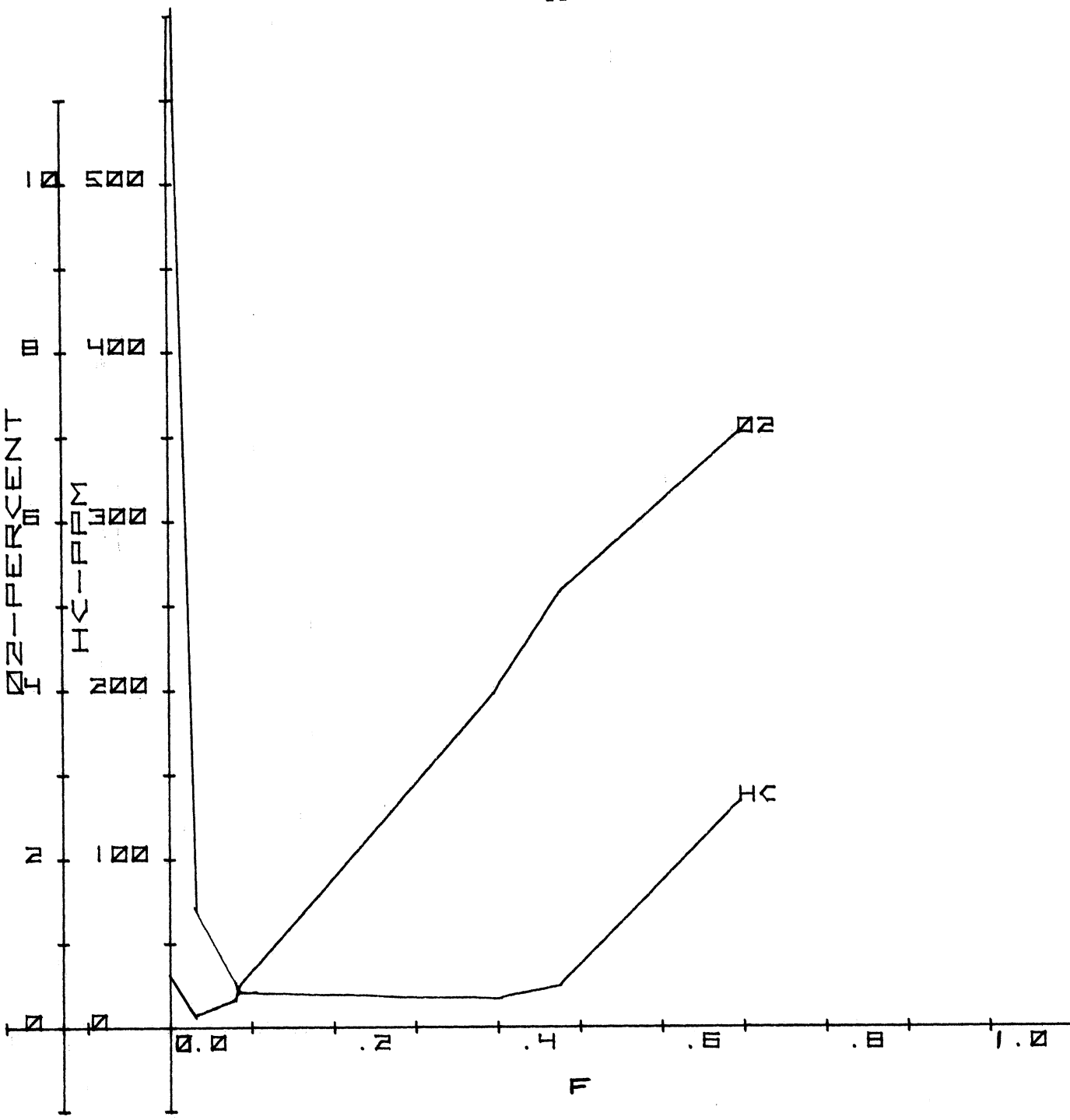


Fig. 7 - Corrected HC and O<sub>2</sub> vs. Injection Fraction for Reactor C. Exhaust Sampled 1-1/2" Downstream of Reactor Exit. Engine 4000 RPM, 28 ft-lbf,  $\dot{m}_a = 170$  lbm/hr,  $\dot{m}_f = 14.5$  lbm/hr. Reactor Inlet - 5.6% CO, 690 ppm n-hexane, 1780° F.

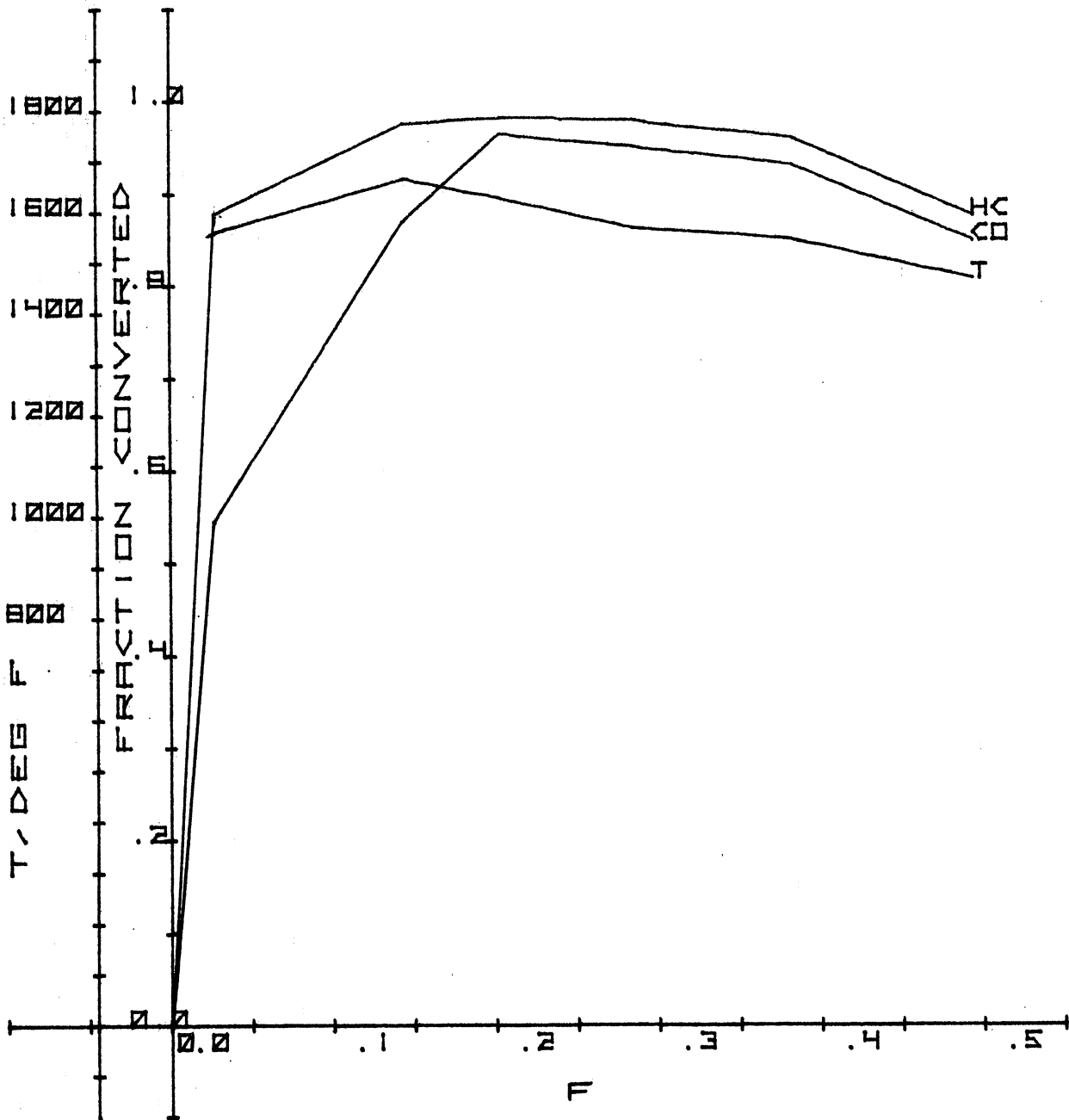


Fig. 8 - CO and HC Conversion and Reactor Temperature vs. Injection Fraction for Reactor D. Exhaust and Temperature Measured 1-1/2" Downstream of the Reactor Exit. Engine - 3000 RPM, 24 ft-lbf,  $\dot{m}_a = 109$  lbm/hr,  $\dot{m}_f = 9.5$  lbm/hr. Reactor Inlet - 5.5% CO, 682 ppm n-hexane, 1665°F.

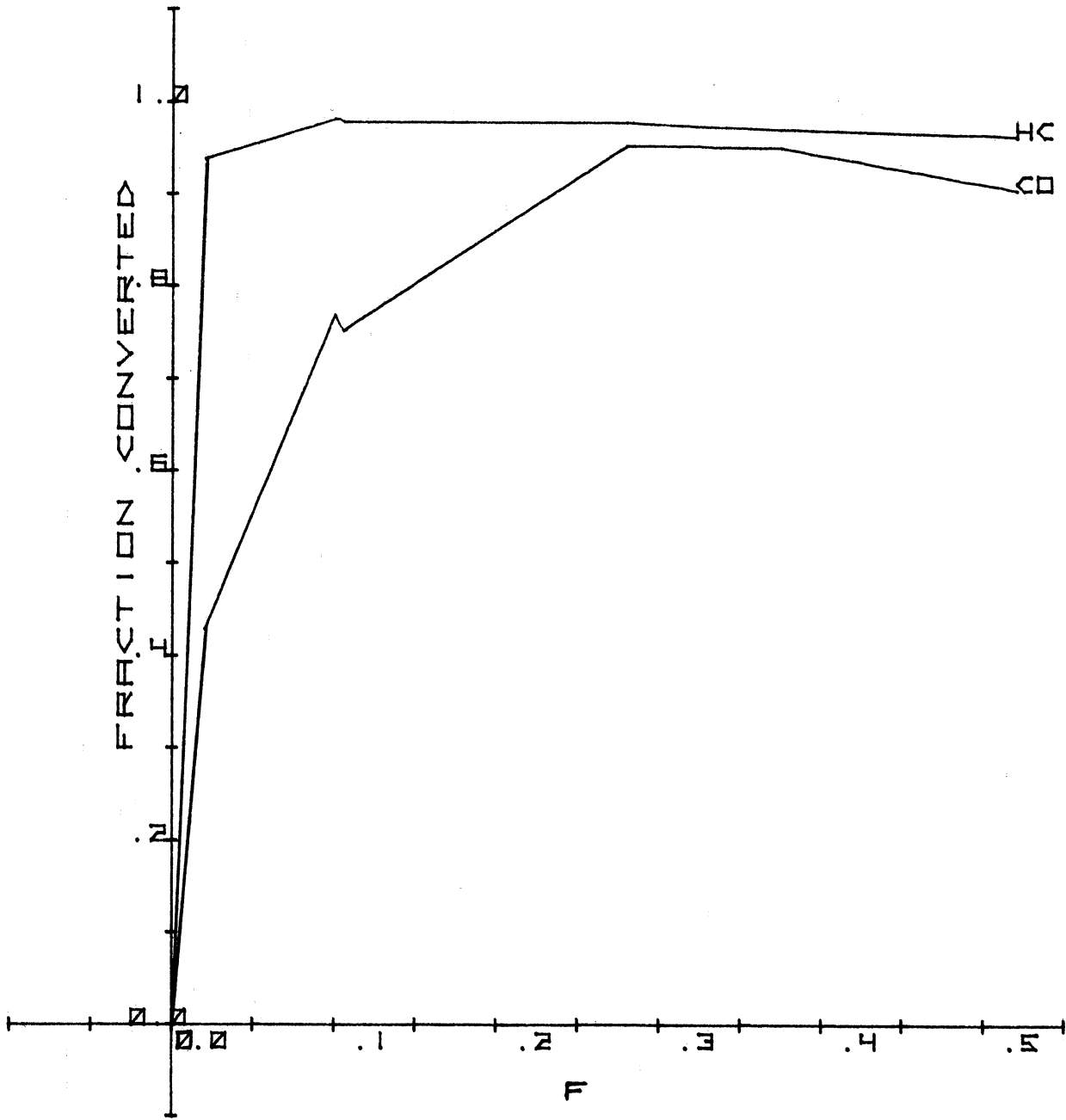


Fig. 9 - CO and HC Conversion vs. Injection Fraction for Reactor D. Exhaust Sampled 1-1/2" downstream of Reactor Exit. Engine - 4000 RPM, 26 ft-lbf,  $\dot{m}_a = 158$  lbm/hr.,  $\dot{m}_f = 13.5$  lbm/hr. Reactor Inlet - 5.5% CO, 594 ppm n-hexane, 1815° F.

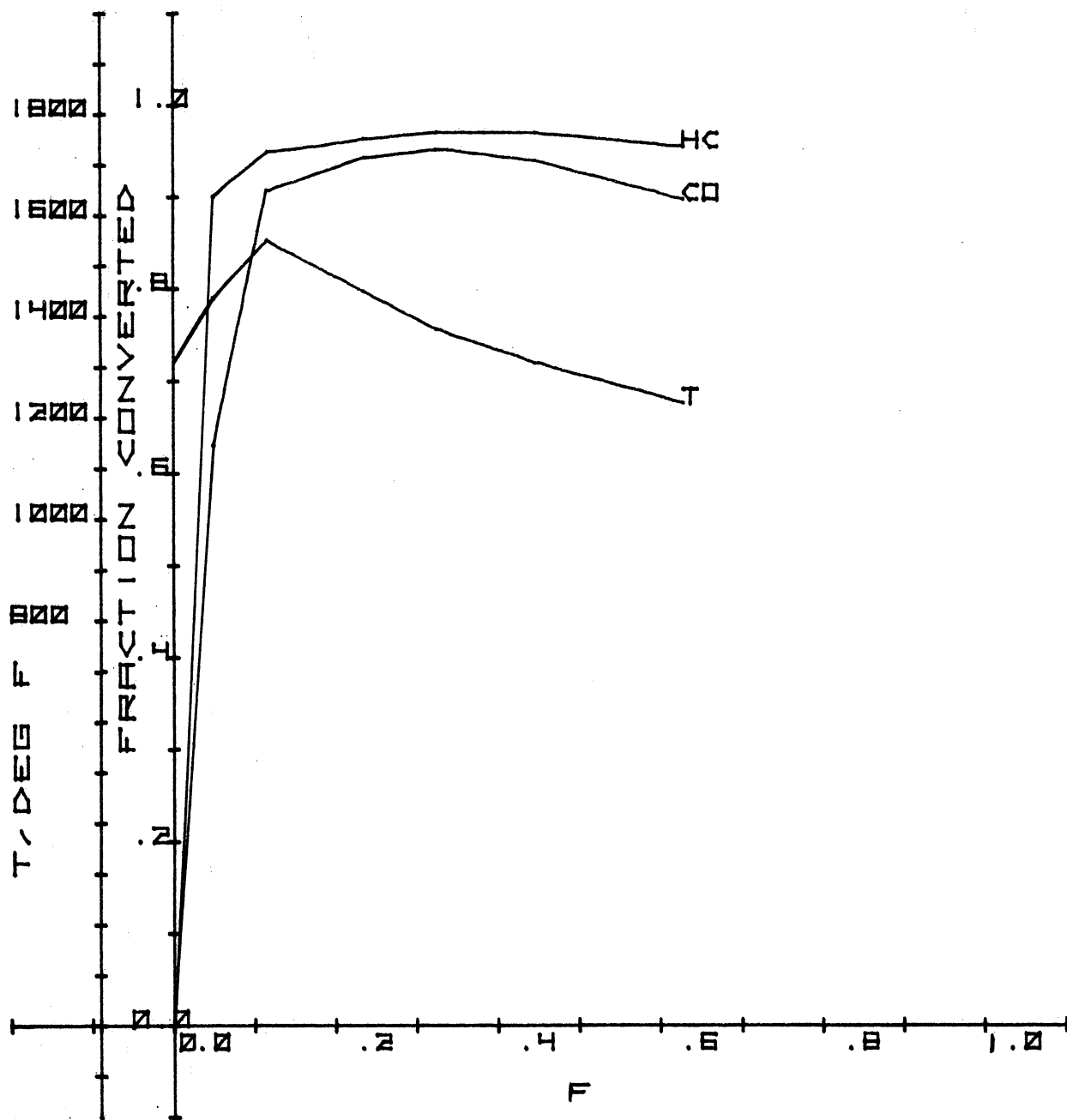


Fig. 10 - CO and HC Conversion and Reactor Temperature vs. Injection Fraction for Reactor E. Exhaust and Temperature Measured 1-1/2" Downstream of Reactor Exit. Engine - 3000 RPM, 24 ft-lbm,  $\dot{m}_a = 110$  lbm/hr,  $\dot{m}_f = 9.4$  lbm/hr. Reactor Inlet - 5.5% CO, 775 ppm n-hexane, 1615°F.

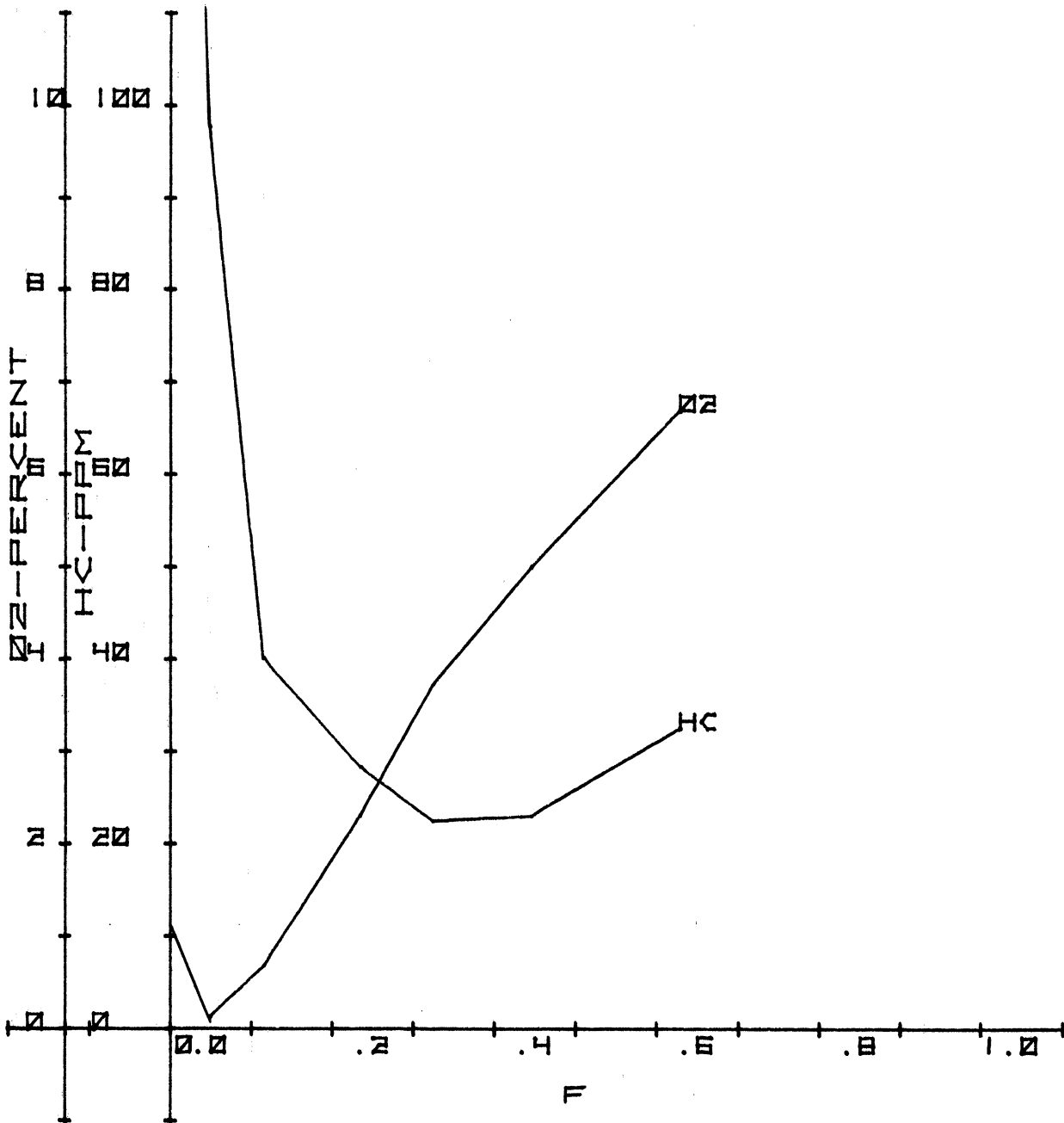


Fig. 11 - Corrected HC and O<sub>2</sub> vs. Injection Fraction for Reactor E. Exhaust Sampled 1-1/2" Downstream of Reactor Exit. Engine - 3000 RPM, 24 ft-lbf,  $\dot{m}_a = 109$  lbm/hr,  $\dot{m}_f = 9.5$  lbm/hr. Reactor Inlet - 5.5% CO, 682 ppm n-hexane, 1618° F.



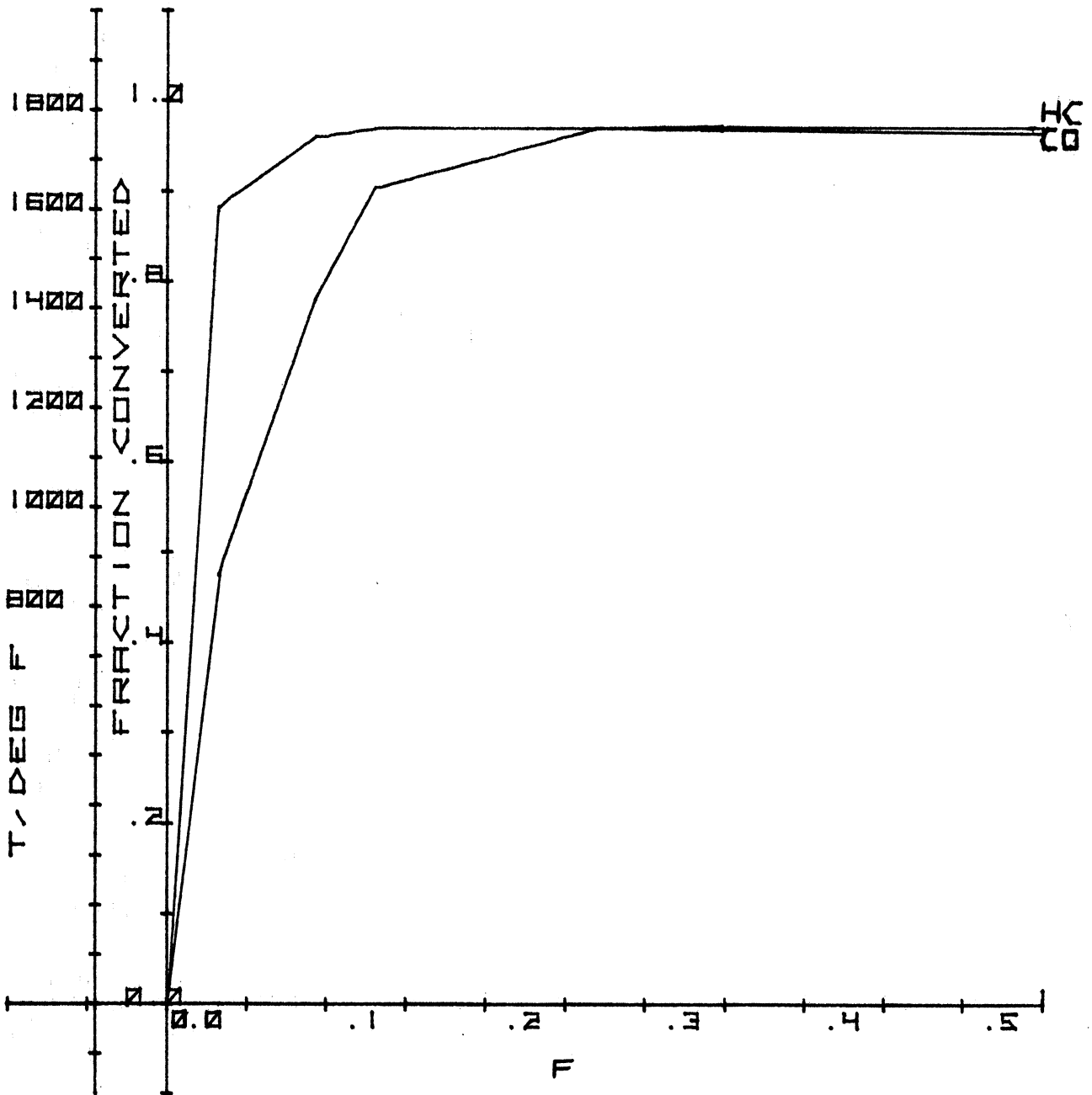


Fig. 12 - CO and HC Conversion vs. Injection Fraction for Reactor E. Exhaust Sampled 1-1/2" Downstream of Reactor Exit. Engine - 4000 RPPM, 26 ft-lbf,  $\dot{m}_a = 161$  lbm/hr,  $\dot{m}_f = 13.8$  lbm/hr. Reactor Inlet - 5.7 % CO, 500 ppm n-hexane, 1770°F.

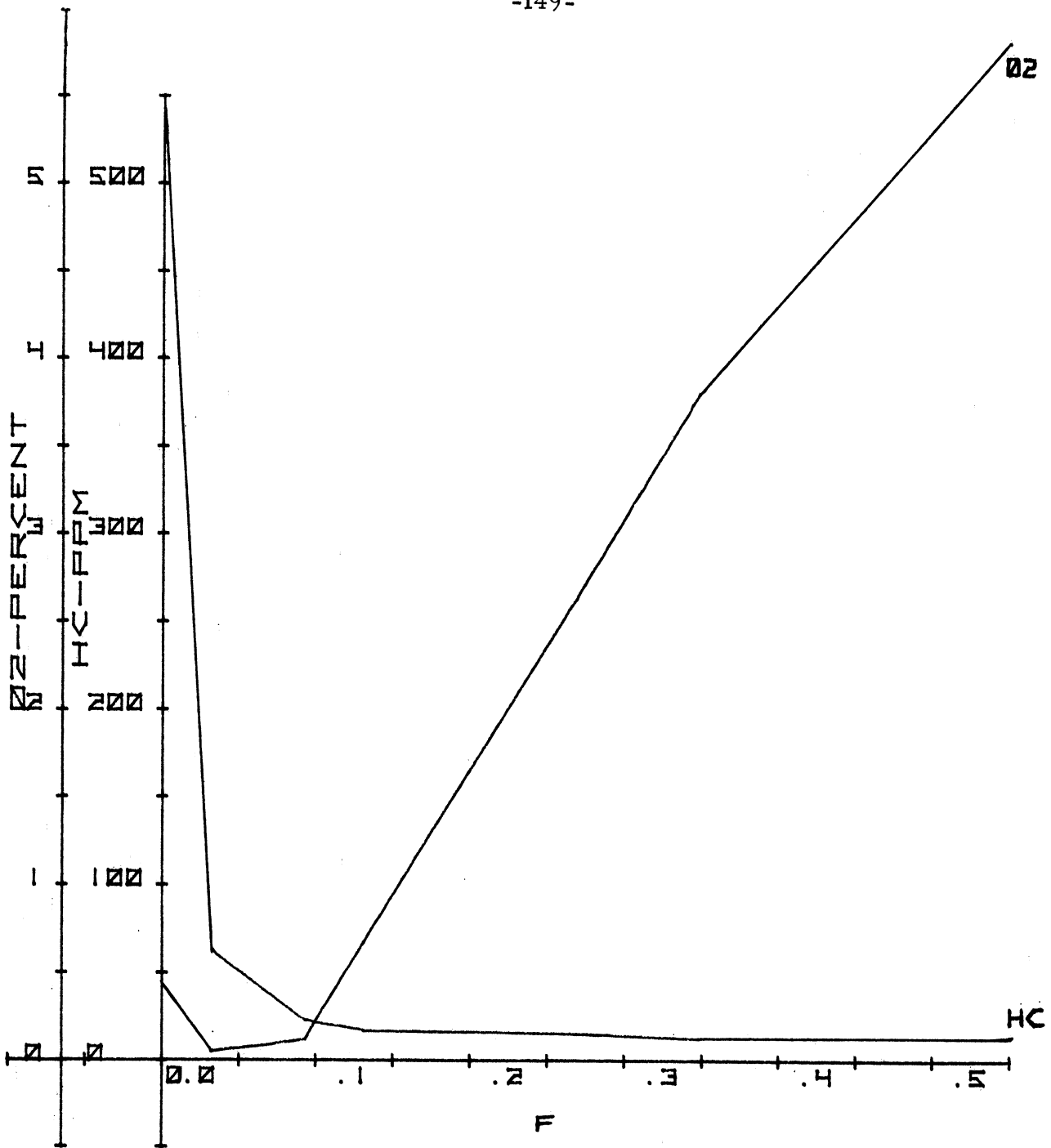


Fig. 13 - Corrected HC and O<sub>2</sub> vs. Injection Fraction for Reactor E. Exhaust Sampled 1-1/2" Downstream of Reactor Exit. Engine - 4000 RPM, 26 ft-lbf,  $\dot{m} = 161$  lbm/hr,  $\dot{m}_f = 13.8$  lbm/hr. Reactor Inlet - 5.7% CO, 500 ppm n-hexane, 1770 °F.

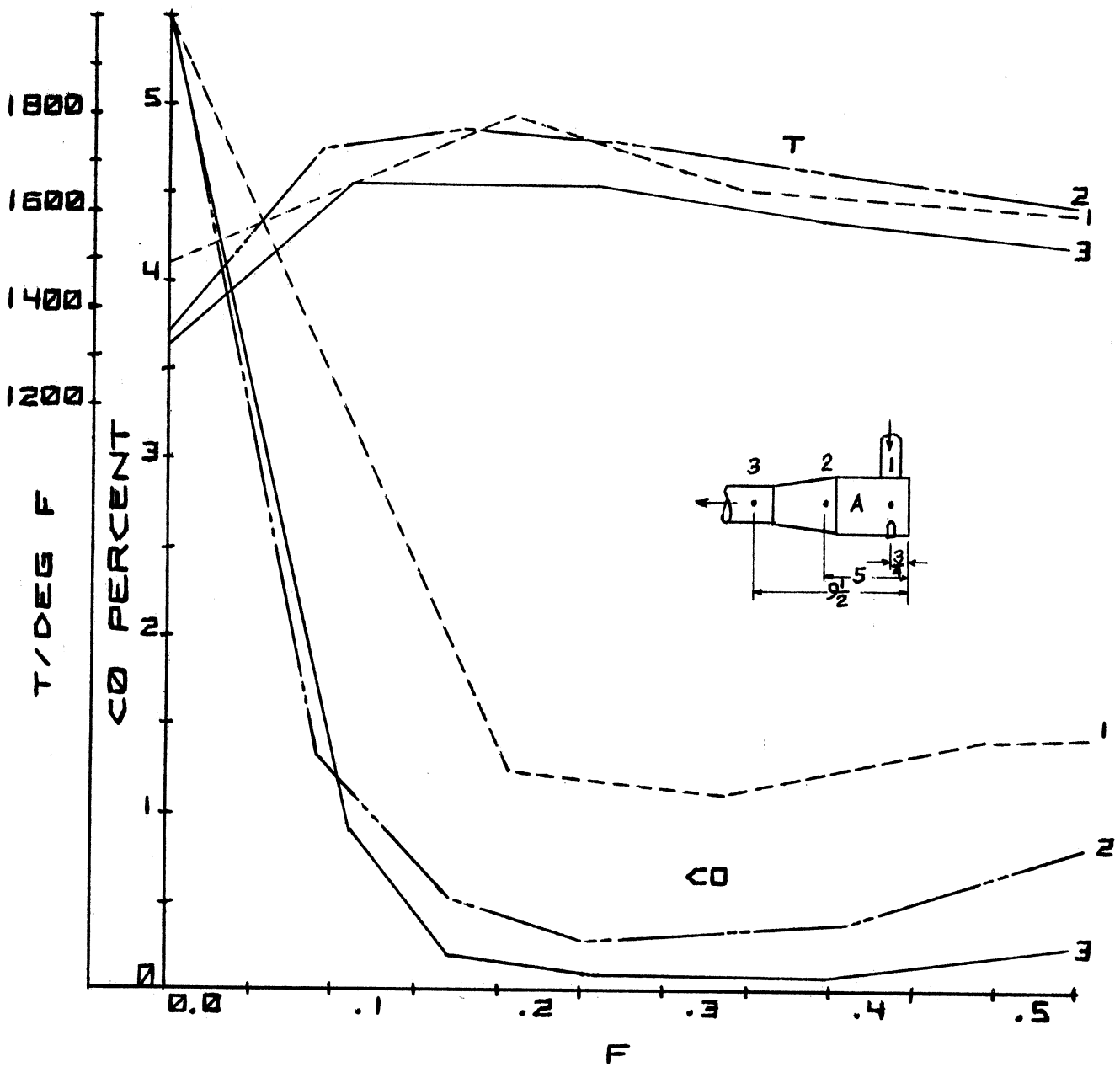


Fig. 14 - Corrected CO Concentration and Temperature Along the Length of Reactor A vs. Injection Fraction. Engine-3000 RPM, 24 ft-lbf,  $\dot{m}_a = 107$  lbm/hr,  $\dot{m}_f = 9.3$  lbm/hr, Reactor Inlet  $1638^\circ\text{F}$ .

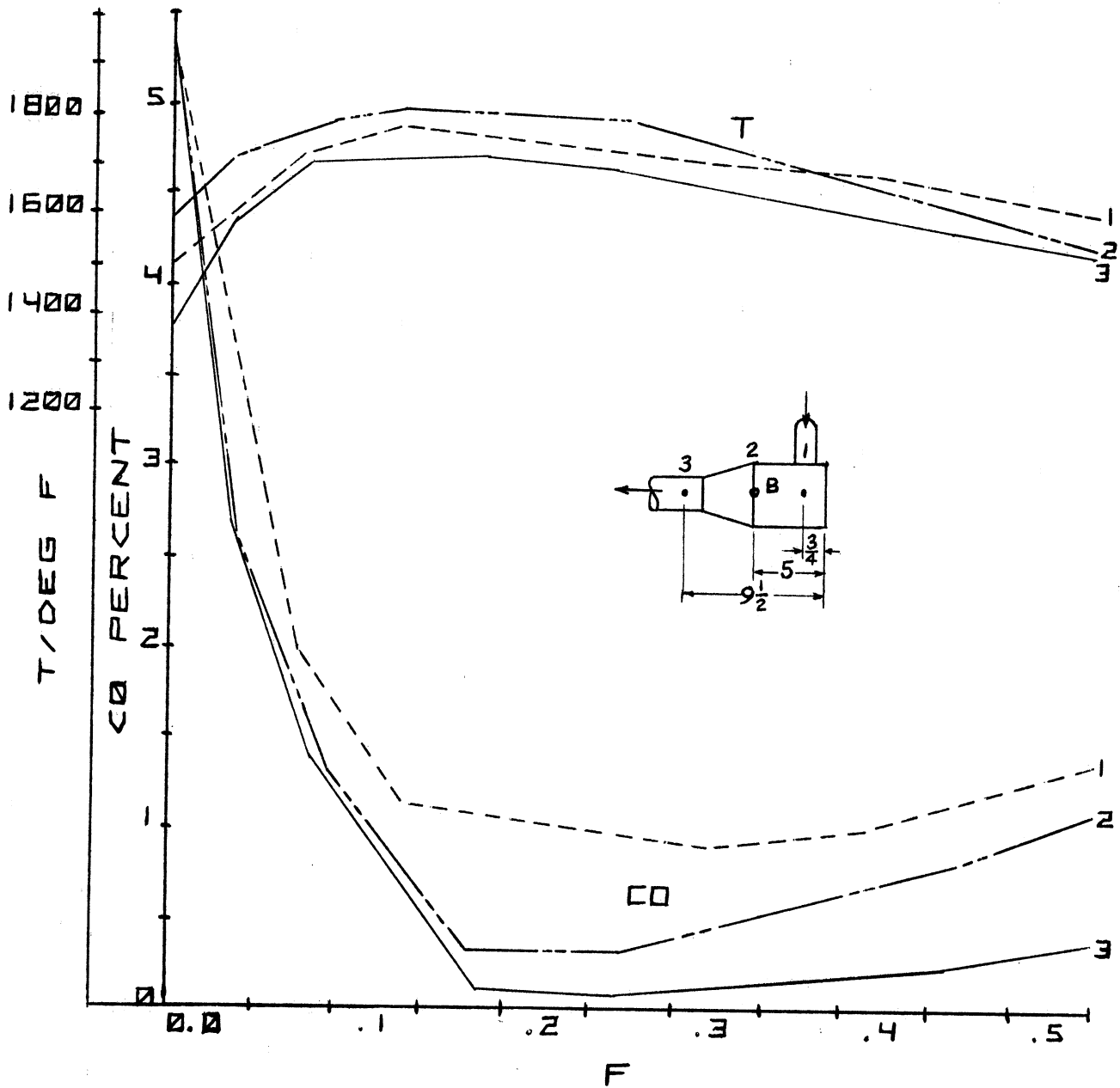


Fig. 15 - Corrected CO Concentration and Temperature Along the Length of Reactor B vs. Injection Fraction. Engine-3000 RPM, 26 ft-lbf,  $\dot{m}_a = 113$  lbm/hr,  $\dot{m}_f = 9.9$  lbm/hr, Reactor Inlet  $1610^\circ\text{F}$ .

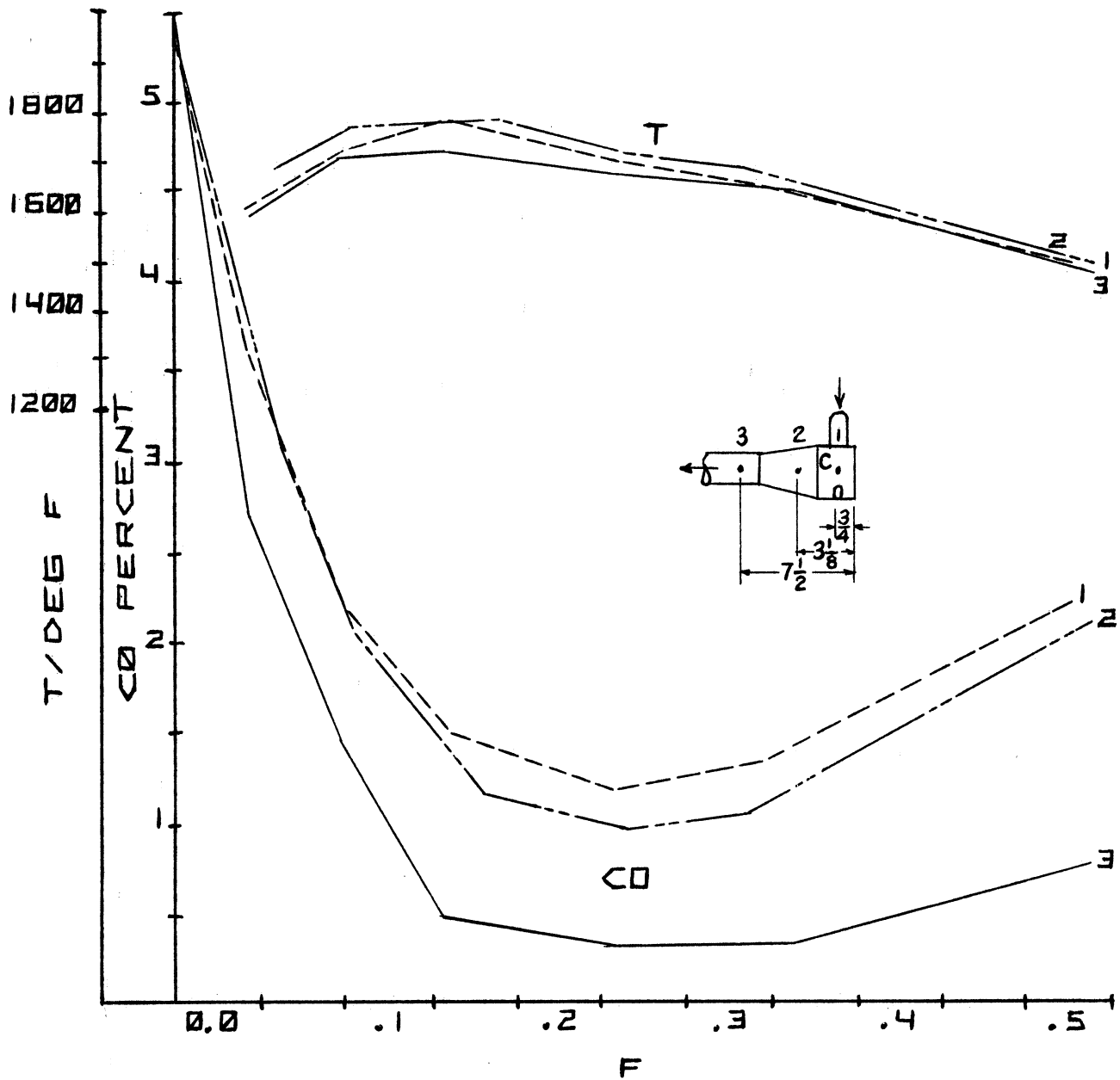


Fig. 16 - Corrected CO Concentration and Temperature Along the Length of Reactor C vs. Injection Fraction. Engine-3000 RPM, 26 ft-lbf,  $\dot{m}_a = 110$  lbm/hr,  $\dot{m}_f = 9.5$  lbm/hr. Reactor Inlet 1615°F.

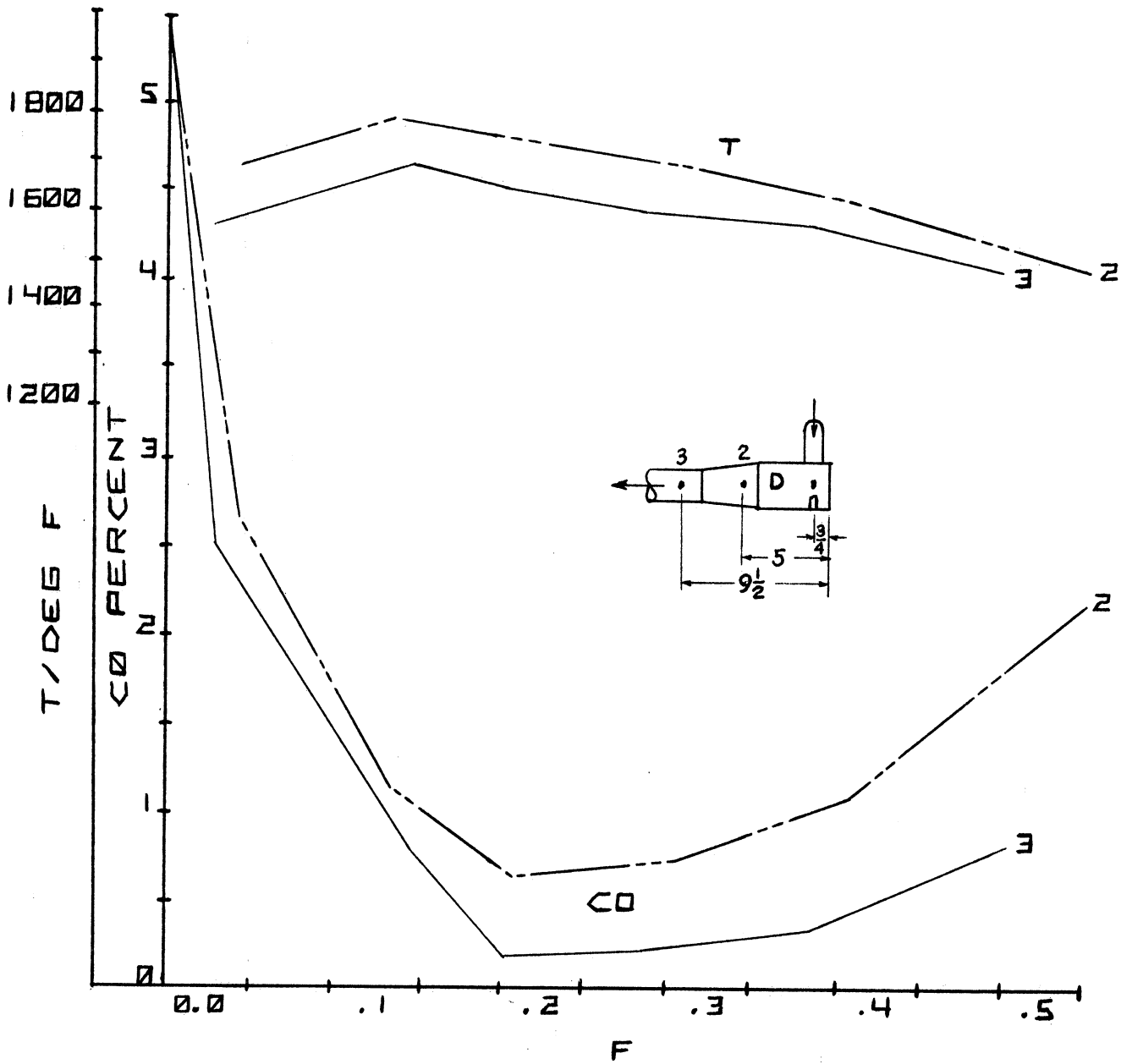


Fig. 17 - Corrected CO Concentration and Temperature Along the Length of Reactor D vs. Injection Fraction. Engine-3000 RPM, 24 ft-lbf,  $\dot{m}_a = 109$  lbm/hr.,  $\dot{m}_f = 9.5$  lbm/hr. Reactor Inlet 1665°F.

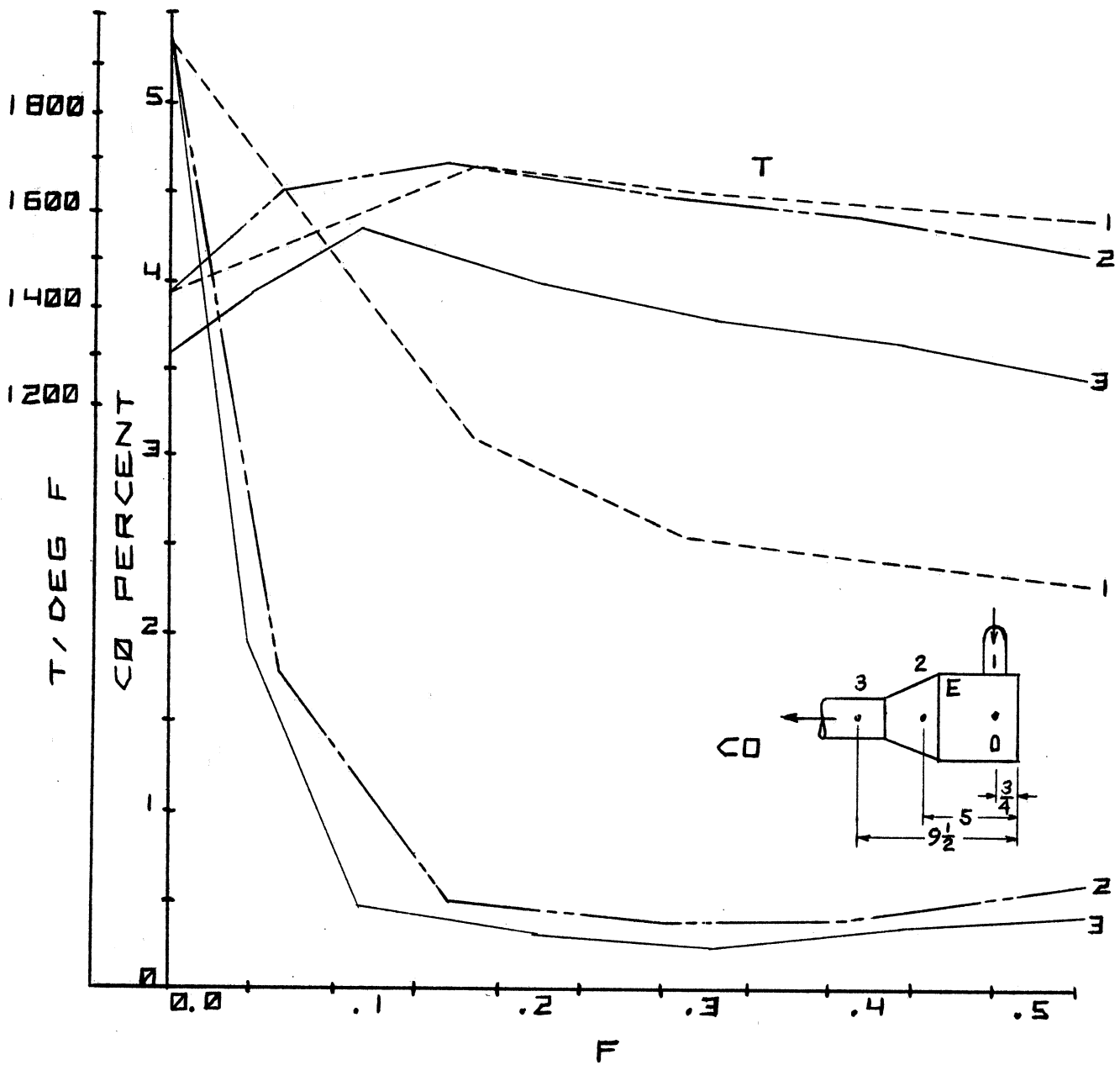


Fig. 18 - Corrected CO Concentration and Temperature Along the Length of Reactor E vs. Injection Fraction. Engine-3000 RPM, 24 ft-lbf,  $\dot{m}_a = 109$  lbm/hr.,  $\dot{m}_f = 9.5$  lbm/hr. Reactor Inlet 1618°F.

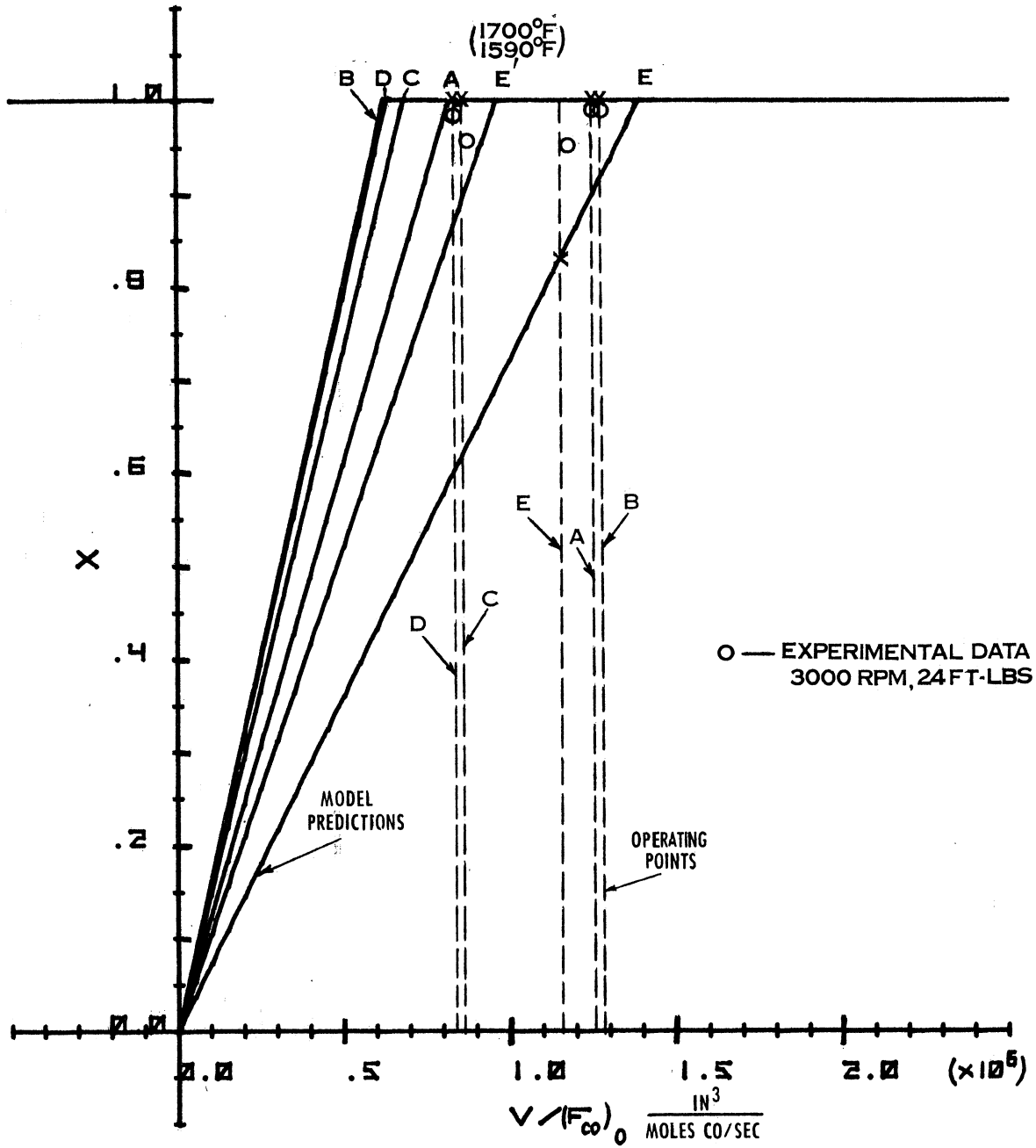


Fig. 19 - Prediction of CO Conversion Fraction(x) using Two-Stirred Tank Model, (solid lines). Experimental ratios of reactor volume divided by molar flow rate of carbon monoxide are indicated by dotted lines, x's are theoretical operating points, circles are experimental results.



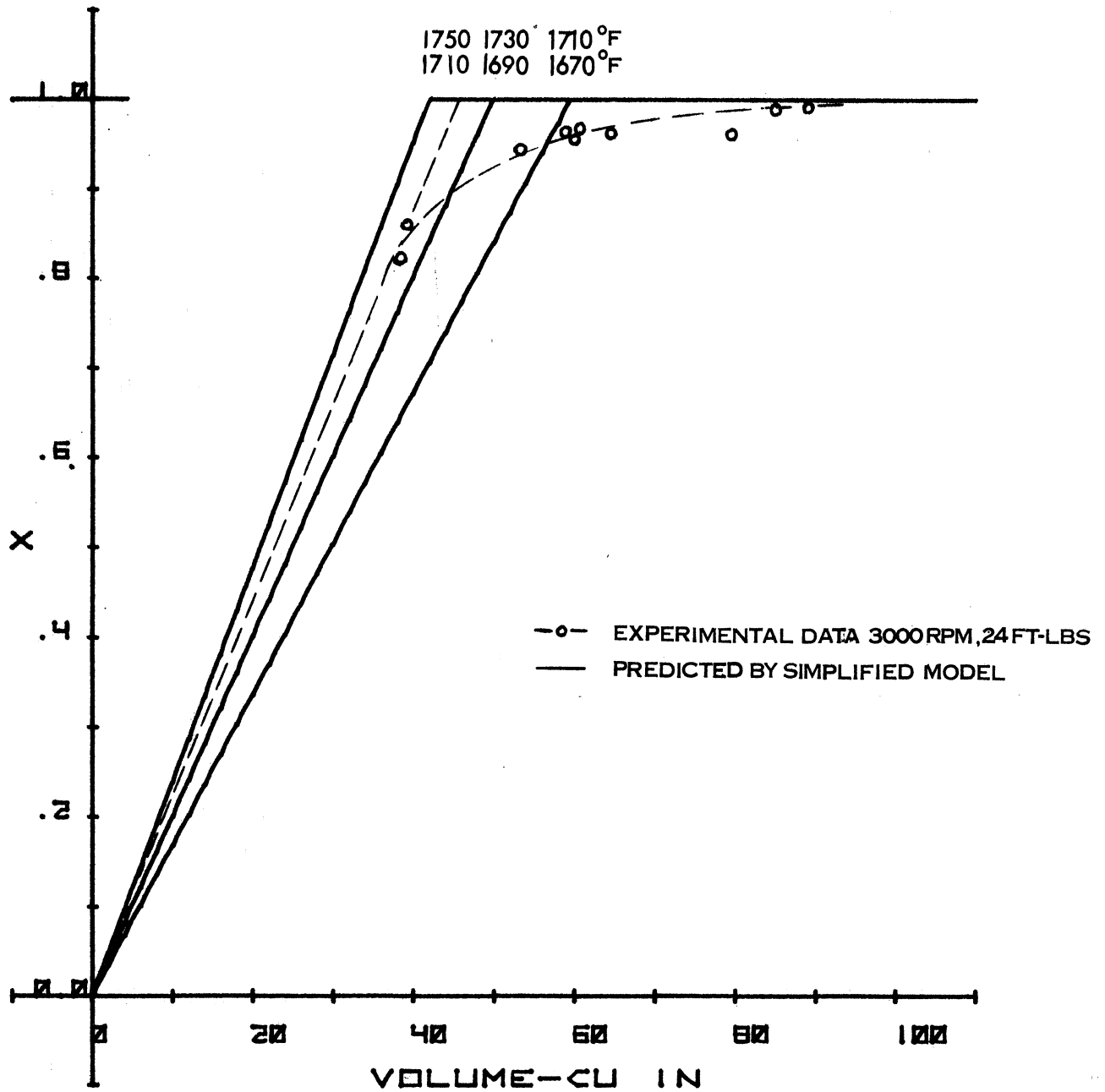


Fig. 20 - Comparison of Theoretical Predictions and Experimental Data for Reactors A, B, C, D and E. Tank 1, CO = .95%, Tank 2, CO = .4%, NO = 300 ppm, f = .73

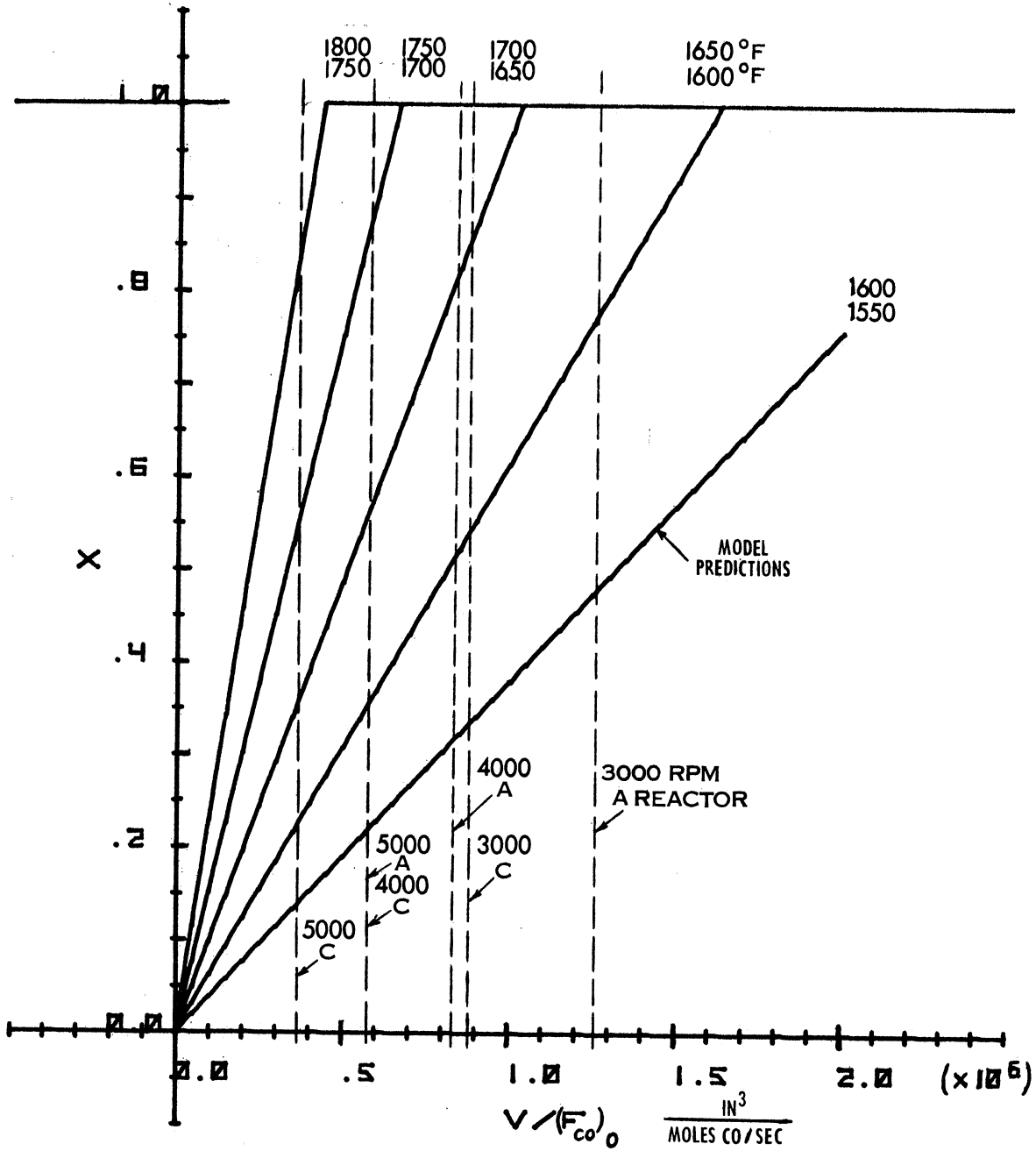


Fig. 21 - Effect of Temperature on CO Conversion Predicted from Two-Stirred Tank Model, assuming a 50°F Difference in Tank Temperatures,  $CO_1 = .95\%$ ,  $CO_2 = .4\%$ ,  $f = .73$ ,  $NO = 300$  ppm. Vertical lines show values of volume divided by carbon monoxide molar flow rate for engine operation at 3000, 4000 and 5000 rpm. Predictions are for a large reactor, Reactor A, and a smaller one, Reactor C.

APPENDIX A

Typical Engine Characteristics  
with Reactor and Secondary Air \*

Speed rpm	Intake Vacuum in. Hg.	Torque ft-lb.	m <sub>a</sub> lbm/hr.	m <sub>f</sub> lbm/hr.	A/F
2100	2.7	28	86	7.1	12.1
2500	2.4	20	83.7	6.8	12.3
2500	2.2	20	82.5	7.2	11.5
2500	2.7	26	95.7	7.6	12.5
2800	1.5	34	142.5	11.8	12.1
3000	2.2	26	115	10.2	11.3
3000	2.4	24	111	9.6	11.6
3000	3.0	25	107	9.3	11.5
3500	1.8	25.5	142.2	12.2	11.6
3500	1.8	26	141.5	12.3	11.5
3500	2.5	25	121.4	11.3	10.8
4000	2.0	28	170.0	14.5	11.7
4000	2.5	28	159.0	13.7	11.6
4000	2.0	28.5	171.6	14.7	11.7

\*Two engines (same model) used during testing period

Appendix B

UM-CRC Computer Program Development

Phase I - Computer Program Revision

A major revision has been completed of the Patterns of Flow (POF) computer program written by Dr. Everett Sondreal, et. al., for the CRC study on Thermal Reactors for Gasoline Engine Exhaust. The purpose of this revision was: 1) to correct a few minor errors previously detected; 2) to strengthen the functional layout of the program; 3) to permit a larger variety of flow cases, such as recycle streams; and 4) to optimize those sections of the program which were the most time consuming. The latest version of the computer program is entitled, Dynamic Patterns of Flow (DPOF).

As part of the computer program revision, the subroutine (CYCLE) which provides the cyclic variations in temperature, flow rate, and composition was rewritten to simulate the variations expected for a Wankel rotary engine.

Phase II - Simulation Results

For purposes of the simulation, the following engine parameters were used:

Air Flow Rate (dry basis) - 140 lbm/hr.

Fuel Flow Rate (H/C = 1.85) - 12 lbm/hr.

A/F = 11.7

Crank Speed - 2800 RPM

Exhaust Concentrations - 6% CO, 10% CO<sub>2</sub>, 0.6% O<sub>2</sub>,  
965 ppm HC as n-hexane

The base case parameters for the thermal reactor were:

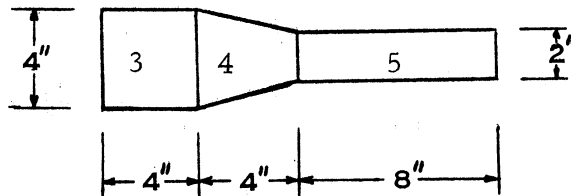
Air flow rate (dry basis) - 33 lbm/hr

Exhaust Port temperature - 1712°F

Reactor Exhaust temperature - >1800°F

Pressure - 15.0 psia

Dimensions - typical of Model A reactor



The reactor was considered to be 3 distinct modules (2 CSTR's followed by a PFR) with volumes of 50.0, 30.0, and 25.0 cu. in. As a first approximation of the mixing, the I/2 values were set to 4.0 for the first CSTR, 2.0 for the second CSTR, and 1.0 for the PFR.

Mass balances around the engine on carbon, oxygen, and hydrogen were employed to calculate the total exhaust flow rate and the concentrations of H<sub>2</sub>O and H<sub>2</sub>. Because of the large pre-exponential factor in the rate expression for hydrogen oxidation, it would have been necessary to use an extremely small stepsize for the integration of the cell differential equations. The added expense of performing the extra calculations was deemed unreasonable and so the entering hydrogen was considered to be completely consumed along with the residual oxygen before the exhaust reached the thermal reactor. The following average exhaust concentrations were used for all simulation cases:

	<u>Mole Fraction</u>
CO	0.06
H <sub>2</sub>	0.0
HC	0.000965
O <sub>2</sub>	0.0
CO <sub>2</sub>	0.10
H <sub>2</sub> O	0.1477
N <sub>2</sub>	Balance

The average exhaust flow rate was 5.288 lbmoles/hr and the average injected air flow rate (for the base case) was 1.144 lbmoles/hr. This produced a dilution ratio of 1.216 and a stoichiometric ratio of 1.269. The exhaust flow was split into 40 cells and the injected air flow was split into 10 cells. This resulted in approximately equal size (molar) cells for the base case air flow rate.

Several preliminary simulation runs indicated that 6 cycles should be sufficient to flush out the startup conditions and to give a reasonable indication of reactor performance when the results of the last 3 cycles were averaged. (Such averaging is required since the model is a stochastic process).

Because the heat loss is an independent parameter for the computer model, the first parametric study was made in an attempt to find reasonable operating temperatures based on the experimental steady-state dynamometer tests.

Tables I and II detail the heat losses for each case for each of the reactor modules and the resulting average temperatures per output cell. Cases which have the same heat losses have different startup temperatures (the higher the case number the higher the startup temperature). The higher temperatures were needed to ensure that the CSTR modules could go their upper operating points.

Although changing the startup temperatures did not have a significant effect on the final averaged temperatures. The heat losses

of case 1-10 were selected for the remainder of the cases.

Table III presents the parameters and results for a comparison of reactor performance versus mixing intensity and reactor volume. The reactor module volumes for cases 2 and 3 correspond to a reduction from 4 inches to 3.5 inches for the diameter of the largest part of the reactor. The results show that the conversions and temperatures drop off as the volume is decreased and that increased mixing is effective only for the larger reactor. These results confirm then that the reactor must be large enough to provide overlapping of the early high temperature cells with the low temperature air cells, and that increasing the mixing is not beneficial unless this overlap is present.

Table IV presents the parameters and results for a comparison of reactor performance versus mixing intensity and random seed number. In general, as the mixing intensity is increased the better the performance. The variation between the cases with different random seed numbers illustrates the range of results one can expect from a stochastic model. Presumably, such variations could be minimized by increasing the number of cells in the reactor, but this would result in an unreasonable cost for running the model.

Finally, Table V presents the parameters and results for a comparison of reactor performance versus the dilution ratio and random seed number. The mixing intensity for this series of cases was 8.0, 4.0, and 2.0 for modules 3, 4, and 5. Note that the temperature increased for the lowest dilution ratio case which is a result of adding less low temperature inert gas ( $N_2$ ). The fact that the reactions are effectively quenched for the highest dilution ratio case is a result of specifying too large a heat loss rather than a result of adding too much air. It might be advantageous sometime in

the future to change the procedure for calculating the heat balance so that it is not necessary to specify an overall heat loss but merely an overall heat transfer coefficient and an outside temperature.

In summary, the Dynamic Patterns of Flow computer model has served as a useful tool in the understanding and evaluation of thermal reactors. It suggests that reactor temperature must be 1750°F or higher for complete conversion. This is a result of the kinetic expression used which underestimates reaction rate at the higher temperatures. Moreover, the experimental data showing close to 100% conversion suggests that mixing is much better than anticipated in this initial investigation.



TABLE I

<u>Heat Loss (BTU/hr) per Module</u>			
<u>Case #</u>	<u>Module #3</u>	<u>Module #4</u>	<u>Module #5</u>
1-3	3000	2000	2000
1-4	4000	4000	4000
1-5	8000	6000	6000
1-6	6000	6000	6000
1-7	6000	6000	6000
1-8	5000	5000	5000
1-9	5000	5000	5000
1-10	4000	6000	6000

TABLE II

<u>Average Temperature(°F) per Output Cell</u>			
<u>Case #</u>	<u>Module #3</u>	<u>Module #4</u>	<u>Module #5</u>
1-3	1875.7	2036.3	2127.8
1-4	1839.3	1950.5	2002.1
1-5	1604.4	1518.3	1437.8
1-6	1645.9	1701.0	1712.5
1-7	1630.8	1699.7	1713.7
1-8	1787.3	1890.1	1935.4
1-9	1772.9	1877.3	1927.9
1-10	1864.7	1958.0	1962.0

TABLE III

<u>Comparison of Reactor Performance versus Mixing Intensity and Reactor Volume</u>								
Case #	Mixing Level	Volume	% Conversions			Average Temperature per Output Cell		
			CO	HC	O <sub>2</sub>	Module #3	Module #4	Module #5
1-10	Low	Large	90	93	62	1864.7	1958.0	1962.0
2	Low	Small	72	87	58	1714.9	1794.2	1831.3
3	High	Small	58	85	49	1656.1	1697.8	1718.6
4	High	Large	90	96	70	1853.8	1945.5	1963.0

Mixing Levels for Modules 3, 4, & 5 - Low: 4.0, 2.0, 1.0; High: 6.0, 3.0, 1.5  
 Reactor Volume for Modules 3, 4, & 5 - Large: 50.0, 30.0, 25.0; Small: 40.0, 25.0, 25.0

TABLE IV

<u>Comparison of Reactor Performance versus Mixing Intensity and Random Number Seed</u>								
Case #	Mixing Level	Random # Seed	% Conversions			Average Temperature per Output Cell		
			CO	HC	O <sub>2</sub>	Module #3	Module #4	Module #5
1-10	Low	999	90	93	62	1864.7	1958.0	1962.0
4	Medium	999	90	96	70	1853.8	1945.4	1963.0
5	High	999	97	97	74	1908.4	2023.4	2018.3
6	High	111	98	98	70	1971.8	2045.8	2020.1
7	Medium	111	94	98	70	1889.0	1978.9	1991.2
8	Low	111	86	93	63	1808.9	1910.8	1929.4

Mixing Levels for Modules 3, 4, & 5 - Low: 4.0, 2.0, 1.0; Medium: 6.0, 3.0, 1.5;  
 High: 8.0, 4.0, 2.0

TABLE V

<u>Comparison of Reactor Performance versus Dilution Ratio and Random Number Seed</u>								
Case #	Dilution Ratio	Random # Seed	% Conversions			Average Temperature per Output Cell		
			CO	HC	O <sub>2</sub>	Module #3	Module #4	Module #5
5	1.216	999	97	97	74	1908.4	2023.4	2018.3
6	1.216	111	98	98	70	1971.8	2045.8	2020.1
9	1.108	111	95	82	93	2106.8	2189.6	2156.3
10	1.108	999	96	82	96	2118.9	2180.2	2165.1
11	1.433	999	9	45	10	1344.7	1271.3	1196.4
12	1.433	111	8	43	3	1349.7	1259.2	1170.7

DISTRIBUTION LIST

	<u>No. of Copies</u>
<u>Walker Manufacturing</u>	
Mr. Robert Balluf	10
Walker Manufacturing Company	
Research and Engineering Center	
3901 Willis Road	
Grass Lake, Michigan 49240	
<u>Internal Distribution</u>	
Professor D. E. Cole	1
Professor D. J. Patterson	1
Mr. F. Ament	1
Project file	7



---

THE UNIVERSITY OF MICHIGAN

DATE DUE

---

9/30 19.27